

The spatial regulation of Auxin Response Factors

Jingyi Han B.Sc

Thesis submitted to the University of Nottingham for the
Doctor of Philosophy

March 2021

Abstract

Auxin regulates plant growth and development through the transcription factors (TFs) of the AUXIN RESPONSE FACTOR (ARF) gene family. Class A ARFs, ARF5, 6, 7, 8 and 19 are transcriptional activators, and control many developmental processes. However, we only have limited understanding on how these ARFs can mediate such diverse developmental responses. In this study we investigated expression patterns of ARFs in the root and shoot apical meristems and showed that they have specific domains of expression. Through a yeast one-hybrid and protoplast assay, we identified a network of transcriptional repressors which regulated these ARFs. To validate this network, we over-expressed candidate TFs in ARF reporter lines, generated new reporter lines to check the co-expression of TFs and ARFs in specific tissues and carefully quantified auxin specific phenotypes in the mutants of candidate TFs. Collectively, these results support a mechanism in which the spatial and temporal expression of ARFs is modulated mainly by tissue specific repression.

In order to understand ARF promoter specificity in auxin responses in the most efficient manner, we saw the opportunity to improve the mechanism for creating reporter constructs. In order to improve live imaging of gene expression in its geometric context, we developed a new series of lines (DEAL) showing cellular anatomy which can efficiently combine with auxin sensors and other reporters by Greengate cloning.

Analysing the 5 ARF reporter lines, we found ARF7 has an interesting expression pattern. A broad expression of ARF7 was observed in root tips only in the reporter containing an in-frame fusion of GFP from 3kb promoter to the second exon. Whilst this region upstream of the transcriptional start site had no effect on expression in the shoot. I demonstrated that the first intron plays an important role in transcriptional regulation in the root meristem. A swap experiment in which the first intron was moved to the 5' -UTR showed the position of intron is not essential

for the correct expression. Therefore, we propose that it is the sequence within this intron that is required and that key transcription factors bind to this region. Bioinformatic analysis into potential binding sites within this promoter suggests that NACs and MYBs bind in this intron to regulate ARF7 expression in the root apical meristem. Collectively these data support a role in which root- and shoot-specific binding motifs coordinate the elaborate expression patterns of ARFs.

Acknowledgements

I would like to thank my supervisor, Anthony Bishopp, who give me strong support in project and life. His encouragement is a big energy for me during PhD. He gives me courage to explore scientific question and enjoy this unfamiliar country. Thanks to Malcolm Bennett encouraging me to stand out of my small circle. Thanks also to Ute Voß giving me lots of support in project and encouragement.

Thanks to all those in CPIB and my lab mates, John Vaughan-Hirsch, George Janes, Britta Kümpers, Elina Chrysanthou, Khulud Albalawi and Alex Ware, who patiently help me and communicate with me. They made my time at Sutton Bonington is colourful. Especially thanks to Kamal Swarup and Nicky Leftley doing a lot to keep the lab in order.

I am grateful to collaborate with Jekaterina Truskina and Tave Vernoux (ENS de Lyon) who gave plant material and microscope support. It is a brilliant experience to work with a big group.

I would like to thank all friends in Nottingham during 4 years. They warmed me in a fresh country. Thanks to my mother, without her support, I cannot finish my PhD. Thanks everybody I met in Nottingham, who decorate my PhD life and let this four-year is a memorable chapter of my life.

Contents

ABSTRACT	I
ACKNOWLEDGEMENTS	III
CONTENTS	IV
ABBREVIATIONS	VI
INTRODUCTION	1
1. ROOT DEVELOPMENT	2
1.1 <i>Root apical meristem development</i>	2
1.2 <i>Primary root elongation</i>	7
1.3 <i>Lateral root development</i>	8
2. SHOOT DEVELOPMENT	9
3. OBSERVATION OF GENE EXPRESSION THROUGH LIVE IMAGING	10
4. AUXIN	11
4.1 <i>Auxin signalling</i>	12
4.2 <i>ARFs</i>	14
4.3 <i>The role of Auxin in development</i>	16
4.4 <i>The role of Auxin in root stimuli response</i>	20
4.5 <i>The subfunctionalisation of auxin signalling components</i>	21
AIM OF THESIS	25
STATEMENT ABOUT JOINT AUTHORSHIP	31
CHAPTER 1	32
1. MANUSCRIPT	32
2. METHODS	33
2.1 MATERIAL	33
2.2 ROOT PHENOTYPE ANALYSIS OF TF MUTANTS	33
2.3 INDUCIBLE OVEREXPRESSION OF TFs	34
CHAPTER 2	35

1. MANUSCRIPT	35
2. METHODS.....	62
2.1 <i>Material</i>	62
2.2 <i>Microscopy</i>	62
CHAPTER 3	63
1. METHODS.....	63
1.1 <i>Constructs of transcriptional reporter lines</i>	63
1.2 <i>Microscopy</i>	64
1.3 <i>Expression level analysis by qRT-PCR</i>	64
1.4 <i>Transcript splicing analysis by RT-PCR</i>	64
1.5 <i>Methodology for motif analysis</i>	64
2. MANUSCRIPT	65
DISCUSSION	81
1. CLASS A ARFs HAVE UNIQUE EXPRESSION PATTERN IN RAM AND SAM	81
2. THE REPRESSOR NETWORK IS A CRUCIAL PART FOR CLASS A ARFs REGULATION.....	83
3. POST TRANSCRIPTIONAL REGULATION ALSO PLAYS A ROLE IN CLASS A ARFs REGULATION	87
4. THE DUAL EXPRESSION AND ANATOMY LINES (DEAL) PROVIDE A ROBUST WAY OF IMAGING DYNAMIC CHANGES IN GENE RESPONSE.....	88
5. THE FIRST INTRON CAN REGULATE ARF7 TRANSCRIPTION VIA <i>CIS</i> -REGULATORY ELEMENTS.....	89
6. NAC AND MYBs TRANSCRIPTION FACTORS COULD BIND IN ARF7 FIRST INTRON.....	91
REFERENCES.....	95
APPENDIX.....	116

Abbreviations

4-Cl-IAA	4-chloroindole-3-acetic acid
bHLH	Basic helix-loop-helix
bp	Base pair
cDNA	Complementary DNA
CDS	Coding DNA Sequence
CEI	Cortex/endodermal initial
CK	Cytokinin
CZ	Central Zone
DAP-seq	DNA affinity purification sequencing
DNA	Deoxyribonucleic acid
DZ	Differentiation zone
EZ	Elongation zone
GFP	Green fluorescent protein
IAA	indole-3-acetic acid
kb	Kilo base
LR	Lateral Root
LRP	Lateral Root Primordium
miRNA	Micro RNA
mRNA	Messenger RNA
MS	Murashige and Skoog
MZ	Meristematic zone
OC	Organizing Centre
PAA	Phenylacetic acid
PI	Propidium Iodide
plantRegMap	Plant Transcription Regulation Map
PZ	Peripheral Zone
QC	Quiescent centre
qRT-PCR	Quantitative Reverse Transcription-PCR
RAM	Root apical meristem

RNA	Ribonucleic Acid
ROS	Reactive oxygen species
RT-PCR	Reverse Transcription-PCR
RZ	Rib Zone
SAM	Shoot apical meristem
SCN	Stem cell niche
T-DNA	Transfer-DNA
TF	Transcription factor
Trp	Tryptophan
TZ	Transition zone
UTR	Untranslated region
Y1H	Yeast one-Hybrid

Introduction

The population is near 9 billion today, and feeding this growing population is a great challenge. Currently, we must grow more food in the face of climate change. The climate is getting warm, and water stress is proving to be a significant limit to yields. Producing sufficient nutritious food is a great challenge for many parts of the globe. The increased industrialisation of agriculture has helped to increase yields. This relies on the high fertilizer use and is very dependent on the local soils. This is a key concern in areas with impoverished soils and limited access to fertilisers.

In vascular land plants, the root system anchors the plant in the soil providing support for the above ground parts of the plant. Roots provide the main interface through which water and nutrients are absorbed from the soil. As well as the roots providing nutrients to the plant, roots can also protect the top layer of soil from soil erosion, a factor further exacerbating the threat of our food in security.

Root system architecture exhibits great plasticity in response to the environment (Khan et al., 2016). Previous approaches to crop improvement have focused on the above ground parts of the plant, however it has recently been proposed that optimisation of the root system can improve the ability of plant to capture water and nutrients (Bishopp & Lynch, 2015). There are broadly two types of root networks. Monocots have complex fibrous root systems, that includes different types of branched root. For example, rice has 4 root types; the primary root, embryonic crown roots, the postembryonic crown roots and lateral roots. Compared with cereal crops, dicots such as *Arabidopsis* have a simple tap root system comprising one primary root and many branching lateral roots. The tap root system normally is deep into the soil, but the fibrous root system forms a dense network of roots closer to the soil surface. As our understanding of root development is most advanced in *Arabidopsis*, this will need further studies to translate this knowledge into crops.

1. Root development

To understand root development, it is convenient to use a simple system. The model plant *Arabidopsis* is popular because of relatively simple root system, short life cycle and detailed genetic resources (Redei, 1975).

In *Arabidopsis* a set of asymmetric cell divisions during embryogenesis establishes the root pole, which includes the future root apical meristem for the primary root. During embryogenesis, the fertilised egg cell undergoes a series of cell division, dividing from the zygote to the 1-cell, 2-cell, 4-cell, Octant, Dermatogen, Globular, Transition and Heart stage (Fig1) (ten Hove et al., 2015). In the first stages of embryo development, the zygote divides asymmetrically to form a small apical cell and a larger basal cell (Yoshida et al., 2014). The basal cell transversely divides to form the suspensor connecting the embryo to maternal tissue. The uppermost cell of the suspensor is later specified as the hypophysis and forms the founder cell of the root meristem, including a smaller lens-shaped cell which produce the quiescent centre (QC) and a larger basal cell that produce the distal stem cells of root meristem, such as columella stem cell and columella (Scheres et al., 1994). These cells coordinate subsequent tangential divisions, producing protoderm and the inner cells. After these two round cell division, embryos have two developmental niches that can go on to form aerial tissues, hypocotyl and root tissues (ten Hove et al., 2015).

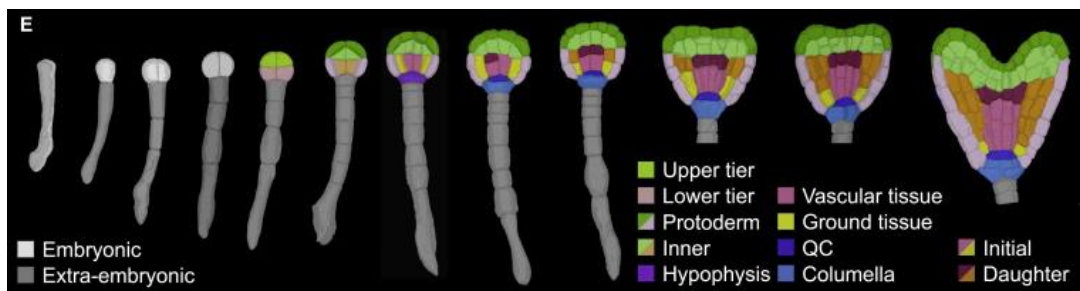


Figure 1. *Arabidopsis* embryo development (Yoshida et al., 2014).

1.1 Root apical meristem development

The developing root axis consists of the meristematic zone (MZ), elongation zone (EZ) and differentiation zone (DZ) (Fig2). The root meristem continuously produces new cells at the root tip. New cells will transit through these three

developmental stages and root reach maturity in the differentiation zone, leading to the developmental zone spread along the longitudinal axis (Sozzani & Iyer-Pascuzzi, 2014). In the EZ, cells lose their ability to divide and undergo an increase in length contributing to elongation of the root (Petricka et al., 2012). In the DZ, cell differentiate into individual cell types. This includes processes such as producing the casparian strip for endodermal cells and the formation of root hairs in a subset of epidermal cells (Petricka et al., 2012).

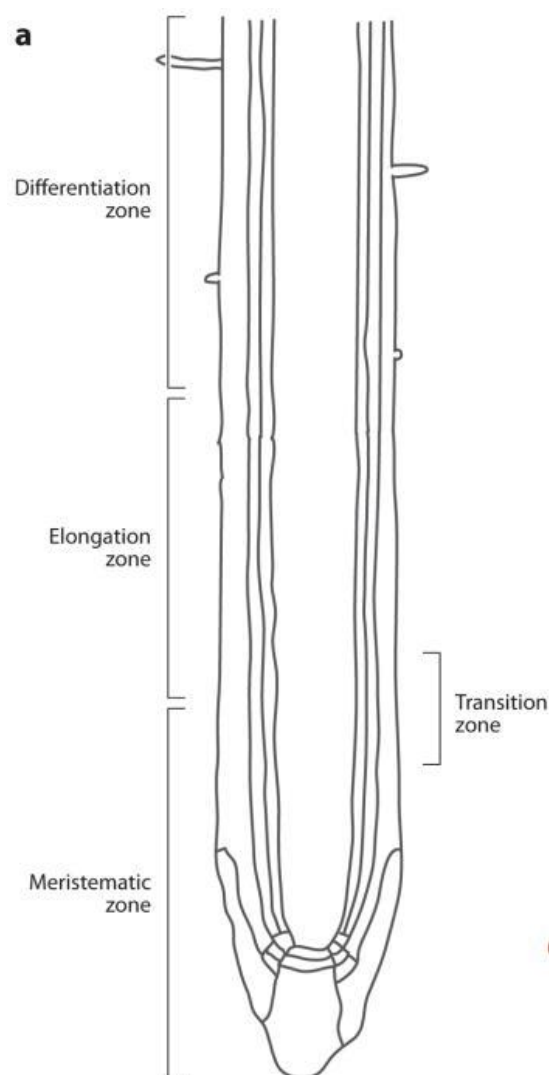


Figure 2 Developmental zoom of Arabidopsis root. This figure shows a longitudinal section of the primary root. Cells divide within the meristematic zone. Cells expand and elongate within the elongation zone. Cells differentiate within the differentiation zone, which can be readily observed through the formation of root hairs in this zone. (Petricka et al., 2012)

The QC is a group of less mitotically active cells and together with the surrounding stem cells forms the stem cell niche (SCN) (Perilli et al., 2012). The QC represses the differentiation of the surrounding stem cells, and promotes their cell division (van den Berg et al., 1997). Transit amplifying cells are daughters of stem cells in the proximal meristem. As the daughter cells become increasingly distant from the QC, they lose their ability to divide and eventually undergo differentiation (van den Berg et al., 1997). The stem cells on shootward side form the vascular, endodermal, cortex, epidermal and lateral root cap cells, whilst the stem cells on rootward side form the columella root cap (Petricka et al., 2012) (Fig3).

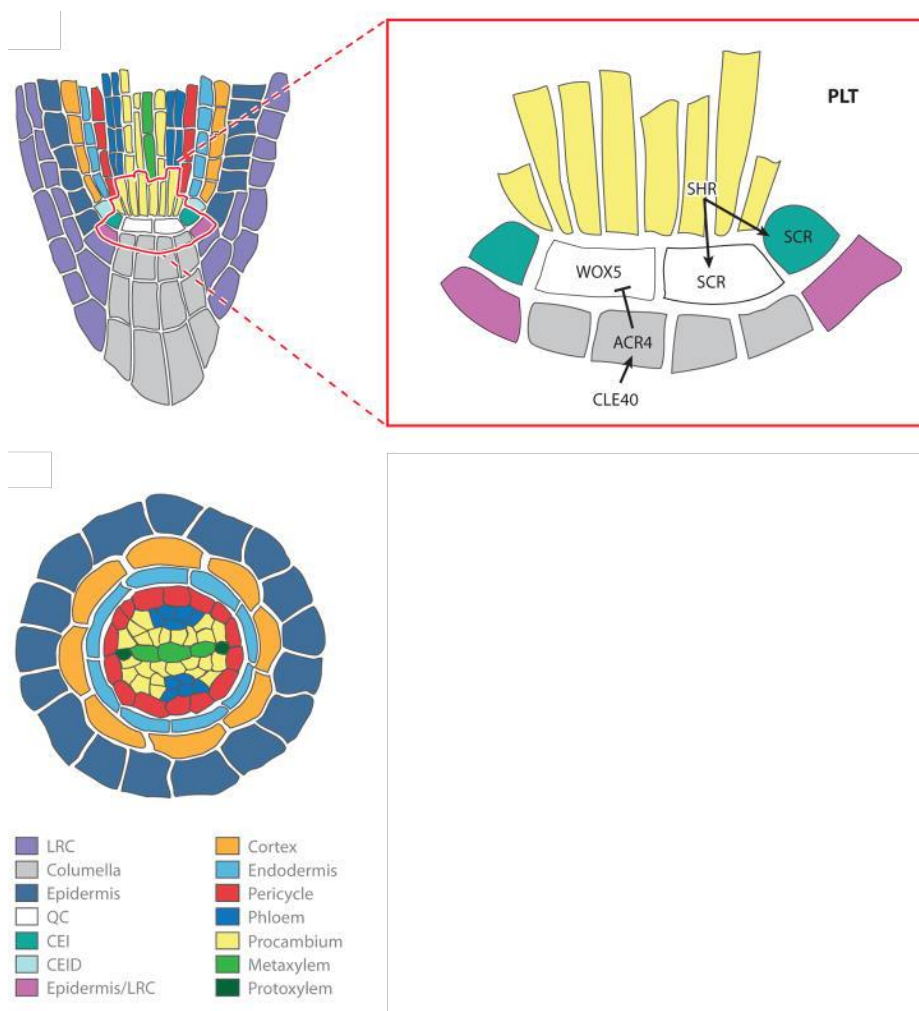


Figure 3 Organization of the root apical meristem The upper image shows the longitudinal section of root apical meristem. The magnified region shows the regulatory network that maintains the meristem identity. The lower image shows the cross section of root tip. (Petricka et al., 2012)

Many transcription factors and other proteins control SCN maintenance and cell differentiation (Fig. 4). SCARECROW (SCR) and SHORTROOT (SHR) are required cell-autonomously for distal specification of the QC and to maintain stem cell activity (Sabatini et al., 2003). SCR is expressed in QC precursor cells in embryogenesis at first, then extends to initial cells for ground tissue. It promotes radial cell division, as well as controlling cell identity via the asymmetric division of the cortex/endodermis initial cell (Wysocka-Diller et al., 2000). The mutant of SCR (*scr-1*) has an aberrant shape of its QC and fails to make the asymmetric cell division in the cortex/endodermal initial (CEI) that forms two distinct cell lineages (Sabatini et al., 2003). SHR is a signal originating from the provascular cells (Helariutta et al., 2000). It activates endodermal cell division and identifies the QC via activation of SCR (Nakajima et al., 2001; Sabatini et al., 2003). *shr* mutants only have a single cortex cell layer (Helariutta et al., 2000). PLETHORA (PLTs), AP2-domain transcription factors, are key factors for establishment of the SCN (Aida et al., 2004). PLTs are essential for QC specification and stem cell activity, providing positional information via distal accumulation which overlaps with SHR and SCR (Aida et al., 2004). PLTs are regulated by auxin, which will be discussed in more detail in section 4.3.1. PLTs are expressed in the basal embryo region that gives rise to hypocotyl, root and root stem cell during embryogenesis (Aida et al., 2004). PLTs are up-regulated at posttranscriptional level by root meristem growth factors (RGFs), which are tyrosine-sulfated peptides (Matsuzaki et al., 2010). The RGF triple mutant *rgf1rgf2rgf3* has a short primary root (Matsuzaki et al., 2010). RGF1 expression defines a gradient of distribution of PLT to maintain SCN and proliferate transit amplifying cell which are mediated by RGF receptors (RGFRs) also known as RGF INSENSITIVE (RGIs) (Galinha et al., 2007; Matsuzaki et al., 2010; Ou et al., 2016). In transit-amplifying cell, GROWTH-REGULATING FACTOR (GRF) class of proteins promote rapid cell divisions, at same time repress PLT to establish the gradient expression (Rodriguez et al., 2015). GRF-INTERACTING FACTORS (GIFs) interact with GRF, including ANGUSTIFOLIA3 (AN3/GIF1) (Ercoli et al., 2018). AN3 interacts with GRFs to modify root meristem size, and can directly bind to the promoter of PLT1 and SCR to control QC organization (Ercoli et al., 2018). WUSCHEL-RELATED HOMEODOMAIN5 (WOX5) is expressed in the QC and represses columella cell differentiation to maintain the distal stem cells in an

undifferentiated state (Sarkar et al., 2007). WOX5 expression depends on SHR/SCR induction, whereas PLT only plays a minor role on WOX5 expression (Sarkar et al., 2007). On the rootward side, CLE40 is a peptide closely related to CLAVATA3 (CLV3) belonging to CLE family expressing in differentiating columella cells (Stahl et al., 2009). The differentiation of columella stem cell daughters into columella cells was delayed in *cle40* mutants (Stahl et al., 2009). CLE40 upregulates the receptor-like kinase ARABIDOPSIS CRINKLY4 (ACR4) which is expressed in columella stem cells to promote stem cell differentiation by inhibiting WOX5 (Stahl et al., 2009).

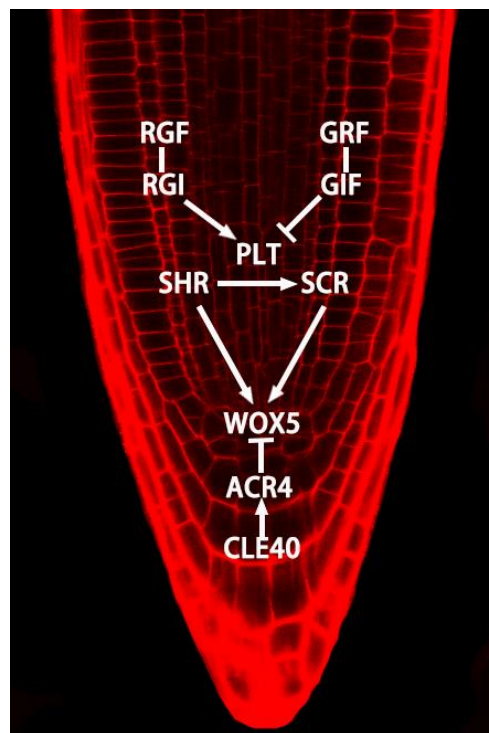


Figure 4 Schematic showing the gene regulatory network controlling root apical meristem development in Arabidopsis. SHR and SCR control distal specification of the QC. PLT expression overlaps with SHR and SCR and provides position information. RGF and GRF regulate the gradient of PLT expression. SHR/SCR induce WOX5 expression in the QC. CLE40 induces ACR4 to regulate cell differentiation by repressing WOX5.

For root meristem growth, some ubiquitin-specific proteases effect RAM development. UBP12/13 can interact with RGF1 receptor (RGFR1) and RGFR2 to counteract RGF1-induced RGFR1 ubiquitination to stabilize RGFR1 and maintain the sensitivity of RGF1 in root cells, thereby promoting RAM development (An et

al., 2018). Reactive oxygen species (ROS) are also involved in this process by controlling the transition between cell proliferation and differentiation in RAM. The transcription factor UPBEAT1 (UPB1) regulates the expression of a set of peroxidases which regulate hydrogen peroxide and superoxide, to modulate the balance of ROS in boundary of MZ and regulate cell differentiation (Tsukagoshi et al., 2010).

1.2 Primary root elongation

Primary root growth depends on cell division and cell elongation. The meristematic zone produces a pool of cells. These cells elongate and differentiate in elongation zone. the expansion of cells in the EZ contributes towards the elongation of the primary root.

The boundary between the meristematic zone and elongation zone is termed the transition zone (TZ), where cells start to elongate (Perilli et al., 2012). This cell elongation requires specific adaptations of the cell wall (Verbelen et al., 2006). Cellulose microfibrils in parallel alignment need to move apart or past one another, and this determines the orientation of expansion (Vissenberg et al., 2000). Cellulose and xyloglucan form cross network to bear tension in the cell wall (Vissenberg et al., 2000). XYLOGLUCAN ENDOTRANSGLUCOSYLASE/HYDROLASE (XTH) is an enzyme that modifies the cellulose-xyloglucan network by cleaving xyloglucans and rebinding the new end to a free nonreducing end to form xyloglucan chains or oligosaccharides (Verbelen et al., 2006). Therefore, XTH increase the distance of two adjacent cellulose microfibrils thereby loosening the cell wall and allowing growth (Verbelen et al., 2006). At the plasma membrane-cell wall interface, COBRA (COB), an extracellular Glycosyl-Phosphatidyl-Inositol (GPI) anchored protein (Roudier et al., 2005; Schindelman et al., 2001), affects the cellulose content of the cell wall and is highly expressed in the elongation zone (Schindelman et al., 2001). It is involved in cellulose microfibril orientation (Roudier et al., 2005), suggesting, COB could contribute to oriented cell expansion (Verbelen et al., 2006).

After the TZ, cells start elongating rapidly. The elongation is inhibited by ethylene.

Ethylene can quickly down regulate cell elongation and instead lead to increasing the width of root (Le et al., 2001). In soil compaction condition, ethylene diffusion is reduced by reduction of air-filled pores, then ethylene is accumulated in root expansion zone cells and inhibits elongation growth (Pandey et al., 2021). In addition, ethylene induces root hair formation. Root hair formation is used as a visual marker as it shows where in the root cells stop to elongate and start to differentiate (Le et al., 2001).

1.3 Lateral root development

The lateral root is an important component of root system. Different species have distinct root systems. Dicotyledonous species such as Arabidopsis have a single primary root from which lateral roots branch (Hochholdinger & Zimmermann, 2008). In cereal crops, the root system comprises embryonic (primary and seminal) and postembryonic (lateral, crown and nodal) roots (Rogers & Benfey, 2015). The degree of root branching affects water uptake, nutrient acquisition and anchorage of the plant (Peret et al., 2009). Lateral roots increase the surface to volume ratio thereby enhancing the uptake of water and nutrients (Rogers & Benfey, 2015). Also, the rate of root growth and the growth angle are key factors for water and nutrient uptake. Arabidopsis lateral roots originate in DZ, where pericycle founder cells are formed opposite to the xylem poles. Lateral root development is divided to 8 stage spanning the earliest divisions to the emergence of the full Lateral Root Primordium (LRP) from the primary root (Fig.5). In the first initiation stage, pericycle founder cells undergo anticlinal divisions to create a single-layer primordia composed of up to ten small cells of equal length (Casimiro et al., 2001; Malamy & Benfey, 1997). In stage II, cells within this layer divide to form inner and outer layers. During stage III, the outer layer undergoes periclinal divisions to form the dome shape LRP. LRP divides to four layers in stage IV. In stage V, LRP begins to penetrate through the cortex layer of the primary root. In stage VI, LRP start to differentiate several cell type as mature root tips, including epidermal, cortex and endodermal cell layers. During stage VII, the LRP enlarges due to anticlinal cell division, and the stele that forms within the primordia can be distinguished. In the last stage VIII, LRP emerges from the epidermis of the parental root (Malamy &

Benfey, 1997). After emergence, the lateral root meristem is activated and the lateral root elongates (Goh et al., 2016).

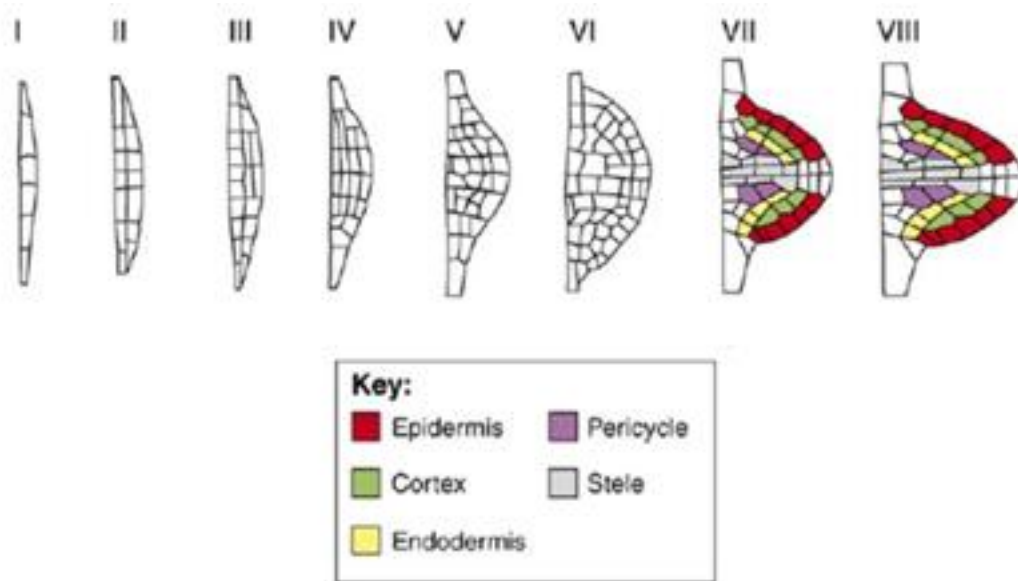


Figure 5 Lateral root developmental stage (Peret et al., 2009)

2. Shoot development

The shoot apical meristem (SAM) contains a group of stem cells and surrounding cells that produce lateral organs for the above-ground parts such as leaves.

The SAM is organized into several zones and cell layers (Fig.6). In the centre of the meristem, The Central Zone (CZ) contains a group of stem cells to maintain the meristem (Bowman & Eshed, 2000). The Peripheral Zone (PZ) surrounding CZ, initiates primordia and is the progenitor of new lateral organs (Murray et al., 2012). The Organizing Centre (OC) is located under and maintains the CZ (Murray et al., 2012). The basal zone is termed Rib Zone (RZ) which forms stem tissue. In dicotyledonous species, the SAM comprises of 3 cell layers (Bowman & Eshed, 2000). From outside to inside these are the epidermal layer (L1) and the subepidermal layer (L2); cells within these layers divide anticlinally and form the tunica layer (Bowman & Eshed, 2000). Inner to these is corpus (L3) which undergoes nonuniform-orientated cell divisions (Bowman & Eshed, 2000).

CLV3 and WUSCHEL (WUS) play important roles to maintain the SAM, and control its function (Truskina & Vernoux, 2018). CLVs promote the transition of meristem

cells to differentiated cells, leading to organ initiation (Schoof et al., 2000). A lack of CLV3 leads to a large SAM (Fletcher et al., 1999). CLV3 is expressed in the outermost layer of the CZ and is perceived by receptor kinase CLV1 and CLV2 in deeper cell layer to repress WUS expression (Brand et al., 2000). WUS is expressed from the 16-cell stage during embryogenesis (Mayer et al., 1998) and represses the differentiation of stem cells in the organizing centre (Sarkar et al., 2007; Schoof et al., 2000). At the same time, WUS can induce CLV3 which forms a feedback loop to control the size of stem cell niche (Schoof et al., 2000). WUS not only works with CLV3 to maintain the stem cell niche, but also represses other genes which are expressed in the boundary domain, such as KANADI1 (KAN1) (Fig.6) (Yadav et al., 2013). Ectopic expression of KAN produces seedlings that lack SAM and vascular tissues in the hypocotyl (Kerstetter et al., 2001), suggesting that KAN promotes peripheral tissue differentiation (Kerstetter et al., 2001; Yadav et al., 2013).

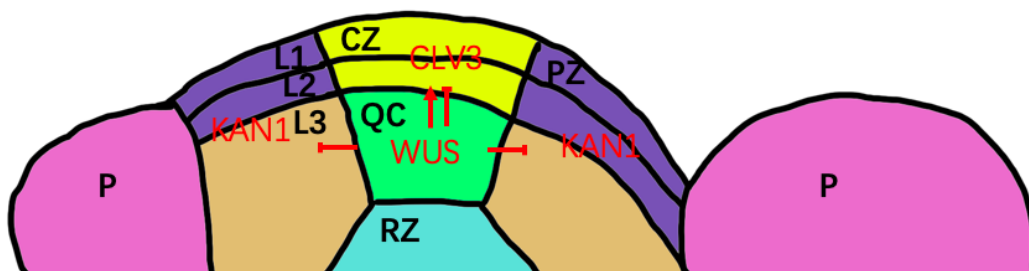


Figure 6 The organization of Arabidopsis SAM This figure shows the structure of SAM in black. The gene network regulating SAM maintenance is shown in red.

3. Observation of gene expression through live imaging.

Observing and analysing expression pattern distribution of specific proteins is crucial to determine the function of a gene. Using a combination of fluorescent microscopes and fluorescent proteins it is possible to observe transcriptional and translational markers in real time. Gene regulation relies on both the spatial and temporal dynamics of gene expression and protein accumulation in specific cell types or tissues. This is crucial, as plants must quickly respond to changes in their environment.

There are many different fluorescent proteins such as the green fluorescent protein (GFP) (Chalfie, 1995), that can be employed to visualise the cell type a specific gene is expressed in. To define the cell type, it is also necessary to present the outline of the cell. One traditional way is using transmitted light, but the cellular resolution is limited by overlying cell layers. Also, this cannot reveal the 3D structure and is not appropriate for continuous observation. Several fluorescent dyes can be used to stain the cell membrane or cell wall, such as propidium iodide or calcofluor white (Hughes & McCully, 1975; Khunkitti et al., 1997). However, staining cells for a long period with these dyes can be toxic for cell and lead to death. In addition, the intensity of the stain diminishes over time. These problems are also confounded by differential staining intensity between the outer layer and inner layers. Alternatively, fluorescent tags can be fused with membrane proteins to form genetically encoded membrane markers that define cell outlines. An example of this is the WAVE lines (Geldner et al., 2009). However, combining these with markers of interest takes time as plants carrying the membrane marker and the marker of interest need to be crossed. This leaves a gap for developing a new membrane marker system that can be introduced to plants in a single event for simultaneous visualization of fluorescent markers and cellular anatomy in both *Arabidopsis* primary and lateral roots.

4. Auxin

Auxin plays an essential role in regulating many growth and developmental processes in plants, such as the formation of SAM and root apical meristem RAM, vascular patterning, establishment of phyllotaxy, shoot phototropism, root gravitropism and female gametophyte development (Avsian-Kretchmer et al., 2002; Berleth et al., 2000; Beyer, 1972; Krogan et al., 2016; Liu et al., 2018). The natural active auxin isoforms include indole-3-acetic acid (IAA), 4-chloroindole-3-acetic acid (4-Cl-IAA) and phenylacetic acid (PAA) from which IAA is most abundant and most studied (Korasick et al., 2013). Auxin (IAA) levels can be affected via biosynthesis, degradation, conjugation and transport. IAA biosynthesis has two major pathways, including synthesis from tryptophan (Trp) by the Trp-dependent pathway and from an indolic Trp precursor by the Trp-independent pathway (Woodward & Bartel, 2005). Conjugation of IAA converts it

to an inactive form and this is an important way to store auxin that can later be released rapidly by hydrolysis (Ludwig-Muller, 2011). The major types of conjugation are ester-linked simple and complex carbohydrate, amide-linked amino acid conjugates, and amide-linked peptide and protein (Ludwig-Muller, 2011). Some types of conjugates lead to degradation (permanently inactive) such as covalent conjugation of aspartate and glutamate (Ludwig-Muller, 2011). Auxin can be synthesised locally and undergo polar transport leading to formation of auxin gradients with minima and maxima in tissues. This transport is controlled by auxin influx and efflux carriers which are AUX (AUX/LAX) and PIN (PIN-FORMED) (Galweiler et al., 1998; R. Swarup & Peret, 2012). As auxin influx transporters, the *AUX/LAX* gene family encodes multimembrane-spanning transmembrane proteins, and IAA can bind to AUX1 depending on the pH (Peret et al., 2012). PINs are located on the plasma membrane or ER and export auxin (R. Swarup & Peret, 2012). The polarity of PIN localization directs auxin transport (Wisniewska et al., 2006). The ATP-binding cassette (ABC) transporter, such as the members of ABCB subfamily, are considered to be Auxin transporters (Geisler & Murphy, 2006). Indole-3-butyric acid (IBA) can be converted to IAA (Woodward & Bartel, 2005). Some of ABCGs are transporters of IBA including ABCG36 and ABCG37 (Ruzicka et al., 2010; Strader & Bartel, 2009). Also ABCD1 is considered to be essential for IBA transport (Zolman et al., 2001).

4.1 Auxin signalling

Plant cells must coordinate their response to auxin changes in order to execute the desired developmental programme. Several gene families comprise the auxin signalling network and mediate transcription of downstream response genes based on cellular auxin levels (Fig. 7). The binding of auxin promotes the interaction between the SCF^{TIR1} ubiquitin protein ligase complex and the Aux/IAA co-repressors (X. Tan et al., 2007). The SCF-type complex comprises an F-box protein such as TIR1 (TRANSPORT INHIBITOR RESPONSE1) alongside the Skp1 and Cullin proteins (Smalle & Vierstra, 2004). This complex transfers an activated ubiquitin from a ubiquitin activating enzyme and conjugates the Aux/IAAs (Dharmasiri et al., 2005; Kepinski & Leyser, 2005). The Aux/IAAs themselves act to stabilize auxin binding, leading to them being considered as co-receptors for

auxin (Tiwari et al., 2001). Following the ubiquitination of the Aux/IAAs, these proteins are degraded by the 26S proteasome (Dharmasiri & Estelle, 2004; Gagne et al., 2002). A group of transcription factors (ARFs) bind to Auxin Response Elements (AuxRE) within promoters of auxin responsive genes (Ulmasov et al., 1999). In the absence of auxin, the Aux/IAA proteins bind these ARFs and inhibit their transcriptional activity (Ulmasov et al., 1997). Aux/IAA proteins can also recruit corepressors TPL (TOPELESS) to maintain repression (Szemenyei et al., 2008). In high auxin concentrations, the Aux/IAA proteins are degraded, releasing ARFs and allowing them to regulate thousands of downstream responses (Worley et al., 2000; Zenser et al., 2001). In *Arabidopsis thaliana* Aux/IAA, ARF, and TIR genes are represented by multigene families. The TIR1/AFB (TIR1/AUXIN SIGNALING F-BOX) gene family consists of 6 members in *Arabidopsis thaliana* (Dharmasiri et al., 2005), the AUX/IAA gene family contains 29 members (Remington et al., 2004) and the ARF gene family includes 23 transcription factors (Okushima et al., 2005). It is hypothesized that this range makes it possible that plants respond to auxin by executing so many different developmental programmes.

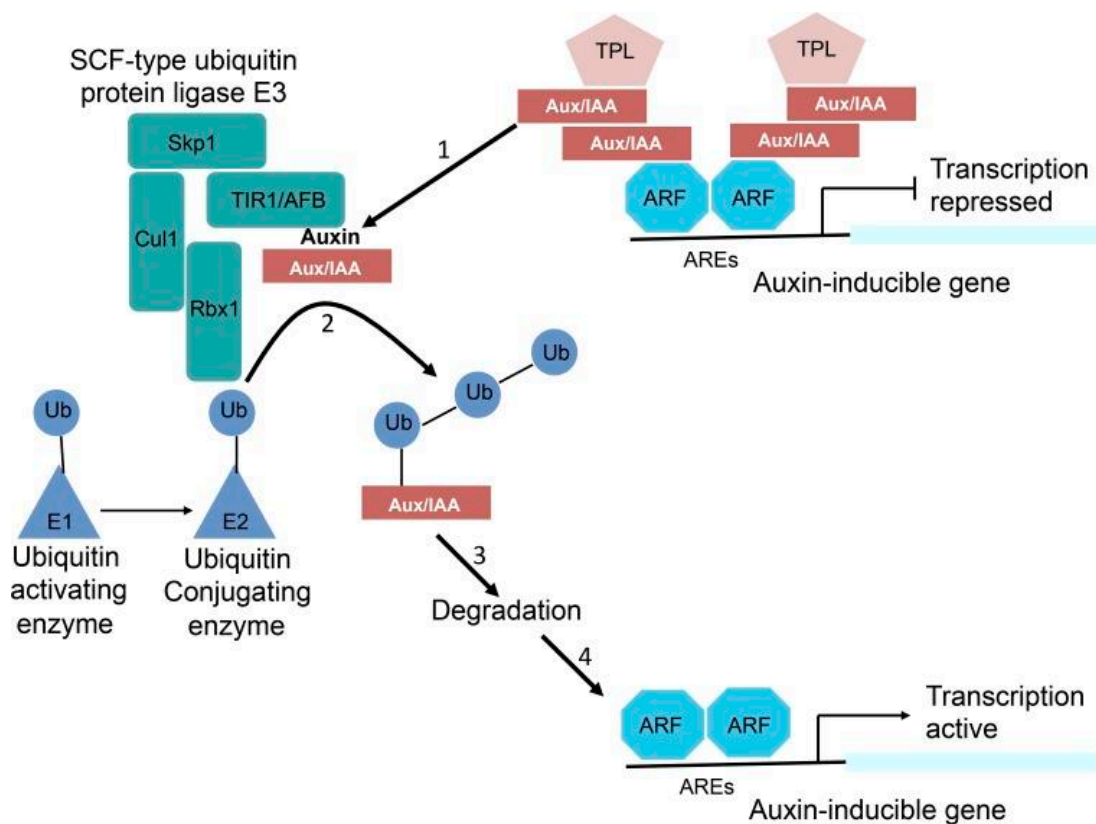


Figure 7 The main pathway of auxin signalling. The steps in the auxin response pathway are indicated by the numbered arrows. 1, Auxin acts as a molecular glue

bringing together Aux/IAAs and F-box proteins of the TIR1/AFB family. 2, These F-box proteins are part of an SCF-type E3 ubiquitin protein ligase complex that transfers activated ubiquitin (Ub) from an E1/E2 enzyme system. 3, Polyubiquitination of the Aux/IAAs results in their degradation. 4, This releases repression at ARE-containing promoters (Leyser, 2018).

4.2 ARFs

As ARFs regulate gene expression in response to auxin levels, they thus form an important part of the auxin signalling machinery. The Arabidopsis genome encodes 23 ARF proteins which control distinct developmental processes (Okushima et al., 2005). ARF proteins contain an N-terminal DNA-binding domain (DBD), Middle Region (MR) and a C-terminal Phox and Bem 1 (PB1) domain (Mutte et al., 2018). PB1 mediates ARF and Aux/IAA proteins homo- and hetero-oligomerization (Mutte et al., 2018). They are divided into 3 classes based on phylogenetic analysis. Class A has 5 members, including ARF5, ARF6, ARF7, ARF8 and ARF19 (Finet et al., 2013). They have been shown to be transcriptional activators and their middle region is rich in glutamine (Ulmasov et al., 1999). In Arabidopsis Class C contains just three members, ARF10, ARF16 and ARF17 (Finet et al., 2013). The ARFs belonging to Class B and C are considered to be repressors (Okushima et al., 2005).

ARF5 is arguably the most critically required, and is the only single mutant with a seedling lethal phenotype (Berleth & Jurgens, 1993). It is essential for patterning of the embryonic root (Berleth & Jurgens, 1993). Besides its role during embryogenesis, ARF5 also targets the transcription factor gene *TARGET OF MONOPTEROS (TMO5)* to regulate vascular tissue development (Schlereth et al., 2010). In addition the BODENLOS/IAA12-ARF5 complex is required in lateral root initiation (De Smet, 2010). In the SAM, ARF5 regulates stem cell homeostasis by regulating *CLV3* expression via repression of *DORNROSCHEN* and *ENHANCER OF SHOOT REGENERATION1* (Luo et al., 2018). Roles have also been identified in flower primordia where ARF5 promotes flowering through *LEAFY* (Yamaguchi et al., 2013).

ARF6 and ARF8 act redundantly in flower maturation (Nagpal et al., 2005). ARF6 and ARF8 also act together to modulate jasmonic acid homeostasis, as well as controlling adventitious root initiation (Gutierrez et al., 2012; Lakehal et al., 2019). ARF8 has also been shown to regulate nitrogen response in lateral root emergence (Gifford et al., 2008), and a recently identified network of transcription factors acting upstream of ARFs predicts that ARF8 is regulated by many genes associated with biotic and abiotic stress response. NAC92 represses *ARF8* to inhibit primary root development (Xi et al., 2019). ARF6 together with BZR1 and PFI4 form a BAP regulatory module (Boure et al., 2019) to regulated cell elongation in the hypocotyl (Oh et al., 2014).

In roots, ARF7 and ARF19 are well known for their partially overlapping roles in regulating lateral root organogenesis via activation of the transcription factors LBD16 and 29 (Harper et al., 2000; Okushima et al., 2007; Okushima et al., 2005). ARF7 and 19 have also been shown to control other processes within the root, such as cell wall composition and pectin dynamics during root hair tip growth through ERULUS (Schoenaers et al., 2018), adventitious root formation via regulating LBD16 and LBD18 (Lee et al., 2019) as well as in tropic responses such as gravitropism (Okushima et al., 2005; Weijers et al., 2005). There has been a role proposed for ARF7/19 in bending of the apical hook but that recent studies show that they may only initiate bending when there are no other external cues (Baral et al., 2021). Auxin is important for root hair elongation in low external phosphate mediated by ARF19 (Bhosale et al., 2018). In the aerial parts of the plant, ARF7 is expressed in veins of maturing leaves, especially in older procambial strands, where it works together with other activating ARFs to control leaf formation (Schuetz et al., 2019). ARF7 works redundantly with ARF19 to control expansion of leaf cells. *arf19* mutants have little effect on leaf elongation, but can enhance the leaf cell expansion phenotype of the *arf7* mutants (Wilmoth et al., 2005). Consequently, the leaf blade area and rosettes of *arf7arf19* are reduced. ARF7 also works alongside ARF5 to control leaf organogenesis, with the double *arf5arf7* mutant either not forming leaves or halting leaf initiation after the formation of one or two leaves (Schuetz et al., 2019). ARF7 and ARF19 are both induced by senescence (Ellis et al., 2005). Whilst miss-expression of these ARFs alone cannot

affect the senescence of leaves, mutations of these genes can enhance the *arf2* effect, which in turn regulates leaf senescence and floral organ abscission (Ellis et al., 2005).

4.3 The role of Auxin in development

4.3.1 Auxin and crosstalk with cytokinin in RAM development

During embryo development at the early globular stage, the hypophysis, the uppermost cell of the suspensors, divides asymmetrically to a smaller lens-shaped cell (precursor of QC) and a large basal cell (precursor of the distal stem cell) (Yoshida et al., 2014). Auxin controls the asymmetric distribution of auxin leads to this asymmetric hypophysis division and subsequent RAM formation (Moller & Weijers, 2009). High auxin levels cause the degradation of the AUX/IAA gene BODENLOS (BDL), thereby releasing ARF5 (Hamann et al., 2002). ARF5 can then activate downstream genes such as *TARGET OF MP7 (TMO7)*, a helix-loop-helix (bHLH) transcription factor. BDL and ARF5 are both expressed in the hypophysis-adjacent embryo cells where they activate *TMO7* expression. *TMO7* is then transported to the hypophysis precursor, where it regulates cell division and hypophysis specification (Schlereth et al., 2010). A cell-autonomous auxin signalling module consisting of ARF9 and other redundant ARFs with their inhibitor IAA10 can mediate hypophysis specification and prevent transformation to embryo identity (Rademacher et al., 2012).

The antagonistic interaction of auxin and cytokinin (CK) plays an important role in RAM development (Fig. 8). The balance of cell differentiation and division is required for RAM maintenance. Opposite to auxin, CK promotes cell differentiation and restricts RAM size (Dello Iorio et al., 2007). CK distribution can be shown by the synthetic reporter TCS (B. Muller & Sheen, 2008). The LONELY GUY (LOG) family encodes CK activating enzymes releasing CK nucleobase and ribose 5'-monophosphate (Kuroha et al., 2009). The level of active CK can be decreased by conjugation (Bajguz & Piotrowska, 2009). CK signals through a phosphorylation relay system. CK is received by transmembrane receptors (CRE1, AHK2 and AHK3), triggering autophosphorylation and subsequent transfer of the

phosphate from histidine to aspartate (Higuchi et al., 2004). Then the phosphate is transferred to AHP (ARABIDOPSIS HISTIDINE PHOSPHOTRANSFER PROTEIN) (Punwani et al., 2010). AHPs are intermediates to transfer phosphate to downstream response regulators ARR (ARABIDOPSIS RESPONSE REGULATORS) (Suzuki et al., 1998). Finally, ARRs lead cellular changes in CK response. During embryogenesis, auxin activates ARR7 and ARR15 in the basal cell which are repressors of cytokinin signalling (B. Muller & Sheen, 2008). After embryogenesis, the antagonistic interaction of auxin and CK plays a crucial role in the maintenance of the root meristem and for regulating root growth. SHY2 (SHORT HYPOCOTYL 2), an auxin signalling repressor (Aux/IAA) which is induced by CK, a key factor to regulate this process, (Dello loio et al., 2008). *SHY2* expression can be induced by the CK response factor (Dello loio et al., 2008). Then, SHY2 binds ARF5 to repress PIN to change auxin distribution and thereby induce cell differentiation (Dello loio et al., 2008; Weijers et al., 2005). On the other hand, auxin can degrade SHY2 protein to release active ARF5 and sustain PIN activities and active cell division (Dello loio et al., 2008).

BREVIS RADIX (BRX) plays a role in auxin and CK cross talk in the proximal meristem and protophloem (Scacchi et al., 2010). The loss-of-function mutant of *brx* has a decrease RAM size and asynchronous developmental distal protophloem (Scacchi et al., 2010). *BRX* is a target of ARF5 and promotes vascular development and can increase PIN3 expression to promote meristem growth in young roots (Scacchi et al., 2010). Whereas at later developmental stage SHY2 is induced by CK, leading to a reduction in BRX expression coupled with a de-repression of PIN3 and subsequent inhibition of meristem growth (Scacchi et al., 2010). Together BRX and SHY2 balance the regulation of ARF5 to coordinate both RAM growth and protophloem development (Scacchi et al., 2010). Other hormones are also involved in the SHY2 pathway to regulate RAM activity. Gibberellin represses the DELLA protein REPRESSOR OF GA 1-3 (RGA) which in turn then repress ARR1 during the early stages of meristem development (Moubayidin et al., 2010). Ethylene plays a weak role to inhibit cell proliferation at RAM via SHY2 to effect CK signalling, but it is not essential for CK signalling (Street et al., 2015).

TMO5 is another factor in auxin and CK interaction. ARF5 not only plays a critical role in embryo development, but also in maintaining vascular tissue (De Rybel et al., 2013). Together with LHW (LONESOME HIGHWAY), this protein forms bHLH transcription heterodimers to target downstream genes (De Rybel et al., 2013; Ohashi-Ito et al., 2014). TMO5/LHW promotes the expression of *LONELY GUY3* (*LOG3*) and *LOG4* as direct targets in xylem precursor cells. These CK biosynthesis genes then increase CK levels in surrounding cells to induce procambial cell proliferation (De Rybel et al., 2014; Ohashi-Ito et al., 2014). On the contrary, TMO5/LHW also promotes AHP6 expression (Ohashi-Ito et al., 2014). AHP6 is a pseudophosphotransfer protein repressing CK signalling and CK can negatively regulate the spatial domain of AHP6 expression, so specifies the meristematic versus differentiated nature of procambial cell files (Mahonen et al., 2006).

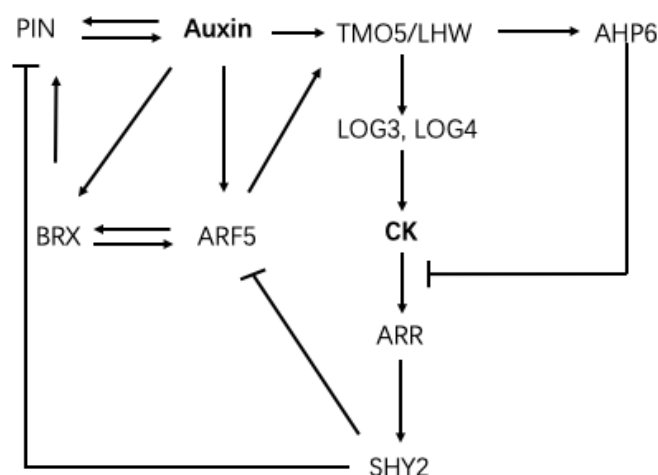


Figure 8 Auxin and CK crosstalk in root development. This network shows the interaction of key factors TMO5, SHY2 and BRX in Auxin and CK crosstalk.

4.3.2 Auxin in lateral root development

Auxin is involved in many stages of lateral root development. During the priming stage, an asymmetric localization of auxin is needed to define the site for LRs to form. At first, auxin accumulation leads pericycle cells to become pericycle founder cells, which regulates the position of lateral organs (De Smet et al., 2007). The pericycle cells initiate the formation of the LRP in basal meristem, and the

auxin influx carrier AUX1 accumulates auxin in this area (De Smet et al., 2007). Auxin accumulation in the primed xylem pole pericycle cell activates the auxin signalling cascade (Peret et al., 2009). The transcription factor GATA23 controls specifying pericycle cells to LR founder cells which is regulated by Aux/IAA28 (De Rybel et al., 2010), also GATA may be an indirect target of ARF7 (Lavenus et al., 2015).

Auxin affects LRP formation and development by forming an auxin gradient to regulate asymmetric cell division. The GNOM protein seems to be required for these initial asymmetric cell division (Geldner et al., 2004). GNOM is a membrane-associated guanine-nucleotide exchange factor on ADP-ribosylation factor G protein (ARF-GEF) (Steinmann et al., 1999). GNOM-dependent vesicle trafficking may establish cell polarity and regulates polar localisation of PINs which build up an auxin gradient (Steinmann et al., 1999). Auxin accumulates in the central cell of LRP at first, then in the tip of LRP (Peret et al., 2009). This high auxin concentration promotes Aux/IAA degradation and activates ARF7 and ARF19, then activates downstream genes such as (LBDs) to regulate the lateral root patterning. ARF7 and ARF19 directly regulate LBD16 and LBD29 activating LR formation (Okushima et al., 2007). LBD18 can interact with LBD16 to regulate LR formation (Lee et al., 2009).

During the LR emergence, the overlaying cell actively accommodates organ outgrowth. This process is also regulated by auxin, and might rely on the shoot-derived auxin by phloem transport (Bhalerao et al., 2002; Overvoorde et al., 2010). Auxin induces the auxin influx carrier *LAX3* by degrading IAA14 to release ARF7 then activating LBD29, and *LAX3* form a positive feedback loop by increasing the auxin uptake in adjacent cortex and epidermis cells (Porco et al., 2016). Then, *LAX3* induces cell wall remodelling enzymes which promote cell separation to allow LRP emergence (K. Swarup et al., 2008).

4.3.3 Auxin in SAM development

Auxin is the major hormone to regulate organ initiation and positioning at SAM. This relies on polar auxin transport leading a local auxin accumulation (Truskina

& Vernoux, 2018). The auxin influx and efflux carrier proteins AUX1 and PIN1 are expressed in L1, cooperatively transporting auxin upwards into the meristem through the epidermis and the outermost meristem cell layer (Reinhardt et al., 2003). AUX1 restricts auxin located in existing leaf primordia to the outer cell layer and PIN1 promotes transportation of auxin to the tip of meristem and leaf primordia (Reinhardt et al., 2003). Via the Aux/IAA-ARF signalling pathway the accumulation of auxin in the meristem is essential to create robust patterns at shoot apex (Vernoux et al., 2011). Especially, ARF5 is necessary to mediate periodic organ formation. PIN1 contributes by regulating local auxin accumulation (Bhatia et al., 2016).

In addition, Auxin can mediate the response pathways for other hormones to control organ initiation. For example, the CK signalling inhibitor AHP6 is produced in an auxin-dependent manner in primordia and moves to adjacent cell to establish the patterns of CK signalling activity, thereby imposing a temporal sequence on organ initiation (Besnard et al., 2014).

4.4 The role of Auxin in root stimuli response

During root development, as well as following internal developmental cues, roots must also respond to various environmental stimuli. Many of these adaptive responses, such as gravitropism and hydrotropism, are controlled by auxin.

Roots respond to gravity to direct their orientation of growth vertically in soil to maximise uptake of water and nutrients. Lateral roots emerge from the primary root in a stereotypical manner and quickly change angle, named gravity set point angle (GSA) (Su et al., 2017). The columella cells of the root cap sense the gravity signal. The starch-filled plastids (amyloplasts) accumulate in the first and second layer of columella cells and sediment to the bottom of the cell due to the force of gravity (Leitz et al., 2009). The moving of amyloplasts is thought to redistribute the auxin efflux carriers PINs, mainly PIN3 and PIN7 to the bottom side of gravity-sensing root cells (Kleine-Vehn et al., 2010). This redirects auxin flux toward the lower side of the root. AUX1 and PIN2 transport auxin through the epidermal cells into the elongation zone, where auxin promotes the differential expansion of

epidermal cells triggering bending of the root tip (Bennett et al., 1996; A. Muller et al., 1998; R. Swarup et al., 2005). For lateral roots, strong repression of PIN4/PIN7 and transient PIN3 expression limit auxin redistribution in young LR columella cells to temporally limit the asymmetric auxin fluxes in the LR tips (Rosquete et al., 2013). In addition, ARF7 and ARF19 are both involved gravitropism in a redundant manner. The mutant of ARF7 *nhp4-1* displays a disturbed gravitropism response, whereas *arf19-1* show normal phenotype (Harper et al., 2000; Okushima et al., 2005). In *nhp4-1arf19-1*, the growth orientation has stronger effect than *nhp4-1* (Okushima et al., 2005). ARF7 may directly bind to the SAUR19 promoter to modulate the response to tropism in hypocotyls (Wang et al., 2020). SAURs (Small Auxin Up RNAs) are early auxin response genes and their asymmetric expression contributing bending growth (Wang et al., 2020).

Water uptake from soil is critical for plant survival. During the hydropatterning response, plants sense microscale heterogeneity in water availability across the circumference of their roots and initiate lateral roots preferentially towards the side where there is more moisture (Bao et al., 2014; Scharwies & Dinneny, 2019). The position of lateral root branches is regulated by auxin. Water locally promotes auxin accumulation by induction of *TAA* which mediates the first step in auxin biosynthesis, Tryptophan to IAA (Bao et al., 2014). Differential transport of auxin by PINs is also necessary to maintain local differences in auxin concentration between the air and contact sides (Bao et al., 2014). ARF7 plays an important role in LR initiation, and also regulates hydropatterning (Orosa-Puente et al., 2018). ARF7 SUMOylation regulates the ability of ARF7 to recruit IAA3 on the air side of the root, thereby inhibiting ARF7 to initiate lateral root development via LBD16 activation (Orosa-Puente et al., 2018).

4.5 The subfunctionalisation of auxin signalling components

Auxin regulates many specific developmental processes, including tropic responses, SAM and RAM development. The key auxin signalling components are TIR1/AFB, Aux/IAA, and ARF. Each component is consisted of gene family, which give the possibility of various auxin response and members of these have sub-

functionalised to have unique expression patterns and functions. Although this project focuses on Class A ARFs, it is important to note that other components have expanded and specialised functions. For example, TIR1/AFB F-box proteins include 6 members which have spatial expression pattern (Prigge et al., 2020). TIR1/AFB contribute unequally to auxin response in root (Parry et al., 2009; Prigge et al., 2020). Especially, AFB1 has a role in rapid auxin inhibition of root growth and the initial phase of root gravitropism (Prigge et al., 2020).

Aux/IAA specificity occurs in embryogenesis, hypocotyl and shoot is transcriptionally regulated. In embryo, the promoter of BDL or IAA13 were fused with IAA13 or BDL coding region in each homologous stabilizing proline to serine domain II mutations. The phenotype and Western blot analysis prove that Aux/IAA specificity is regulated in part by transcriptional regulation (Weijers et al., 2005). The pairs of co-expressed Aux/IAA and ARF regulate developmental specificity of auxin response, such as SHY2 and BDL can interact with ARF5 in embryo, whereas only SHY2 interact with ARF7 and ARF19 in root development (Weijers et al., 2005).

Class A ARF comprises only five members compared with 15 members for Class B ARFs (Finet et al., 2013; Okushima et al., 2005) (Fig. 9A). Secondly, Class A ARFs have been associated with specific auxin responses; for example, ARF7 and ARF19 control LR development and ARF6 and ARF8 control flower maturation. Also, their mutants have clear phenotypes. These 5 ARFs gene structures are shown in Fig.9B. In particular, I draw the reader's attention to the large first introns present in ARF7 and ARF19, that are discussed later in this thesis. These 5 ARFs have unique expression patterns in roots and shoots. Using 2kb promoter fragments upstream of each ARF to drive reporter genes shows cell-type-specific and distinct expression patterns in primary root (Rademacher et al., 2011). However, it is unclear whether these faithfully recapitulate the pattern of mRNA in the plant. RNA *in situ* hybridization show different ARF expression patterns in the SAM (Vernoux et al., 2011). For example, ARF6 has a more restricted expression in boundary domain compared with 2kb promoter reporter lines. Additionally, when MP is driven by a promoter including only 2kb upstream sequence it can only partly complement the *mp* mutant (Schlereth et al., 2010). This suggests that these

2kb promoters may not be sufficient to fully recapitulate the endogenous patterns of gene expression. Normally, gene promoters contain a core promoter region which recruits the RNA pol II complex, and proximal and distal transcription factor binding regions (Davuluri et al., 2003). A typical promoter length ranges from 500bp to over 2000bp (Davuluri et al., 2003). But there are several examples both longer sequences and in which introns play an important role in regulating transcription (Bradnam & Korf, 2008; Friede et al., 2017).

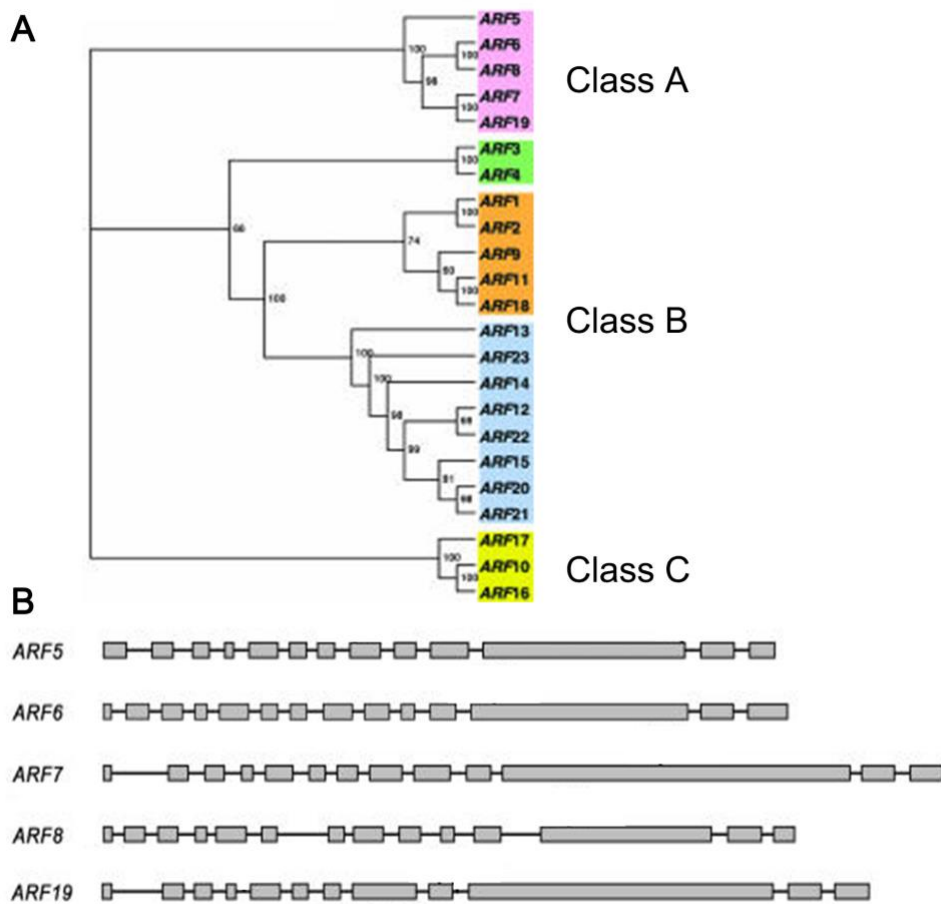


Figure 9 ARFs gene family. (A) Phylogenetic analysis indicated ARFs are split into 3 subfamilies. Class A is shaded pink. Class C is shaded yellow. Others are belonging to Class B. (B) Schematic showing the gene structure of Class A ARFs. Boxes showed exons (Finet et al., 2013; Okushima et al., 2005).

Individual or pairs of ARFs regulate different developmental processes. But how can ARFs mediate such diverse function? Firstly, these ARFs regulate different downstream target genes. For example, ARF5 targets TMO5 regulating RAM

establishment (Schlereth et al., 2010). ARF7 can directly interact with LBD29 and LBD16, or targets ARF19 then regulates LBD16. Secondly the transcription of all these different ARFs is tightly and specifically regulated, ensuring only the desired target genes will be activated in response to increasing cellular auxin levels, but this is less well understood.

This project focus on the transcriptional regulation of the 5 activating class A ARFs, ARFs 5,6,7,8 and 19.

Aim of thesis

This thesis focuses on the special regulation of Class A ARFs. It addresses a central question of how ARFs can mediate such diverse function. Whilst there is wealth of knowledge about the processes downstream of ARFs (produced by either microarray or RNASeq experiments, there is a knowledge-gap on the upstream regulation of ARFs. This thesis is divided into three chapters, with each chapter having a distinct yet overlapping aim. Below I outline the central aims and objectives for each chapter. As these chapters all contain collaborative work done by a group of people, I highlight the questions that drove the research overall, as well as those that relate specifically to the part of the work that I was involved with.

Manuscript 1

A network of transcriptional repressors modulates auxin responses

Jekaterina Truskina, Jingyi Han, Elina Chrysanthou, Carlos S. Galvan-Ampudia, Stéphanie Lainé, Géraldine Brunoud, Julien Macé, Simon Bellows, Jonathan Legrand, Anne-Maarit Baġman, Margot E. Smit, Ondřej Smetana, Arnaud Stigliani, Silvana Porco, Malcolm J. Bennett, Ari Pekka Mähönen, François Parcy, Etienne Farcot, Francois Roudier, Siobhan M. Brady, Anthony Bishopp and Teva Vernoux, Nature 2021

Central Objective

As highlighted above, one of the central questions in auxin biology relates to the conundrum of how one molecule can regulate so many developmental processes. The simplest system of auxin signalling has been observed in the liverwort *Marchantia polymorpha*. Here, each gene family (TIR1/AFB, Aux/IAA, Class A, Class B and Class C ARFs) are represented by a single component (Kato et al., 2020). Consequently, despite the relative simplicity of the auxin response machinery, this hormone drives many developmental processes, such as rhizoid

initiation and elongation, thallus growth, regeneration from excised thalli, and the relative growth between lobes. In *Arabidopsis* auxin signalling components exist in large gene families and there is great complexity in the number of auxin responses. Both experimental and theoretical studies have revealed that the complexity of the auxin pathway does not result exclusively from the large number of components. It also follows from the intrinsic, modular structure of the pathway, which endows it with a rich potential for different dynamical behaviours. Auxin signalling output composes many aspects of the signalling pathway including the TIR1 auxin perception process, the binding to Aux/IAA proteins and their subsequent degradation, the distribution of different oligomers composed of ARF, Aux/IAA proteins and co-regulators, all of which have potentially distinct transcriptional regulatory properties (Weijers et al., 2005). For these components to have acquired different roles requires a degree of subfunctionalisation. Such subfunctionalisation would require both specificity in the expression pattern of individual members and also differences in their biochemical function, such as changes in binding affinities. Such differences could include the presence of different post-translational modifications, the ability to target different DNA motifs or the ability to have different interactors.

In this manuscript we consider only Class A ARFs. We are mindful that these will not be the only components conferring specificity in auxin response, but considering only Class A ARFs allowed the project to keep to a manageable size. We also consider only differences in expression patterns. Therefore, we firstly ask,

1: Are the 5 Class A ARFs in *Arabidopsis* expressed differentially in the root and shoot meristems?

Differential expression patterns could be caused by epigenetic silencing in different tissues, e.g. cell specific marking of the DNA by H3K27, or they could be caused by being the targets of different groups of spatially-specific transcription factors. Therefore, we ask,

2: Are the differences in Class A ARFs expression the result of epigenetic

regulation or due to them being targets of different transcription factors?

After producing a network of upstream ARF regulators suggesting that the expression of each Class A is regulated by a distinct set of transcription factors. We sought to verify this network. In particular my work was focused on asking

3: Are the levels of Class A ARFs miss-regulated in transcription factor mutants predicted to be upstream of auxin response?

I observed alterations in the levels of ARFs expression in plants where levels of putative transcriptional regulators were manipulated. The results suggested AL3 and CRF10 are repressors of ARF7. To investigate the functional role of these TFs, therefore we ask,

4: Are auxin-related responses affected in these same mutants?

I tested whether knock out mutants in transcription factors upstream of ARFs were affected in known auxin-regulated processes, such as root elongation and the speed of gravitropic response. These results confirmed that a majority of the TF mutants identified are involved in auxin-related processes.

Manuscript 2

A Novel Dual Expression Anatomy Lines (DEAL) Vector System allows simultaneous visualization of gene expression and anatomical features during live imaging of Arabidopsis roots.

Britta MC Kümpers, Jingyi Han, John Vaughan-Hirsch, Nicholas Redman, Alexander Ware, Jonathan A Atkinson, Nicola Leftley, George Janes, Giuseppe Castiglione, Paul T. Tarr, Kevin Pyke, Ute Voss, Darren M Wells and Anthony Bishopp

Central Objective

As mentioned before, a combination of fluorescent microscopes and fluorescent

proteins is a vital tool to observe gene expression pattern and protein distribution. To define gene expression in context with the cell identity, it is also necessary to present the outline of the cell. However, the transmitted light, fluorescent dyes and some membrane protein fused fluorescent have limitations. In particular these methods are unsuitable for imaging changes in gene expression in a time-resolved manner, as long-term imaging is not possible with these methods. Genetically encoded proteins offer a solution, but it can be time consuming crossing these with existing markers. This leaves a gap for developing a new membrane marker system for simultaneous visualization of fluorescent markers and cellular anatomy in both Arabidopsis primary and lateral roots.

In this manuscript, we developed a new fluorescent plasma-membrane marker system in which a genetically encoded membrane marker is included within the destination plasmid. We used Tdtomato combined with Greengate destination vectors to aid rapid assembly. This system can combine with target genes efficiently and yield a high number of transformed plants. This research is built around three objectives

1: To design and build a system for the simultaneous visualisation of gene expression alongside the outline of the cell.

We need a marker that is bright and easy to visualise with a standard confocal set up and does not degrade over time. In addition, in order to facilitate rapid cloning, we need an assembly method that is quick, efficient and does not rely on expensive enzymes.

2: Evaluate how efficient this dual visualisation system is in comparison to treatment with propidium iodide.

PI is a common fluorescent stain for showing cell membrane, but it is limited by cell layers. For example, the dye does not penetrate the vascular cylinder outside of the meristem. We compared images between PI and the DEAL plants to test if this can offer a better system for these tissues. In addition, PI has previously been

shown to penetrate lateral root primordia poorly. We compared images between PI with DEAL.

3: Evaluate the efficiency of the Dual visualization system for long-term observation.

To confirm this fluorescent marker can work in long-term observation, we set two tasks. The first was to follow expression of a marker through the process of LR primordia emergence. Ideally this would start at an early stage of root development (such as stage 3) and we would continue imaging through until the root emerges, a period of around 48h. The second was to test how gene expression changes in response to a changing environment. In this context we use the auxin sensor DII and observe how it's pattern changes on auxin treatment.

Manuscript 3

NACs and MYBs specify ARF7 expression patterns in the root apical meristem through binding sites in the first intron.

Jingyi Han, Rahul Bhosale, Ute Voß, Anthony Bishopp

Central Objective

The first manuscript showed Class A ARFs shows a unique but partially overlapping expression pattern in both the root and shoot apical meristems. The expression of all five activating ARFs was investigated in transgenic reporters containing either only sequence 3' to the transcriptional start site or in reporters containing an in-frame fusion of GFP to the second exon. ARF7 has an interesting expression pattern. A broad expression of ARF7 was observed in root tips only in the reporter containing an in-frame fusion of GFP to the second exon, whilst for ARFs 5,6,8 and 19, there was no discernible difference between the two promoter fragments. This result suggested that these regulatory sequences appeared to increase GFP transcription, and that transcriptional activators likely bound these sequences. This was in sharp contrast with the majority of components identified

within the ARF regulatory networks that were predicted to be transcriptional repressors.

In this manuscript, we explore the role of the sequences 3' of the transcription site including first intron in ARF7 transcriptional regulation, and identify which transcription factors bind in this region to coordinate root development. We ask,

1: Is the ARF7 first intron required for ARF7 expression in the RAM?

To test whether the first intron lead different expression pattern, we use different length 5' sequence with or without first intron drove GFP to investigate ARF7 expression pattern in roots. We used the DEAL system developed in manuscript 2 to produce these lines. This marker system gave an efficient positive control, and presence of the red cell marker provided a control to let us know that the transformation was successful. It was vital to confirm that lack of GFP expression was caused because of the missing 3' sequence rather than failed transformation. Further, to test whether the position of intron was required for specifically expression in RAM, we will use swap experiment inserting intron to UTR. The results from these experiments led us to ask:

2: Does the first intron contains potential *cis*-elements?

To explore potential regulator element, we will examine the conservation of intronic sequence within the 1001 Genomes Sequencing project, which shows 1135 *Arabidopsis thaliana* strains. The plantRegMap (Plant Transcription Regulation Map) provided information of TF binding site prediction. DAP-seq (DNA affinity purification sequencing) data is a high-throughput TF binding site discovery method that interrogates genomic DNA with in-vitro-expressed TFs and was used to further identity putative binding sites. Potential binding sites were further dissected to identify the potential *cis*-elements.

Statement about Joint Authorship

1. Chapter 1 ‘A network of transcriptional repressors modulates auxin responses’

As second author, my role was in validating a network of genes upstream of the ARFs. I examined a panel of 24 TF mutants and assayed their response to auxin in root elongation assays as well as gravitropic response. To confirm that these mutants miss-regulated ARF I generated overexpression lines and confirmed elevated levels of Class A ARFs in these. These data are shown in Figure 3 e, Extended Data Figure 8 i and j, Extended Data Figure 9.

2. Chapter 2 ‘A Novel Dual Expression Anatomy Lines (DEAL) Vector System allows simultaneous visualization of gene expression and anatomical features during live imaging of Arabidopsis roots.’

As second author, I evaluated the efficiency of this line by recording the majority of the confocal images for primary roots and lateral roots in this paper. It was critical to prove that the system could be used for long-term imaging, and to do this I observed gene expression in LR primordia development over a 24h period.

3. Chapter 3 ‘NACs and MYBs specify ARF7 expression patterns in the root apical meristem through binding sites in the first intron.’

As first author, I completed all experiments and wrote the draft with inputs from all other authors. The bioinformatic analysis was done by Rahul Bhosale.

Chapter 1

1. Manuscript

A network of transcriptional repressors modulates auxin responses

Jekaterina Truskina¹, Jingyi Han, Elina Chrysanthou, Carlos S. Galvan-Ampudia, Stéphanie Lainé, Géraldine Brunoud, Julien Macé, Simon Bellows, Jonathan Legrand, Anne-Maarit Bågman, Margot E. Smit, Ondřej Smetana, Arnaud Stigliani, Silvana Porco, Malcolm J. Bennett, Ari Pekka Mähönen, François Parcy, Etienne Farcot, François Roudier, Siobhan M. Brady, Anthony Bishopp and Teva Vernoux, Nature 2021

A network of transcriptional repressors modulates auxin responses

<https://doi.org/10.1038/s41586-020-2940-2>

Received: 9 October 2018

Accepted: 4 September 2020

Published online: 18 November 2020

 Check for updates

Jekaterina Truskina^{1,2}, Jingyi Han^{2,9}, Elina Chrysanthou^{2,9}, Carlos S. Galvan-Ampudia¹, Stéphanie Lainé¹, Géraldine Brunoud¹, Julien Macé¹, Simon Bellows³, Jonathan Legrand¹, Anne-Maarit Bågman^{4,5}, Margot E. Smit^{4,5}, Ondřej Smetana^{6,7}, Arnaud Stigliani⁸, Silvana Porco², Malcolm J. Bennett², Ari Pekka Mähönen^{6,7}, François Parcy⁸, Etienne Farcot^{2,3}, Francois Roudier¹, Siobhan M. Brady^{4,5}, Anthony Bishopp²✉ & Teva Vernoux¹✉

The regulation of signalling capacity, combined with the spatiotemporal distribution of developmental signals themselves, is pivotal in setting developmental responses in both plants and animals¹. The hormone auxin is a key signal for plant growth and development that acts through the AUXIN RESPONSE FACTOR (ARF) transcription factors^{2–4}. A subset of these, the conserved class A ARFs⁵, are transcriptional activators of auxin-responsive target genes that are essential for regulating auxin signalling throughout the plant lifecycle^{2,3}. Although class A ARFs have tissue-specific expression patterns, how their expression is regulated is unknown. Here we show, by investigating chromatin modifications and accessibility, that loci encoding these proteins are constitutively open for transcription. Through yeast one-hybrid screening, we identify the transcriptional regulators of the genes encoding class A ARFs from *Arabidopsis thaliana* and demonstrate that each gene is controlled by specific sets of transcriptional regulators. Transient transformation assays and expression analyses in mutants reveal that, in planta, the majority of these regulators repress the transcription of genes encoding class A ARFs. These observations support a scenario in which the default configuration of open chromatin enables a network of transcriptional repressors to regulate expression levels of class A ARF proteins and modulate auxin signalling output throughout development.

Previous research aimed at understanding how auxin elicits diverse downstream responses in different tissues has focused on asymmetries in the distribution of the hormone^{2,4}. However, differences in expression of signalling components could also contribute to the specificity in auxin response. Among the 23 ARFs in *Arabidopsis*, ARF5, ARF6, ARF7, ARF8 and ARF19 are class A ARF activators of transcription³ and key regulators of both embryonic and post-embryonic development^{6–13}. In the stem cell niches driving post-embryonic plant development, the root and shoot apical meristems⁶, tissue-specific variation in the expression of class A ARF genes (Fig. 1a, b) is thought to be a key determinant of the diversity of auxin responses^{14,15}.

Transcriptional regulation of class A ARF genes

Class A ARF proteins are encoded by genes with 11–14 introns, with the first introns of ARF7 and ARF19 being around three times larger than the other introns. We tested the role of upstream sequences in determining the expression of class A ARF genes by comparing the patterns in meristems from transcriptional reporter lines (Fig. 1a, b, Extended Data Fig. 1a–j) using either the sequences 3–5 kb 5' of the

ATG and 3' of the ATG up to the end of the first intron of ARF6, ARF7 and ARF19 or the 5' sequences alone (designated respectively *pARF* and *pARF*^{–intron}). We observed a difference between the two reporters only for ARF7 (Fig. 1a, b, Extended Data Fig. 1c, h): the ARF7 transcriptional reporter including the first intron, but not the version lacking it, showed strong expression in the root apical meristem (Fig. 1b), implying that the 3' sequence contains regulatory information required for ARF7 expression in the root. Furthermore, comparison with the patterns of class A ARF expression seen when using reporters with shorter (2-kb) promoters¹⁴ (Extended Data Fig. 1k–o) and with those observed through RNA in situ hybridization^{15,16} (Extended Data Fig. 1p–r) showed that sequences upstream of the first 2 kb 5' of the ATG codon are necessary for the regulation of class A ARF expression.

Chromatin status of class A ARF loci

Specific expression patterns of class A ARF genes could be due to tissue-specific differences in the chromatin accessibility of these loci. We analysed the chromatin status of each class A ARF locus by scoring the presence of the histone H3 lysine 27 and lysine 4 trimethylation

¹Laboratoire Reproduction et Développement des Plantes, Université de Lyon, ENS de Lyon, UCB Lyon 1, CNRS, INRAE, Lyon, France. ²School of Biosciences, University of Nottingham, Loughborough, UK. ³School of Mathematical Sciences, University of Nottingham, Nottingham, UK. ⁴Department of Plant Biology, University of California Davis, Davis, CA, USA. ⁵Genome Center, University of California Davis, Davis, CA, USA. ⁶Institute of Biotechnology, HiLIFE, University of Helsinki, Helsinki, Finland. ⁷Organismal and Evolutionary Biology Research Programme, Faculty of Biological and Environmental Sciences, University of Helsinki, Helsinki, Finland. ⁸Université Grenoble Alpes, CNRS, CEA, INRAE, IRIG-DBSCL-LPCV, Grenoble, France. ⁹These authors contributed equally: Jingyi Han, Elina Chrysanthou. ✉e-mail: Anthony.Bishopp@nottingham.ac.uk; teva.vernoux@ens-lyon.fr

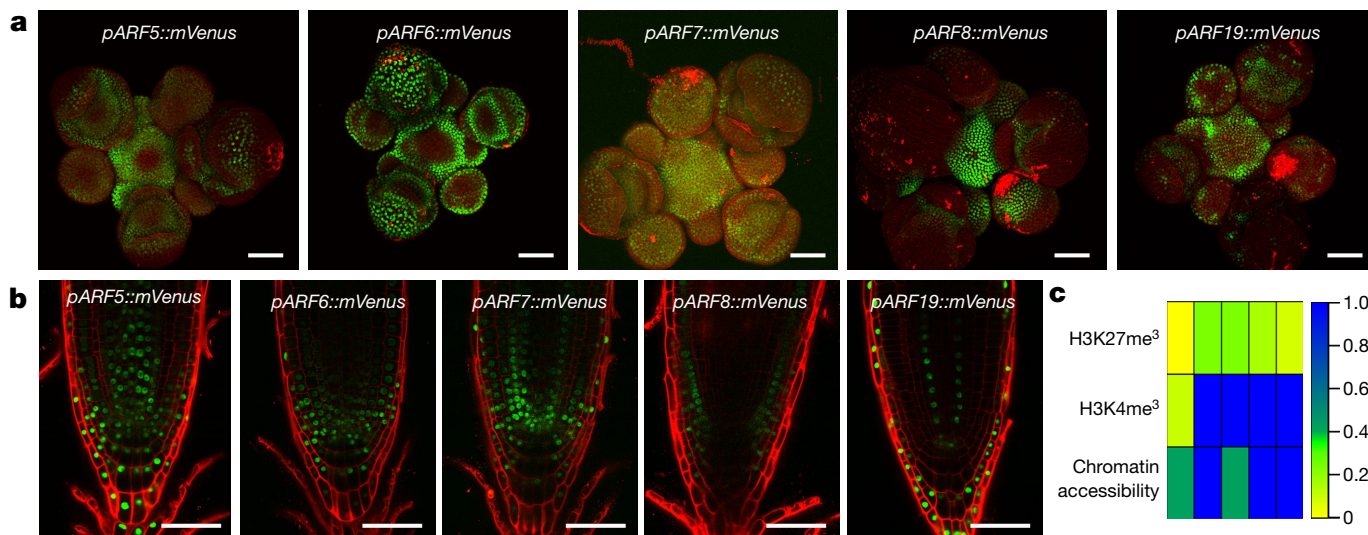


Fig. 1 | Tissue-specific expression patterns and chromatin landscape of *Arabidopsis* class A *ARF* loci. **a, b**, Expression of class A *ARF* genes in the shoot (SAM; **a**) and root apical meristem (RAM; **b**) reported using long promoters containing sequences 5' and 3' of the ATG (*pARF::mVenus*). Scale bars, 50 μ m.

Experiments were performed at least three times with similar results. **c**, Frequency of association of the repressive chromatin marker H3K27me₃, active chromatin marker H3K4me₃ and chromatin accessibility with class A *ARF* loci across all available datasets.

(H3K27me₃ and H3K4me₃) chromatin modifications, which are implicated in repressing and promoting gene expression, respectively¹⁷. Meta-analysis of published datasets covering a range of tissues and developmental stages showed that H3K27me₃ is largely absent, whereas H3K4me₃ is present, at all class A *ARF* loci (Fig. 1c, Extended Data Fig. 2a–c, Supplementary Table 1). These loci are also characterized by accessible regulatory regions in the majority of tissues (Fig. 1c, Extended Data Fig. 2d, Supplementary Table 1). These properties suggest that the chromatin configuration of class A *ARF* loci allows them to be actively transcribed at different tissues and developmental stages, implying that the spatial expression pattern specific to class A *ARF* genes does not result primarily from alternate chromatin states with contrasting accessibility.

Repressors as regulators of class A *ARF* genes

Alternatively, specific spatiotemporal transcription of class A *ARF* loci could arise from regulatory networks made up of transcription factors (TFs). To identify TFs that could regulate the transcription of class A *ARF* genes, we used a semiautomated enhanced yeast one-hybrid (eY1H) assay with baits consisting of promoter sequences identical to those from the transcriptional reporter lines described above. The assay yielded 42 previously unrecognized putative transcriptional regulators of class A *ARF* genes (Fig. 2, Extended Data Fig. 3a, b, Supplementary Table 2). Analysis of this candidate gene-regulatory network indicated that individual class A *ARF* loci are likely to be regulated by specific sets of TFs, as only four TFs were identified as binding multiple class *ARF* sequences. Based on the expression of these TFs, the network may contain proteins that mediate either root- or shoot-specific responses (Extended Data Fig. 3c). Most TFs in the network are involved in development, but many putative regulators of *ARF8* are associated with biotic and abiotic stress (Extended Data Fig. 3a, d, Supplementary Table 2). *ARF8* may therefore act as an environmental hub mediating auxin responsiveness, and indeed it has been shown to be involved in plant responses to both biotic and abiotic stresses^{18,19}.

To validate this regulatory network, we searched the class A *ARF* promoters for the presence of binding sites for the TFs identified by eY1H. We predicted the presence of many of these TF-binding sites within the *ARF* promoters and found that a small proportion of the inferred bindings have been confirmed experimentally (Extended Data Fig. 3e–g, Supplementary Table 3, refs.^{20,21}). Next, we systematically tested the regulatory

activity of each TF through transient expression analysis using the TFs either alone or fused to the VP16 transactivation domain (Extended Data Fig. 4a, b, Supplementary Table 4). Thirty-four of 42 (81%) TFs induced a significant change in expression of their class A *ARF* target(s), corresponding to a decrease in mRNA transcript level for 32 of the 34 class A *ARF* genes (94%, or 76% of the total TFs; Fig. 2, Supplementary Table 4, Supplementary Note 1). We observed transcriptional repression of class A *ARF* genes in the majority of cases, both for TFs alone and for TF-VP16 fusions, indicating a strong repressive activity (Extended Data Fig. 4c, d, Supplementary Table 4). Together, our data reveal a functional regulatory network controlling the transcription of class A *ARF* genes and demonstrate that this is regulated by TF-mediated repression.

Expression of class A *ARF* regulators

If the expression of class A *ARF* proteins is controlled by tissue-specific transcriptional repression, we would expect many of the repressors involved to have expression patterns complementary to those of their target *ARF* gene. To test for complementarity of expression with a high spatial resolution, we generated transcriptional reporters for six TFs and investigated them in seven combinations with class A *ARF* reporters in both root and shoot apical meristem (Fig. 3a, b, Extended Data Fig. 5). We observed complementary expression patterns in the root in five of the seven cases (Fig. 3b, Extended Data Fig. 5a, b). In the shoot, we assessed two combinations involving *WRKY11* and *At2g26940*. We detected *WRKY11* only in meristem layers L2/3, whereas its target *ARF8* is expressed specifically in layer L1 (Fig. 3a). In the shoot apical meristem, *At2g26940* is expressed weakly in the centre of the meristem, whereas *ARF19* is expressed, also weakly, in flower primordia (Extended Data Fig. 5c). Hence, repressors and their target *ARFs* have mostly complementary expression patterns in both shoot and root tissues, although repressors and their targets co-localize in some cells, as for other TFs^{22,23}.

Mutants of class *ARF* regulatory genes

To further test the significance of our results in planta, we characterized mutants of 24 TFs from the regulatory network, representing regulators of all five class A *ARFs* (Supplementary Table 5). We measured the expression of the target class A *ARF* genes using qRT-PCR in whole root and shoot tissues (Extended Data Fig. 6, Supplementary Table 6). We

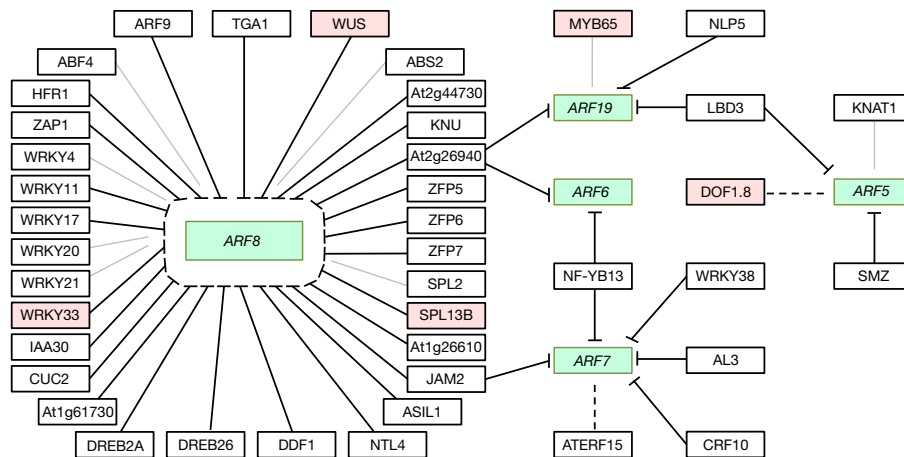


Fig. 2 | Class A ARF transcription is regulated by repressors. eY1H promoter-transcription factor interaction network for class A ARF genes. Interactions between class A ARF promoters (green boxes) and the regulatory TFs listed were tested using transient protoplast assays. Solid lines, confirmed repression; dashed lines, confirmed transcriptional activity; thin grey lines,

unconfirmed interaction. Light red background indicates TFs for which binding has been shown by DNA affinity purification sequencing (DAP-seq) or chromatin immunoprecipitation with sequencing (ChIP-seq; see Supplementary Table 3).

detected changes in the expression of target class A ARF genes identified in our network in 11 of the 24 mutants (46%). Four showed upregulation of their target ARFs, compatible with a repressive activity. The other seven, of which six are ARF8 regulators, showed downregulation of their target ARF. In the case of ARF8, this could be explained by

complex, nonlinear regulation of ARF8 expression by multiple TFs. Indeed, the ARF8 regulators tested are themselves directly or indirectly regulated transcriptionally by ARF8 both negatively and positively, thus establishing a network structure that could result in upregulation of ARF8 in mutants (Extended Data Fig. 7, Supplementary Note 2). The low

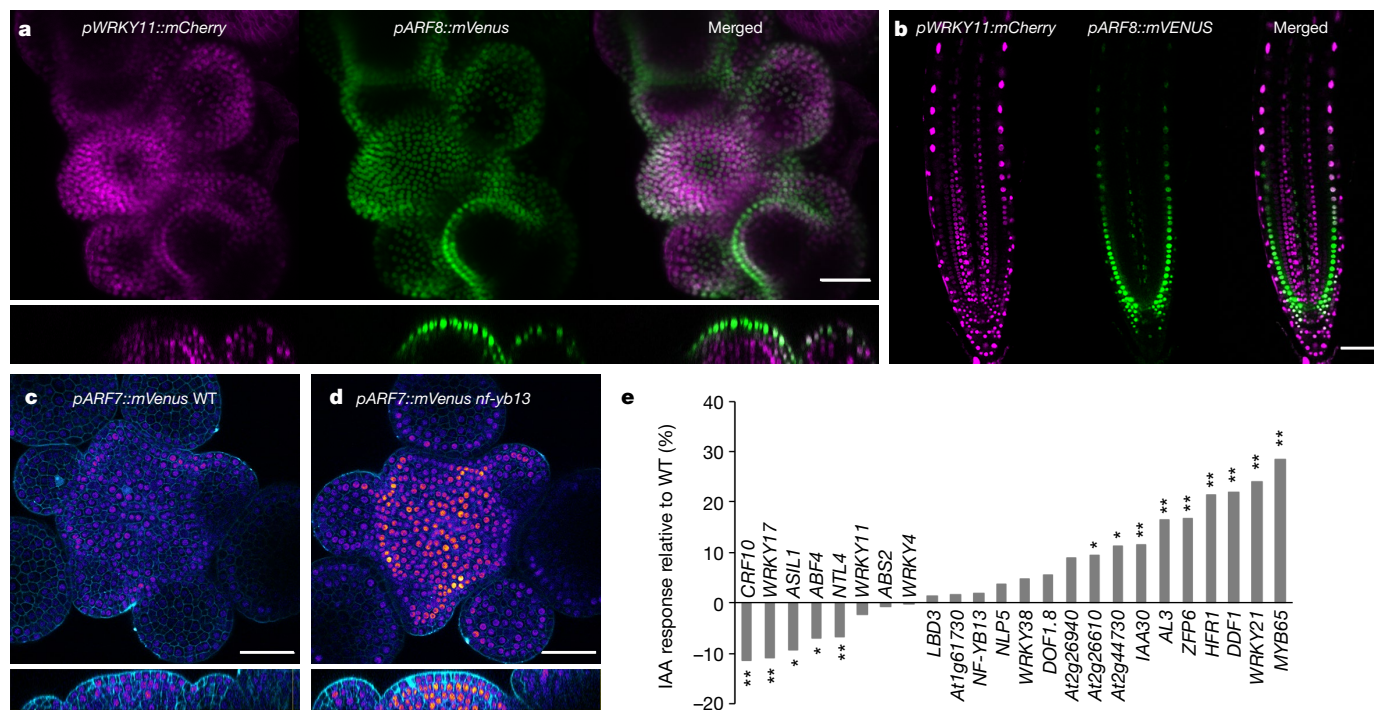


Fig. 3 | Expression levels and patterns of class ARF genes are altered when upstream transcription factors are modulated. a, b, ARF8 and WRKY11 show complementary expression patterns in the SAM (a) and RAM (b). c, d, pARF7-driven patterns are altered in the SAM of *nf-yb13* mutant. Experiments were done twice (a–d). Scale bars, 40 μm (a), 60 μm (b), 45 μm (c, d). For SAM images, orthogonal projections are shown below. (e) Quantification of auxin response in mutant lines. Graph shows percentage change in root elongation at 15 d for plants with mutations in the indicated genes grown on 10 μM indole-3-acetic acid (IAA, the most common natural auxin) as compared to those grown without IAA. All values normalized to those for wild-type controls (WT). n of WT/mutant plants with and without IAA

(P values), left to right: 26/31 and 29/27 (0.002), 24/28 and 28/29 (0.003), 22/31 and 26/23 (0.015), 27/30 and 30/32 (0.03), 30/32 and 29/31 (0.0003), 24/30 and 31/32 (0.61), 31/31 and 29/30 (0.80), 24/31 and 31/32 (0.98), 18/30 and 30/25 (0.72), 30/30 and 31/28 (0.37), 29/30 and 28/27 (0.28), 30/30 and 29/30 (0.07), 29/30 and 31/25 (0.05), 28/28 and 32/30 (0.24), 19/30 and 27/28 (0.19), 22/25 and 29/28 (0.048), 23/27 and 29/32 (0.016), 21/27 and 27/30 (0.003), 28/30 and 31/27 (0.00002), 15/29 and 28/27 (0.004), 24/25 and 31/28 (3×10^{-7}), 15/28 and 29/30 (0.002), 28/31 and 29/29 (1×10^{-9}) and 28/28 and 27/31 (1×10^{-9}). Statistical analyses: two-sided *t*-test comparing variation in the rate of elongation on IAA against that of the WT control; **P* ≤ 0.05, ***P* ≤ 0.01.

sensitivity of expression analysis on whole tissues could also explain our results. This prompted us to determine at higher spatial definition how TF mutations affect class A *ARF* expression. We first crossed *pARF7::mVENUS* and *pARF19::mVENUS* transcriptional reporters into various TF mutants. For the *crf10* and *wrky38* mutants, in which our qRT-PCR results had not revealed changes in *ARF7* mRNA levels, we observed a significant increase in expression and an expansion of the expression pattern for *pARF7::mVENUS* in the root apical meristem (Extended Data Fig. 8a, b, h). We also observed enhanced expression of *pARF7::mVENUS* in the root apical meristem of *nf-yb13*, in this case in agreement with the qRT-PCR results (Extended Data Fig. 8c, h). However, we saw no changes in the expression of *pARF19::mVENUS* in the root of three mutants we analysed (Extended Data Fig. 8d–f, h). In the shoot apical meristem, *pARF7*-driven fluorescence in the *nf-yb13* mutant was identical to that in the wild type in layer L1 but elevated in layers L2 and L3, indicating a change in the spatial pattern of *pARF7* expression (Fig. 3c, d, Extended Data Fig. 8h). We also detected expression pattern changes for *pARF7::mVENUS* in the shoot apical meristem of the *wrky38* mutant (Extended Data Fig. 8g, h). In addition, inducible constitutive overexpression of *AL3* or *CRF10* in the *pARF7::mVENUS* background triggered a decrease in *mVENUS* signal (Extended Data Fig. 8i, j). These results confirm in planta that four TFs are repressors and provide examples of how such repressors shape the expression level or pattern of class A *ARF* genes.

To investigate the functional role of this network, we scored the 24 TF mutants for defects in auxin-regulated root processes (Fig. 3e, Extended Data Fig. 9, Supplementary Table 7). Although none of these mutants had previously been implicated in auxin-dependent responses, 58% (14/24) showed altered root length in response to auxin and 29% (7/24) showed altered gravitropism. Among mutants with altered root length response, 64% (9/14) showed an enhanced response, and all mutants with changes in gravitropism had a faster response. Thus, for both traits, a majority of the TF mutants with altered auxin response show effects opposite to those observed for mutants in loci known to promote auxin signalling^{22,24}, consistent with a repressive role of the TF. We selected two genes with high auxin responsiveness in the root, *IAA13* and *IAA19*, and tested their expression in the TF mutants. Although we mutated only one TF at a time, we found a small but significant increase in the expression of *IAA19* in the roots of seven mutants (-28%), two of which also show elevated levels of *IAA13*. A reduction in either *IAA13* or *IAA19* was observed in a further three mutants (-12%; Supplementary Table 8). A significant number of the mutants also had altered shoot phenotypes, further demonstrating that these TFs have important roles in development (Extended Data Fig. 10, Supplementary Table 9). Taken together, our results support a negative regulation of auxin responses by the corresponding TFs. That mutation of single genes in the class A *ARF* regulatory network can significantly affect auxin-dependent developmental responses further demonstrates the functional importance of individual nodes of this network.

Discussion

Although gene repression mediated by polycomb repressive complex 2 (PRC2) proteins plays a broad role in tissue-specific expression²⁵, the general absence of H3K27me3, a hallmark of PRC2 activity, at class A *ARF* loci indicates that their regulation does not rely on this epigenetic mechanism. This may be because such a system would not allow rapid changes in signalling output. Instead, our data suggest a regulatory system based on the use of transcriptional repressors that modulates expression of constitutively active loci and, in combination with post-translational modifications of class A *ARF* proteins^{26,27}, constantly adjust auxin responsiveness during development. Other transcriptional regulation networks defined in eukaryotes involve both transcriptional activators and repressors²⁸. Instead, the network we characterize resembles the early scenario proposed by Jacob and

Monod²⁹ for transcriptional regulation by repressors only, indicating that there may be a place for the concept that the expression of key developmental regulators may be controlled via transcriptional repression.

Online content

Any methods, additional references, Nature Research reporting summaries, source data, extended data, supplementary information, acknowledgements, peer review information; details of author contributions and competing interests; and statements of data and code availability are available at <https://doi.org/10.1038/s41586-020-2940-2>.

- Sagner, A. & Briscoe, J. Morphogen interpretation: concentration, time, competence, and signaling dynamics. *Wiley Interdiscip. Rev. Dev. Biol.* **6**, e271 (2017).
- Leyser, O. Auxin signaling. *Plant Physiol.* **176**, 465–479 (2018).
- Tiwari, S. B., Hagen, G. & Guilfoyle, T. The roles of auxin response factor domains in auxin-responsive transcription. *Plant Cell* **15**, 533–543 (2003).
- Petrásek, J. & Friml, J. Auxin transport routes in plant development. *Development* **136**, 2675–2688 (2009).
- Finet, C., Berne-Dedieu, A., Scutt, C. P. & Marlétaz, F. Evolution of the ARF gene family in land plants: old domains, new tricks. *Mol. Biol. Evol.* **30**, 45–56 (2013).
- Krogan, N. T., Marcos, D., Weiner, A. I. & Berleth, T. The auxin response factor MONOPTEROS controls meristem function and organogenesis in both the shoot and root through the direct regulation of PIN genes. *New Phytol.* **212**, 42–50 (2016).
- Berleth, T. & Jurgens, G. The role of the monopteros gene in organising the basal body region of the *Arabidopsis* embryo. *Development* **118**, 575–587 (1993).
- Przemek, G. K., Mattsson, J., Hardtke, C. S., Sung, Z. R. & Berleth, T. Studies on the role of the *Arabidopsis* gene MONOPTEROS in vascular development and plant cell axialization. *Planta* **200**, 229–237 (1996).
- Schlereth, A. et al. MONOPTEROS controls embryonic root initiation by regulating a mobile transcription factor. *Nature* **464**, 913–916 (2010).
- Nagpal, P. et al. Auxin response factors ARF6 and ARF8 promote jasmonic acid production and flower maturation. *Development* **132**, 4107–4118 (2005).
- Gutiérrez, L. et al. Phenotypic plasticity of adventitious rooting in *Arabidopsis* is controlled by complex regulation of AUXIN RESPONSE FACTOR transcripts and microRNA abundance. *Plant Cell* **21**, 3119–3132 (2009).
- Okushima, Y. et al. Functional genomic analysis of the AUXIN RESPONSE FACTOR gene family members in *Arabidopsis thaliana*: unique and overlapping functions of ARF7 and ARF19. *Plant Cell* **17**, 444–463 (2005).
- Harper, R. M. et al. The NPH4 locus encodes the auxin response factor ARF7, a conditional regulator of differential growth in aerial *Arabidopsis* tissue. *Plant Cell* **12**, 757–770 (2000).
- Rademacher, E. H. et al. A cellular expression map of the *Arabidopsis* AUXIN RESPONSE FACTOR gene family. *Plant J.* **68**, 597–606 (2011).
- Vernoux, T. et al. The auxin signalling network translates dynamic input into robust patterning at the shoot apex. *Mol. Syst. Biol.* **7**, 508 (2011).
- Hardtke, C. S. & Berleth, T. The *Arabidopsis* gene MONOPTEROS encodes a transcription factor mediating embryo axis formation and vascular development. *EMBO J.* **17**, 1405–1411 (1998).
- Roudier, F. et al. Integrative epigenomic mapping defines four main chromatin states in *Arabidopsis*. *EMBO J.* **30**, 1928–1938 (2011).
- Gifford, M. L., Dean, A., Gutierrez, R. A., Coruzzi, G. M. & Birnbaum, K. D. Cell-specific nitrogen responses mediate developmental plasticity. *Proc. Natl Acad. Sci. USA* **105**, 803–808 (2008).
- Jay, F. et al. Misregulation of AUXIN RESPONSE FACTOR 8 underlies the developmental abnormalities caused by three distinct viral silencing suppressors in *Arabidopsis*. *PLoS Pathog.* **7**, e1002035 (2011).
- O'Malley, R. C. et al. Cistrome and episcistrome features shape the regulatory dna landscape. *Cell* **165**, 1280–1292 (2016).
- Ma, Y. et al. WUSCHEL acts as an auxin response rheostat to maintain apical stem cells in *Arabidopsis*. *Nat. Commun.* **10**, 5093 (2019).
- Zhao, Z. et al. Hormonal control of the shoot stem-cell niche. *Nature* **465**, 1089–1092 (2010).
- Leibfried, A. et al. WUSCHEL controls meristem function by direct regulation of cytokinin-inducible response regulators. *Nature* **438**, 1172–1175 (2005).
- Dharmasiri, N. et al. Plant development is regulated by a family of auxin receptor F box proteins. *Dev. Cell* **9**, 109–119 (2005).
- Kim, D.-H. & Sung, S. Polycomb-mediated gene silencing in *Arabidopsis thaliana*. *Mol. Cells* **37**, 841–850 (2014).
- Orosa-Puente, B. et al. Root branching toward water involves posttranslational modification of transcription factor ARF7. *Science* **362**, 1407–1410 (2018).
- Cho, H. et al. A secreted peptide acts on BIN2-mediated phosphorylation of ARFs to potentiate auxin response during lateral root development. *Nat. Cell Biol.* **16**, 66–76 (2014).
- Ptashne, M. Repressors. *Curr. Biol.* **17**, R740–R741 (2007).
- Jacob, F. & Monod, J. Genetic regulatory mechanisms in the synthesis of proteins. *J. Mol. Biol.* **3**, 318–356 (1961).

Publisher's note Springer Nature remains neutral with regard to jurisdictional claims in published maps and institutional affiliations.

© The Author(s), under exclusive licence to Springer Nature Limited 2020

Methods

Plant material and growth conditions

All transgenic lines were generated in the Col-0 accession of *Arabidopsis thaliana*. T-DNA insertion mutants in transcription factor-coding genes and the *arf8-1* mutant were obtained from NASC. All T-DNA lines were genotyped to confirm that they were homozygous, and qRT-PCR was used to confirm alterations in transcript levels (Supplementary Table 5). The accession numbers of T-DNA lines and further details are listed in Supplementary Table 5.

For root microscopy and in situ hybridization of ARF transcriptional reporter lines, plants were grown on half-strength Murashige and Skoog (1/2 MS) medium supplemented with 1% sucrose and 1% agar in 24 h light conditions (microscopy) or 12 h light/12 h dark conditions (in situ hybridization). For shoot microscopy, plants were grown in 8 h light/16 h dark conditions for 6 weeks and then transferred to 16 h light/8 h dark conditions for 2 weeks to induce bolting. For the qRT-PCR experiments, the seedlings were grown in 24 h light conditions on 1/2 MS plates containing 1% sucrose and 1% agar for 7 d. For the root imaging of crosses between ARF transcriptional reporter lines and TF mutants and for the co-expression analysis of ARF transcriptional reporter lines with TF transcriptional reporter lines, the plants were grown on 1/2 MS medium supplemented with 0.8% agar in 16 h light/8 h dark light. TF overexpression lines were grown for 12 h light/12 h dark light on 1/2 MS medium supplemented with 1% agar.

Cloning

Multisite Gateway cloning technology was used to generate ARF transcriptional reporter lines harbouring DNA sequences both upstream and downstream from the start codon. The promoter fragments were amplified by PCR with the following sequences: *pARF5*: bp -5418 to +134; *pARF6*: bp -3255 to +197; *pARF7*: bp -2973 to +374; *pARF8*: bp -5091 to +42; *pARF19*: bp -4906 bp to +457. For *ARF5*, *ARF6*, *ARF8* and *ARF19*, the fragments were inserted into pDONR P4-P1R and recombined with 3× mVenus-N7 pDONR211 (containing triple mVenus coding sequences and an N7 nuclear localization signal), *OCS* terminator pDONR P2R-P3 (containing the stop codon followed by an octopine synthase terminator) and pK7m34GW (the destination vector containing the kanamycin resistance gene for in planta selection) to produce pARF-3xmVenusN7 constructs. For ARF7, the fragment was cloned into pCR8/GW/TOPO and recombined with a nuclear-localized mVenusN7, 35S terminator and pK7m34GW to produce the pARF7-mVenusN7 construct. Similarly, the shorter promoter fragments were amplified by PCR based on primers designed at the following locations: *pARF5*: bp -5418 to -1; *pARF6*: bp -3255 to -1; *pARF7*: bp -2973 to -1; *pARF8*: bp -5091 to -1; *pARF19* bp -4906 to -1. The fragments were inserted into pDONR P4-P1R and recombined with 3× mVenus-N7 pDONR211, *OCS* terminator pDONR P2R-P3 and pK7m34GW destination vector to yield pARF-3xmVenusN7 shorter transcriptional reporter lines.

All constructs were transformed into *Agrobacterium tumefaciens* C58pMP90 strain by electroporation and then transformed into Col-0 plants by the floral dip method³⁰.

The ARF promoter sequences screened in the eY1H assay were amplified by PCR and sequenced to confirm absence of mutations. The overall ARF promoters screened correspond in length and content to those used in the construction of the transcriptional reporter lines except that the longer promoters were split into two fragments: *pARF5* fragment 1: bp -2796 to +134; *pARF5* fragment 2: bp -5418 to -2481; *pARF6*: bp -3255 to +197; *pARF7*: bp -2973 to +374; *pARF8* fragment 1: bp -2899 to +42; *pARF8* fragment 2: bp -5091 to -2121; *pARF19* fragment 1: bp -2399 to +457; *pARF19* fragment 2: bp -4906 to -1992. The amplified fragments were cloned into either pDONR P4P1R or pENTR 5' TOPO plasmids by the Gateway BP reaction or using the pENTR 5'-TOPO kit, respectively. The resulting plasmids were recombined with the Gateway LR reaction into both pMW2 and pMW3 Gateway destination vectors

designed for yeast expression and containing respectively *HIS3* or *LacZ* reporter genes³¹. The resulting plasmids were transformed into the yeast strain YM4271.

Additional transcription factors were cloned and added to the collection of existing root-specific transcription factors (Supplementary Table 10). The transcription factors were amplified by a PCR from cDNA collections obtained by isolating total RNA from various tissues. Each full-length transcription factor cDNA PCR product (without a stop codon) was inserted into a pENTR-Zeo plasmid by the Gateway BP reaction and then recombined into the pDEST-AD-2μ destination vector designed for yeast expression and containing a *GAL4* activation domain³¹. The vectors were transformed into the yeast strain Yα1867.

To produce the reporter plasmid for the protoplast assays, the promoter fragment of the respective ARF corresponding to the one used in the eY1H assay, and the ARF transcriptional reporter lines described above, were amplified by PCR and cloned into the plasmid pDONR P4-P1R. For the *ARF8* promoter, a short part of the 35S promoter (bp -107 to +1) was inserted at bp -115. Separately, a construct containing an NLS followed by the mVenus coding sequence and an *OCS* terminator was cloned into the plasmid pDONR 211. Third, a construct containing the promoter of *RPS5a* (encoding ribosomal protein S5A) driving TagBFP followed by an NLS and a *nosT* terminator were cloned into the plasmid pDONR P2R-P3. These three plasmids were recombined using a multisite Gateway method to yield the final reporter plasmid pARF-NLS-mVenus-term-pRPS5a-TagBFP-NLS-term. An alternative reporter plasmid contained a shorter ARF promoter fragment that contained sequences upstream and lacked sequences downstream of the start codon (corresponding to the transcriptional reporter lines with shorter promoters described above). To create the effector plasmid for the protoplast assays, the *RPS5a* promoter was cloned into pDONR P4-P1R; the cDNA of the respective transcription factor without the stop codon was cloned into pDONR 211; and the construct, containing the self-cleaving 2A peptide^{32,33} followed by mCherry coding sequence, a NLS and a *nosT* terminator, was cloned into pDONR P2R-P3. Finally, these three plasmids were recombined with a multisite Gateway reaction to yield pRPS5a-cDNA-2A-mCherry-NLS-term. An alternative effector plasmid included an activator VP16 domain from the herpes simplex virus fused to the TF cDNA.

Microscopy

Roots of ARF transcriptional reporter lines were imaged 5 d after germination. Plant cell walls were visualized by staining with 15 μg ml⁻¹ propidium iodide solution. Roots were examined using a TCS-SP5 confocal microscope (Leica) with excitation at 514 nm and emission at 526–560 nm for mVenus and 605–745 nm for propidium iodide.

For analysis of shoot apical meristems, bolted shoots were dissected under a stereomicroscope and transferred to an apex culture medium (1/2 MS medium supplemented with 1% sucrose, 0.8% agarose, 1× vitamin solution (myoinositol 100 mg l⁻¹, nicotinic acid 1 mg l⁻¹, pyridoxine hydrochloride 1 mg l⁻¹, thiamine hydrochloride 10 mg l⁻¹, glycine 2 mg l⁻¹), for overnight incubation. Before microscopy, cell walls were stained with 100 μg ml⁻¹ propidium iodide solution. The shoot apices were then examined using a TCS-SP5 confocal microscope (Leica) with excitation at 514 nm and emission at 526–560 nm for mVenus and 605–745 nm for propidium iodide.

eY1H assay

The eY1H assay was conducted according to³¹. The ARF promoters screened correspond in length and content to those used in the construction of the transcriptional reporter lines except that the longer promoters (*pARF5*, *pARF8* and *pARF19*) were split into two fragments (see Cloning section). With the longer promoters, only 1 out of 39 TFs was identified using the distal fragment of the *ARF8* promoter. This suggests that the other 38 TFs bind in a region of the promoter from bp -2480 to +134 for *ARF5*, bp -2120 to +42 bp for *ARF8* and bp -1991 to +457 for *ARF19*.

We used a TF collection enriched in root-expressed TFs³¹ expanded with additional TFs involved either in development of the shoot apical meristem or in hormonal regulation (see Supplementary Table 10).

Transient expression analysis in *Arabidopsis* protoplasts

For the protoplast assay Col-0 seedlings were grown in short-day conditions (8 h light/16 h dark) for 37–45 d. Leaves of similar size from the second or third pair were collected and digested in an enzyme solution (1% cellulose R10, 0.25% macerozyme R10, 0.4 M mannitol, 10 mM CaCl₂, 20 mM KCl, 0.1% BSA, 20 mM MES at pH 5.7) overnight at room temperature. Protoplasts were collected through a 70-micron mesh, washed twice with ice-cold W5 solution (154 mM NaCl, 125 mM CaCl₂, 5 mM KCl, 5 mM glucose, 2 mM MES at pH 5.7) and incubated on ice for 30 min. The protoplasts were then resuspended in MMG solution (0.4 M mannitol, 15 mM MgCl₂, 4 mM MES at pH 5.7) at a final concentration 150,000 cells per ml. 10 µl of each the effector and the reporter plasmid DNA (concentration 3 mg µl⁻¹) were mixed with 200 µl of the protoplasts. Immediately, 220 µl of PEG solution (40% PEG 4000, 0.2 M mannitol, 0.1 M CaCl₂) was added and the protoplasts were incubated for 5 min at room temperature and then washed twice in W5 solution. The protoplasts were resuspended in 800 µl of the W5 solution and incubated for 24 h in 16 h light/8 h dark growth chamber. Before imaging, the protoplasts were resuspended in 400 µl W5 solution and subsequently transformed into an 8-well imaging chamber.

A Zeiss 710 LSM confocal microscope was used for imaging the protoplasts (Extended Data Fig. 4). Sequential scanning was performed with mVenus (excitation at 514, emission at 520–559), TagBFP (excitation at 405 and emission at 423–491), mCherry (excitation at 561, emission at 598–636) and bright-field channels. z stacks of several protoplasts were taken. The data were analysed using ImageJ software (imagej.net/Fiji). The image with the best focus for each protoplast was selected from the z stack. The nucleus was selected and the mean fluorescence was measured as illustrated in Extended Data Fig. 4. The number of replicates was between 15 and 54 protoplasts with a majority of experiments including at least 20 protoplasts. For most ARF-TF interactions, 4 or 5 independent experiments were performed (Supplementary Table 4): 2 or 3 experiments with the standard effector plasmid and 2 experiments with alternative effector plasmid containing VP16 domain. For the statistical analysis, we first run a Kruskal–Wallis *H*-test on all controls for a given set of experiments (TF or TF-VP16). At a significance level of 0.05, all tests rejected the null hypothesis that control populations have the same median, indicating that the data could not be pooled. The results for each experiment was analysed independently using a one-sided Mann–Whitney *U*-test to test for a significant effect of TF or TF-VP16 and to identify the direction of the change. To take into account the results from several experiments of a given type (TF or TF-VP16), we performed a meta-analysis using the method of Mudholkar and George³⁴ to combine the *P* values from the independent experiments. This allows us to obtain 'meta *P* values' per type of experiment. Note that the meta *P* value was calculated only if the Mann–Whitney test was significant (with a significance level of 0.05) in at least one of the repetitions.

Expression analysis with qRT–PCR

The whole root and the whole shoot parts of the seedlings were collected separately. For one root sample, roots from 30 seedlings grown on the same plate were pooled together. For one shoot sample, 8 shoots from seedlings grown on the same plate were pooled together. Three independent replicates per genotype were collected. RNA was extracted using Spectrum Plant Total RNA kit (Sigma-Aldrich). The DNA was removed using TURBO DNA-free kit (Invitrogen). The cDNA was produced using SuperScript VILO cDNA Synthesis kit (Thermo Fischer) with 500 ng RNA. The cDNA was diluted 1:100 before use. The qRT–PCR was performed using Applied Biosystems Fast SYBR Green Master Mix. Expression of TUB4 gene was used as standard. The statistical

analysis was performed with a one-sided Mann–Whitney test, with *P* < 0.1 considered as statistically significant. *IAA13* and *IAA19* were chosen as auxin-responsive genes for qRT–PCR analysis in roots from ref.³⁵.

Expression analysis of crosses between ARF transcriptional reporter lines and TF mutants

Mutants of the regulatory transcription factors were crossed with pARF7-mVenus transcriptional reporter line described above. The crosses were selected for the presence of homozygous pARF7-mVenus reporter construct. The F3 generation wild-type and mutant plants were compared.

The roots of 5 d-old plants were stained with 15 µg ml⁻¹ propidium iodide and imaged using the TCS-SP8 (Leica) confocal microscope with excitation at 514 nm and emission at 526–560 nm for mVenus and 605–745 nm for propidium iodide.

For the shoot microscopy the images were taken with a Zeiss 710 LSM confocal microscope. mVenus intensity was measured separately in L1 and in L2/L3 layers in each of the 8 cross-sections with 50 nm distance between each cross-sections. Number of replicates: 7 WT and 7 mutant plants for *nf-yb13*, 12 WT and 12 mutant plants for *wrky38*.

Co-expression analysis of ARF transcriptional reporter lines and TF transcriptional reporter lines

Multisite Gateway cloning technology was used to generate TF transcriptional reporter lines. The promoter fragments of TFs were amplified by PCR with sequences: *pWRKY11*: bp –3626 to –1 bp; *pDOF1.8*: bp –4389 to –1; *pAt2g26940*: bp –3179 to –1 bp; *pAt2g44730*: bp –2738 to –1 bp; *pCRF10*: bp –4060 to –1 bp; *pZFP6*: bp –2117 to –1. The fragments were inserted into pDONR P4-P1R and recombined with 2× mCherry pDONR211 (containing double mCherry coding sequences) and N7 pDONR P2R-P3 (containing a nuclear localization signal) and pB7m34GW (the destination vector containing basta resistance gene for in planta selection) to produce pTF-2xmCherryN7 constructs. These constructs were transformed into the *pARF*-mVenus transcriptional reporter line backgrounds by the floral dip method³⁰.

Roots of the plants grown for 5–10 d were imaged using the TCS-SP8 (Leica) confocal microscope, with excitation at 514 nm and emission at 526–560 nm for mVenus and excitation and emission at 587 nm and 610–670 nm respectively for mCherry. Total fluorescence was calculated for individual nuclei from two or three individual roots using a 6-px circular selection in ImageJ. These values were then normalized for each channel based on a scale of 0–1 with the brightest nuclei in each root being set to a value of 1. The shoots were examined using the TCS-SP8 (Leica) confocal microscope, with excitation at 514 nm and emission at 526–560 nm for mVenus and excitation and emission at 587 nm and 610–670 nm respectively for mCherry.

Inducible overexpression of TFs

Multisite Gateway cloning technology was used to generate TF inducible overexpression lines. The chimaeric transcription activator p1R4-pG1090:XVE³⁶ containing XVE followed by the *rbs* and *nos* terminators and LexA operon, expressed under UBQ10 promoter was recombined with TF coding sequence (lacking STOP codon) in pDONR211 and the 2A-mCherry-term pDONR P2R-P3 (containing the self-cleaving 2A peptide^{32,33} followed by the mCherry coding sequence, a nuclear localization sequence (NLS) and a *nosT* terminator) and pB7m34GW (the destination vector containing basta resistance gene for in planta selection) to produce pUBQ10-XVE-TF-2A-mCherry oestradiol-inducible constructs. These constructs were transformed in the pARF7-mVenus transcriptional reporter line background by floral dip method³⁰.

For the overexpression analysis, roots of the plants grown for 5 d were treated with 10 µM β-oestradiol for 24 h and imaged using the TCS-SP8 (Leica) confocal microscope, with excitation at 514 nm and emission at 526–560 nm for mVenus and excitation and emission at 587 nm and 610–670 nm, respectively, for mCherry.

Shoot phenotype analysis of the TF mutants

24 T-DNA insertion mutants and the wild-type Col-0 were grown in 8 h light/16 h dark conditions on soil for 43 d. Leaf number was counted every 3 d starting from day 24. Rosette diameter was measured at 43 d. After 43 d of growth in the above conditions, the plants were transferred to 16 h light/8 h dark conditions to induce bolting. The following parameters were measured after 21 and 27 d in the 16 h light/8 h dark conditions: length of the main stem, number of cauline branches growing from the main stem, number of axillary branches growing from rosette (the main stem not included). The number of replicates per genotype was 12 plants. For the statistical analysis, an unpaired two-tailed *t*-test was conducted with $P \leq 0.05$ considered as statistically significant.

Root phenotype analysis of the TF mutants

For root length measurement and for gravitropic analysis plants were grown on 1/2 MS medium supplemented with 1% agar in 12 h light/12 h dark conditions. For root length analysis, plants were grown either on medium lacking IAA or supplemented with 10 μM IAA. To reduce plate-to-plate variation wild-type plants and mutants were grown on the same agar plate. Images were taken at 15 d and the root length was measured. The number of replicates per genotype was at least 26 plants without IAA and 15 plants with IAA. For the gravitropic response, plants were grown for 5 d, then turned at a 90° angle and images taken every 1 h for 12 h in the dark using an infrared camera. The number of replicates per genotype was at least 26 plants. Rootnav v.1.8 software (<https://www.nottingham.ac.uk/research/groups/cvl/software/rootnav.aspx>) was used for data analysis. Statistical analysis was done with unpaired two-tailed *t*-test with $P \leq 0.05$ considered as statistically significant.

In situ hybridization

For RNA probe synthesis, 300–500-bp templates were amplified from a cDNA library adding the T7 RNA polymerase promoter sequence at the 5' prime overhang. The product was gel purified and used directly as a template for transcription with DIG RNA Labelling Kit (SP6/T7, Roche). The following primers were used: 3'-ctggttcagctctggtagagt-5' and 3'-ggatcctaatacactcactatagggaggcagcggtgagttgtggaatc-5' (ARF5); 3'-gctgctgtgtttccgctatgt-5' and 3'-ggatcctaatacactcactatagggagggtttgacattccgttcggcat-5' (ARF6); 3'-tgctgatggaaggggtgattt-5' and 3'-ggatcctaatacactcactatagggagggtgctgcggaagattctcactca-5' (ARF8). Roots were cut from 4-d-old plants and vacuum-infiltrated in FAA (50% (v/v) ethanol, 5% (v/v) acetic acid, 3.7% (v/v) formaldehyde) 3–4 times for 5 min each and then fixed overnight at 4 °C. The tissue was rinsed with PBS 4 times for 15 min and embedded in 1% SeaKem LE-agarose (in PBS). For paraffin-embedding, a Leica ASP200 vacuum tissue processor was used following the program described in ref.³⁷. The samples were cut into 7 μm sections. During pre-treatment the samples were passed through the following solution series: xylene 2 times 10 min, methanol 5 min, 100% (v/v) ethanol 2 times 2 min, 95% ethanol 1 min, 90% ethanol 1 min, 80% ethanol 1 min, 60% ethanol + 0.75% NaCl 1 min, 30% ethanol + 0.75% NaCl 1 min, 0.75% NaCl 2 min, PBS 2 min, 1 $\mu\text{g}/\text{ml}$ proteinase K in dilution buffer (100 mM Tris pH 7.5, 50 mM EDTA, pH 7.5) 30 min at 37 °C, PBS + glycine (2 mg ml⁻¹) 2 min, PBS 2 min, FAA 5 min, 2 times PBS 5 min, 0.75% NaCl 2 min, 30% ethanol + 0.75% NaCl 30 s, 60% ethanol + 0.75% NaCl 30 s, 80% ethanol 30 s, 90% ethanol 30 s, 95% ethanol 30 s, 2 times 100% ethanol 30 s. The probe (0.3 μg ml⁻¹ per kb probe complexity) was mixed with hybridization solution (50% formamide, 10% dextran sulphate, Denhardt's solution, 500 μg ml⁻¹ tRNA, 5 mM EDTA, 300 mM NaCl, 10 mM Tris pH 7.0, 10 mM sodium phosphate pH 7.0), denatured at 80 °C for 2 min and applied to the samples which were placed into the wet chamber aligned with paper towels soaked in the soaking solution (2 \times SSC in 50% formamide). The samples were hybridized overnight at 50 °C. The samples were washed 4 times with 0.2 \times SSC at 55 °C for 30 min and then once each with 0.2 \times SSC at 37 °C for 5 min and 0.2 \times SSC at room temperature for 5 min,

PBS 5 min. Detection was done by incubating the samples in 1% blocking solution (1% blocking reagent, 100 mM Tris-HCl pH 7.5, 150 mM NaCl, 0.3% Triton X-100) for 45 min and then in a wet chamber with antibody solution (anti-Digoxigenin-AP 1:250 in 1% blocking solution) for 1.5 h, washing 3 times with buffer A (1% BSA in 100 mM Tris-HCl pH 7.5, 150 mM NaCl, 0.3% Triton X-100) for 30 min, washing twice with detection buffer (100 mM Tris pH 9.5, 100 mM NaCl, 50 mM MgCl₂) for 5 min each, applying 200 μl of colour substrate solution (4.5 ml detection buffer + 90 μl NBT-BCIP) and incubating 24 h for *ARF5* and *ARF6* and overnight for *ARF8* at room temperature. The reactions were stopped by washing the samples twice with TE buffer for 5 min each. The samples were then mounted in 50% glycerol and observed under the light microscope.

In silico analyses

Analysis of expression and function of regulatory TFs. Expression of TFs in the root and the shoot apical meristems was analysed using cell type-specific expression profiles from refs.^{38–40}.

Overrepresentation of TF gene families was analysed for families represented by two or more members in the network. The number of gene family members in the network was compared to total number of genes from the same family in the TF library. Statistical analysis was done using a hypergeometric test, with $P \leq 0.05$ considered as statistically significant.

Involvement of TFs in specific developmental processes (development, biotic and abiotic stress) was analysed based on literature description.

Chromatin state analysis. Binary data on H3K27me3- and H3K4me3-marked genes and chromatin accessibility regions were retrieved from multiple datasets covering a range of tissues and developmental stages. For each dataset, at least two biological replicates were considered, and only the presence of a given *ARF* in both gene lists was scored as a positive association with a chromatin mark or an accessible region.

Datasets used for chromatin marking analysis were: H3K27me3, from refs.^{17,41–45} (GEO database GSE24657, GSE7907, GSE24507, GSE50636, GSE24657, GSE24710, GSE19654; ArrayExpress database E-MTAB-4680, E-MTAB-4684); H3K4me3, from refs.^{17,41–44} (GEO GSE24658, GSE7907, GSE50636, GSE24665, GSE19654; ArrayExpress E-MTAB-4680, E-MTAB-4684).

Datasets used for chromatin accessibility analysis were: DNase I hypersensitive sites, from ref.⁴⁶ (GEO GSM1289358, GSM1289362, GSM1289374); FANS-ATAC-defined accessible regions, from ref.⁴⁷ (GEO GSM2260231, GSM2260232, GSM2260235, GSM2260236); ATAC-defined transposase hypersensitive sites, from refs.^{48,49} (GEO GSM2704255, GSM2704256, GSM2719200, GSM2719201, GSM2719202, GSM2719203, GSM2719204, GSM2719205). For each chromatin accessibility dataset, the presence of at least one accessible region within the *ARF* gene and up to 1 kb upstream of its transcription start site was scored using ad hoc scripts.

Visualization of epigenomic data was carried out using the IGV software^{50,51}.

Binding motif search and reanalysis of DAP-seq data. Position weight matrices (PWM) available for TFs identified in the eYIH screen were retrieved from the Jaspar⁵² and CisBP⁵³ databases. Using these PWMs, we computed the best score of the TF binding sites present in each *Arabidopsis* 2-kb promoter with an R script using the Biostrings library (<https://bioconductor.org/packages/release/bioc/html/Biostrings.html>) and ranked the class A *ARF* gene promoter among all *Arabidopsis* promoters based on this score. As negative control, this operation was repeated identically five times for each class A *ARF* promoter with 20 randomly selected TFs (excluding specific TF classes and families identified in the eYIH screen). The distributions of class A *ARF* promoter ranks with eYIH-selected and randomly selected TFs were compared using a one-sided *t*-test.

DAP-seq files containing the peak list from ref.²⁰ were retrieved (GEO accession number GSE60141). Bedtoolsintersect (bedtools.readthedocs.io/en/latest/index.html) was then used with the -wb option to determine which DAP peak overlap with each promoter.

Reporting summary

Further information on research design is available in the Nature Research Reporting Summary linked to this paper.

Data availability

The data including the source data that supports the finding of this study are available within the paper, its supplementary information files or publicly available datasets. Publicly available position weight matrices were obtained from the Jaspar and CisBP databases. Publicly available chromatin marking and accessibility datasets were acquired from the GEO and ArrayExpress databases with the following accession numbers: GSE24665, GSE24658, GSE7907, GSE24507, GSE50636, GSE24657, GSE24710, GSE19654, GSM2260231, GSM2260232, GSM2260235, GSM2260236, GSM2704255, GSM2704256, GSM2719200, GSM2719201, GSM2719202, GSM2719203, GSM2719204, GSM2719205, GSM1289362, GSM1289374, E-MTAB-4680, E-MTAB-4684 and GSM1289358.

30. Clough, S. J. & Bent, A. F. Floral dip: a simplified method for *Agrobacterium*-mediated transformation of *Arabidopsis thaliana*. *Plant J.* **16**, 735–743 (1998).
31. Gaudinier, A. et al. Enhanced Y1H assays for *Arabidopsis*. *Nat. Methods* **8**, 1053–1055 (2011).
32. Kim, J. H. et al. High cleavage efficiency of a 2A peptide derived from porcine teschovirus-1 in human cell lines, zebrafish and mice. *PLoS ONE* **6**, e18556 (2011).
33. Trichas, G., Begbie, J. & Srinivas, S. Use of the viral 2A peptide for bicistronic expression in transgenic mice. *BMC Biol.* **6**, 40 (2008).
34. George, E. O. & Mudholkar, G. S. On the convolution of logistic random variables. *Metrika* **30**, 1–13 (1983).
35. Paponov, I. A. et al. Comprehensive transcriptome analysis of auxin responses in *Arabidopsis*. *Mol. Plant* **1**, 321–337 (2008).
36. Siligato, R. et al. MultiSite Gateway-compatible cell type-specific gene-inducible system for plants. *Plant Physiol.* **170**, 627–641 (2016).
37. Smetana, O. et al. High levels of auxin signalling define the stem-cell organizer of the vascular cambium. *Nature* **565**, 485–489 (2019).
38. Brady, S. M. et al. A high-resolution root spatiotemporal map reveals dominant expression patterns. *Science* **318**, 801–806 (2007).
39. Yadav, R. K., Girke, T., Pasala, S., Xie, M. & Reddy, G. V. Gene expression map of the *Arabidopsis* shoot apical meristem stem cell niche. *Proc. Natl Acad. Sci. USA* **106**, 4941–4946 (2009).
40. Yadav, R. K., Tavakkoli, M., Xie, M., Girke, T. & Reddy, G. V. A high-resolution gene expression map of the *Arabidopsis* shoot meristem stem cell niche. *Development* **141**, 2735–2744 (2014).
41. Oh, S., Park, S. & van Nocker, S. Genic and global functions for Paf1C in chromatin modification and gene expression in *Arabidopsis*. *PLoS Genet.* **4**, e1000077 (2008).
42. Willing, E.-M. et al. Genome expansion of *Arabidopsis alpina* linked with retrotransposition and reduced symmetric DNA methylation. *Nat. Plants* **1**, 14023 (2015).
43. Deal, R. B. & Henikoff, S. A simple method for gene expression and chromatin profiling of individual cell types within a tissue. *Dev. Cell* **18**, 1030–1040 (2010).
44. You, Y. et al. Temporal dynamics of gene expression and histone marks at the *Arabidopsis* shoot meristem during flowering. *Nat. Commun.* **8**, 15120 (2017).

45. Lafos, M. et al. Dynamic regulation of H3K27 trimethylation during *Arabidopsis* differentiation. *PLoS Genet.* **7**, e1002040 (2011).
46. Sullivan, A. M. et al. Mapping and dynamics of regulatory DNA and transcription factor networks in *A. thaliana*. *Cell Rep.* **8**, 2015–2030 (2014).
47. Lu, Z., Hofmeister, B. T., Vollmers, C., DuBois, R. M. & Schmitz, R. J. Combining ATAC-seq with nuclei sorting for discovery of cis-regulatory regions in plant genomes. *Nucleic Acids Res.* **45**, e41 (2017).
48. Maher, K. A. et al. Profiling of accessible chromatin regions across multiple plant species and cell types reveals common gene regulatory principles and new control modules. *Plant Cell* **30**, 15–36 (2018).
49. Sijacic, P., Bajic, M., McKinney, E. C., Meagher, R. B. & Deal, R. B. Changes in chromatin accessibility between *Arabidopsis* stem cells and mesophyll cells illuminate cell type-specific transcription factor networks. *Plant J.* **94**, 215–231 (2018).
50. Thorvaldsdóttir, H., Robinson, J. T. & Mesirov, J. P. Integrative Genomics Viewer (IGV): high-performance genomics data visualization and exploration. *Brief. Bioinform.* **14**, 178–192 (2013).
51. Robinson, J. T. et al. Integrative genomics viewer. *Nat. Biotechnol.* **29**, 24–26 (2011).
52. Khan, A. et al. JASPAR 2018: update of the open-access database of transcription factor binding profiles and its web framework. *Nucleic Acids Res.* **46** (D1), D260–D266 (2018).
53. Weirauch, M. T. et al. Determination and inference of eukaryotic transcription factor sequence specificity. *Cell* **158**, 1431–1443 (2014).
54. Berger, N., Dubreucq, B., Roudier, F., Dubos, C. & Lepiniec, L. Transcriptional regulation of *Arabidopsis* LEAFY COTYLEDON2 involves RLE, a cis-element that regulates trimethylation of histone H3 at lysine-27. *Plant Cell* **23**, 4065–4078 (2011).
55. Yu, C.-P., Lin, J.-J. & Li, W.-H. Positional distribution of transcription factor binding sites in *Arabidopsis thaliana*. *Sci. Rep.* **6**, 25164 (2016).
56. Goda, H. et al. The AtGenExpress hormone and chemical treatment data set: experimental design, data evaluation, model data analysis and data access. *Plant J.* **55**, 526–542 (2008).

Acknowledgements We thank F. Besnard, A. Larriue and R. Azais for their help with data analysis and statistics; M. Herpola for RNA in situ hybridization analysis; G. Castiglione for help with root phenotyping; A. Mathelier for help with JASPAR; and D. Weijers for ARF transcriptional reporter lines. This work was supported by a joint INRA/University of Nottingham PhD grant to J.T.; ANR-2014-CE11-0018 grant and Human Frontier Science Program organization (HFSP) grant RPG0054-2013 to T.V.; a Royal Society University Research Fellowship and enhancement award (UF110249 and RGF\EA\180308) to A.B.; a starting grant from the Programme Avenir Lyon Saint Etienne (ANR-11-IDEX-0007) to F.R.; an HHMI Faculty Scholar fellowship to S.M.B.; ANR-10-LABX-49-01 and ANR-17-EURE-0003 to F.P.; ANR-18-CE12-0014-02 to T.V., F.R. and F.P.; and Aux-ID CNRS PICS grant to T.V., A.B. and E.F.

Author contributions A.B. and T.V. designed the study and supervised the work; J.T., F.P., F.R., E.F., S.M.B., A.B. and T.V. designed the experiments; J.T., A.-M.B. and M.E.S. performed the eY1H screen with the help of S.P. and M.B.; J.T., J.H., E.C., C.S.G.-A., S.L. and G.B. performed all experiments in relation to TF biological activity characterization; J.L. performed the statistical analysis of the protoplast experiment and participated in all statistical analysis; O.S. and A.P.M. performed the in situ hybridization experiments; A.S. and F.P. performed TF binding site analysis; S.B. and E.F. performed the modelling analysis; J.M. and F.R. performed the epigenetic data analysis; all authors were involved in data analysis; J.T., A.B. and T.V. wrote the manuscript with inputs from all authors.

Competing interests The authors declare no competing interests.

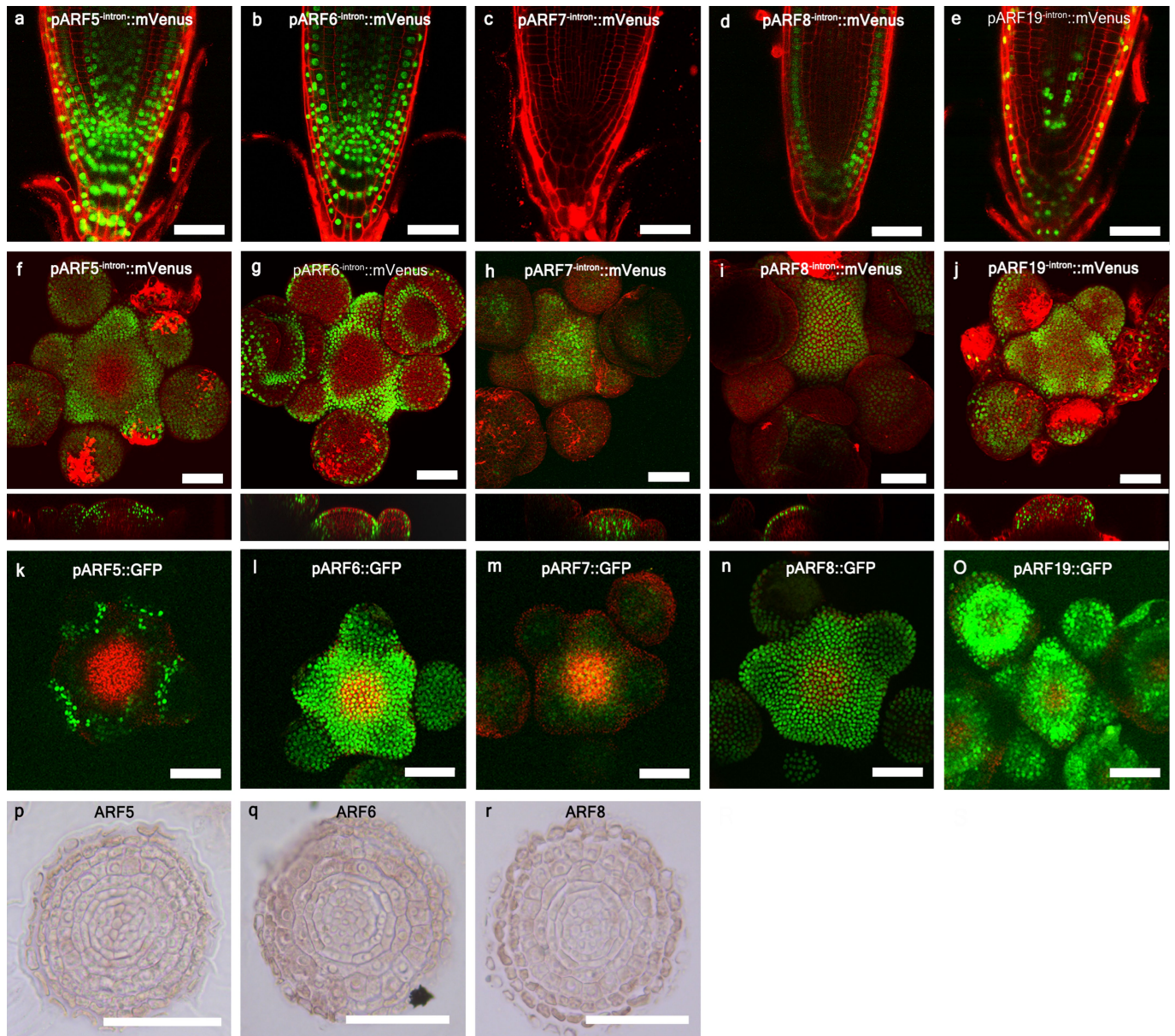
Additional information

Supplementary information is available for this paper at <https://doi.org/10.1038/s41586-020-2940-2>.

Correspondence and requests for materials should be addressed to A.B. or T.V.

Peer review information *Nature* thanks the anonymous reviewer(s) for their contribution to the peer review of this work.

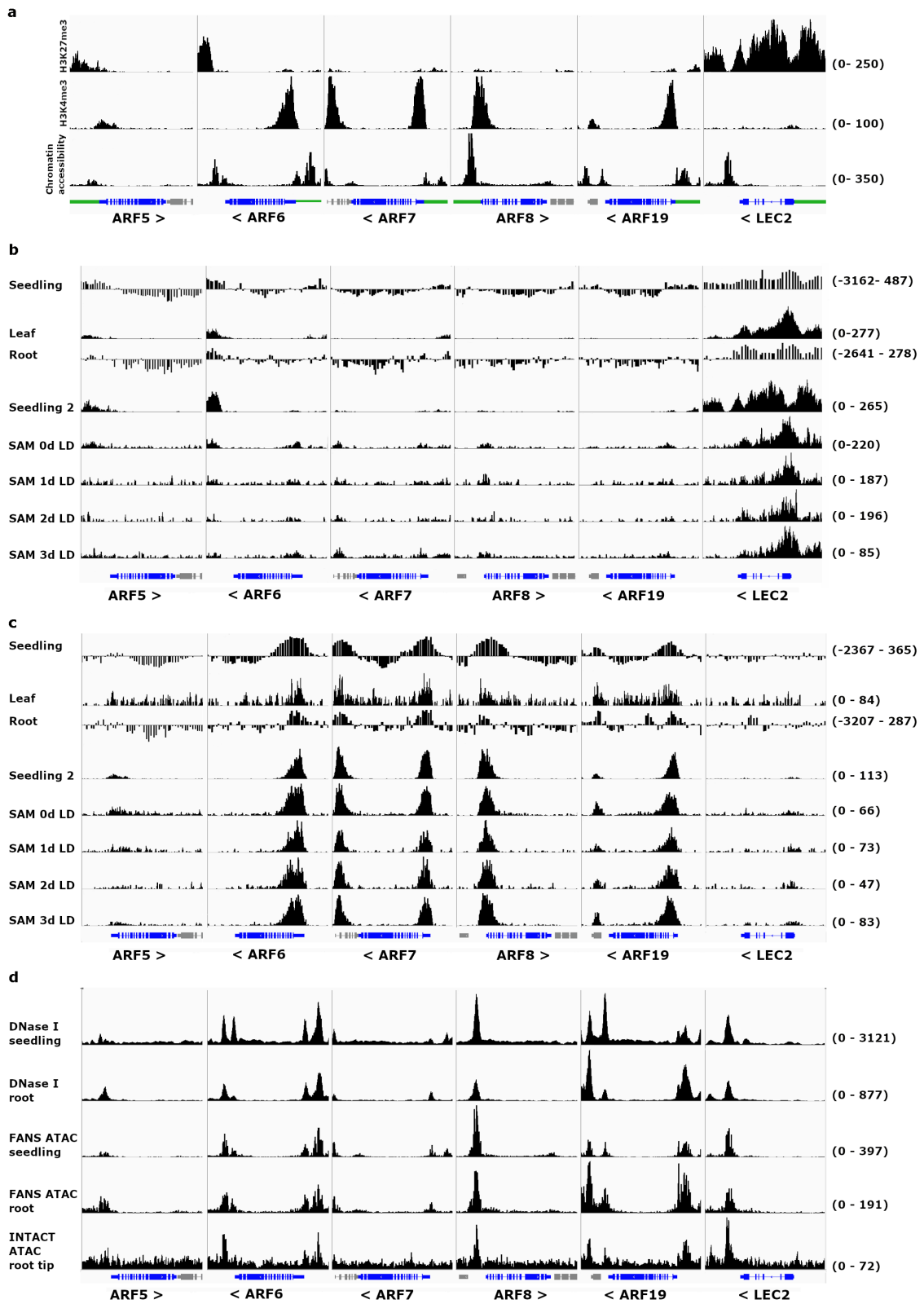
Reprints and permissions information is available at <http://www.nature.com/reprints>.



Extended Data Fig. 1 | Analysis of class A ARF expression in the RAM and the SAM using transcriptional reporter lines and in situ hybridization.

a–j, Confocal images showing expression of *ARF5* (**a, f**), *ARF6* (**b, g**), *ARF7* (**c, h**), *ARF8* (**d, i**) and *ARF19* (**e, j**) in the RAM and the SAM using promoters that lack sequences downstream of the start codon but contain the long upstream sequences (*pARF^{-intron}::mVenus*) (–3 kb for *ARF6* and *ARF7*; 5 kb for *ARF5*, *ARF8* and *ARF19*) (see Methods). For SAM images (**f–j**) an orthogonal projection is shown below to provide information about expression in different layers. **k–o**, For comparison, the expression of each class A *ARF* gene in the SAM using the previously published *pARF::GFP* lines with shorter (–2 kb) promoters containing sequences upstream of the start codon is shown in panels **k–o**¹⁴.

ARF5 (**k**), *ARF6* (**l**), *ARF7* (**m**), *ARF8* (**n**) and *ARF19* (**o**). (**p–r**) In situ hybridizations through the RAM for *ARF5* (**p**), *ARF6* (**q**) and *ARF8* (**r**). Note that expression patterns of the class A *ARF* reporters (**a–j**) differ from those with shorter (2 kb) promoters (**k–o**¹⁴) and recapitulate the patterns observed with RNA in situ hybridization (**p–r**; ref.¹⁶). This was particularly clear in the shoot for *ARF5* and *ARF6*. Shorter promoters drive GFP expression mostly in flower boundaries for *ARF5* and throughout the meristem for *ARF6*, in contrast with detection of both genes throughout the periphery of the meristem both with longer promoters (**k–o**; also Fig. 1f–j) or using in situ hybridization¹⁵. Experiments were done three (**a–e**) and two times (**f–r**). Scale bars: 50 μm.

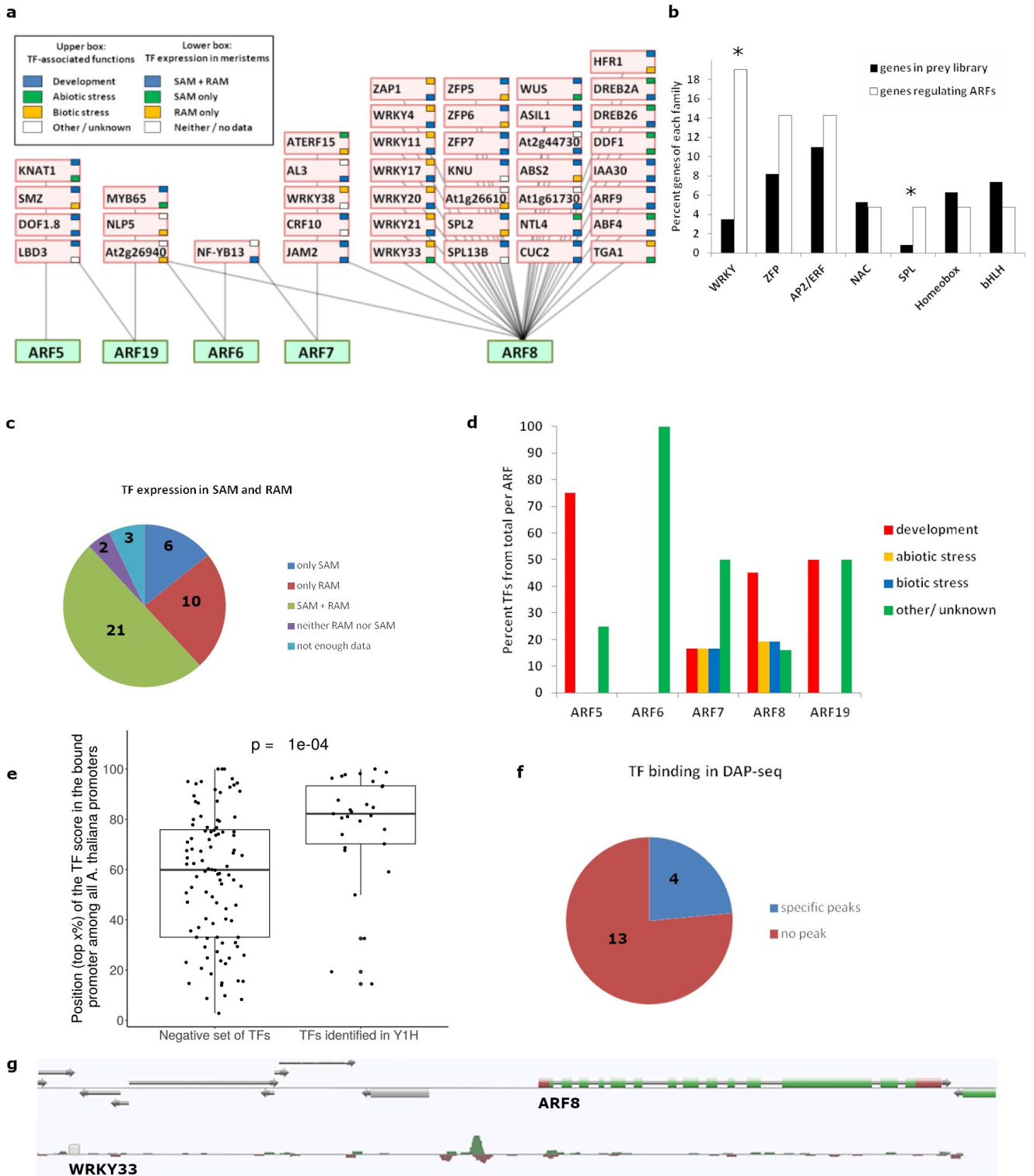


Extended Data Fig. 2 | See next page for caption.

Article

Extended Data Fig. 2 | Distribution of the repressive chromatin marker H3K27me3, the active chromatin marker H3K4me3 and chromatin accessibility at class *AARF* loci. **a**, Chromatin landscape of class *AARF* and *LEC2* in whole seedlings illustrating the chromatin status of class *AARF* loci. Repressive H3K27me3 marker (top row), active H3K4me3 marker (middle row) and FANS-ATAC chromatin accessibility (bottom row; see Supplementary Table 1). **b, c**, Chromatin landscape of class *AARF* and *LEC2* loci showing distribution of the repressive chromatin marker H3K27me3 (**a**) and the active chromatin marker H3K4me3 (**b**) in various tissues. Seedling, whole seedlings¹⁷; leaf, rosette leaves⁴²; root, whole roots¹⁷; seedling 2, whole seedlings⁴⁴; SAM, shoot apical meristems after 0, 1, 2 or 3 d in long-day conditions⁴⁴. Gene models are shown below with arrowheads indicating direction of transcription. **d**, The chromatin landscape of class *AARF* and *LEC2* loci showing chromatin

accessibility in various tissues. DNaseI-seq seedling: DNase I hypersensitive sites in whole seedling⁴⁶; DNaseI-seq root: DNase I hypersensitive sites in root⁴⁶; FANS-ATAC seedling: FANS-ATAC accessible regions in whole seedling⁴⁷; FANS-ATAC roots: FANS-ATAC accessible regions in roots⁴⁷; INTAC-ATAC root tip: INTACT-ATAC transposase hypersensitive sites in root tips⁴⁸. The *LEC2* locus is included as a negative control for H3K4me3 marking and chromatin accessibility, and as a positive control for H3K27me3 marking⁵⁴. The y axis scales (at right) show the minimum and maximum number of reads represented in each windows of the same row, except for the data set related to ref.¹⁷, for which the data range corresponds to the IP/INPUT value of the ChIP-chip experiments. For the x axis the window size is fixed at 8.5 kb and centred on the gene of interest (gene model in blue below each column, 5' sequences in green), with arrowheads by the gene name showing the direction of the locus.

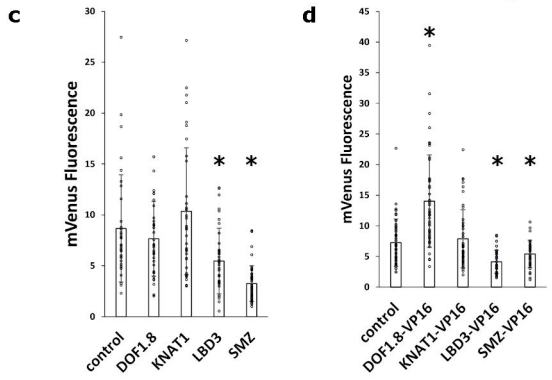
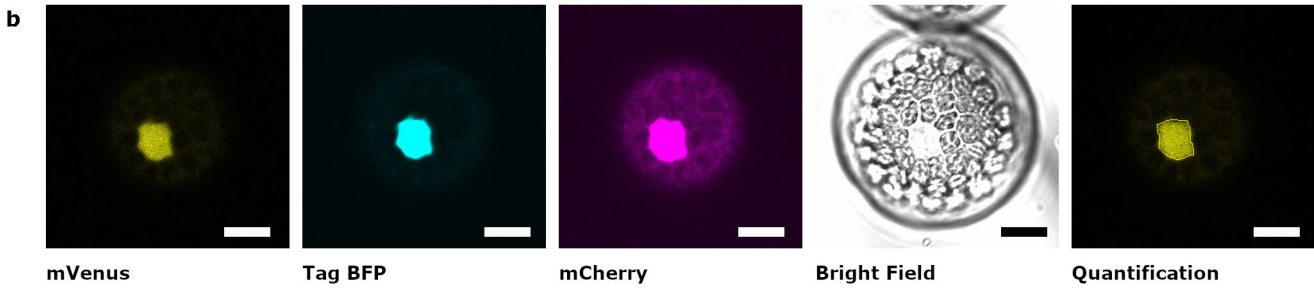
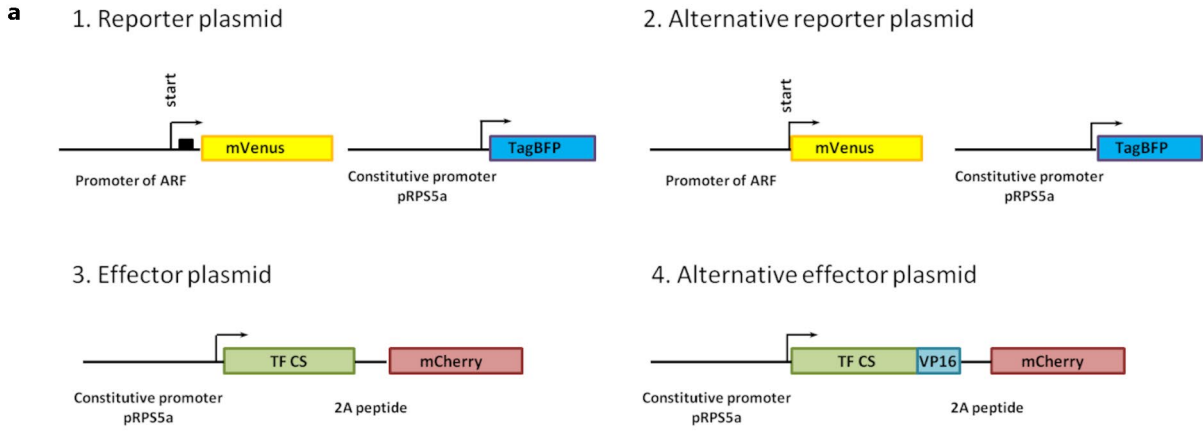


Extended Data Fig. 3 | See next page for caption.

Article

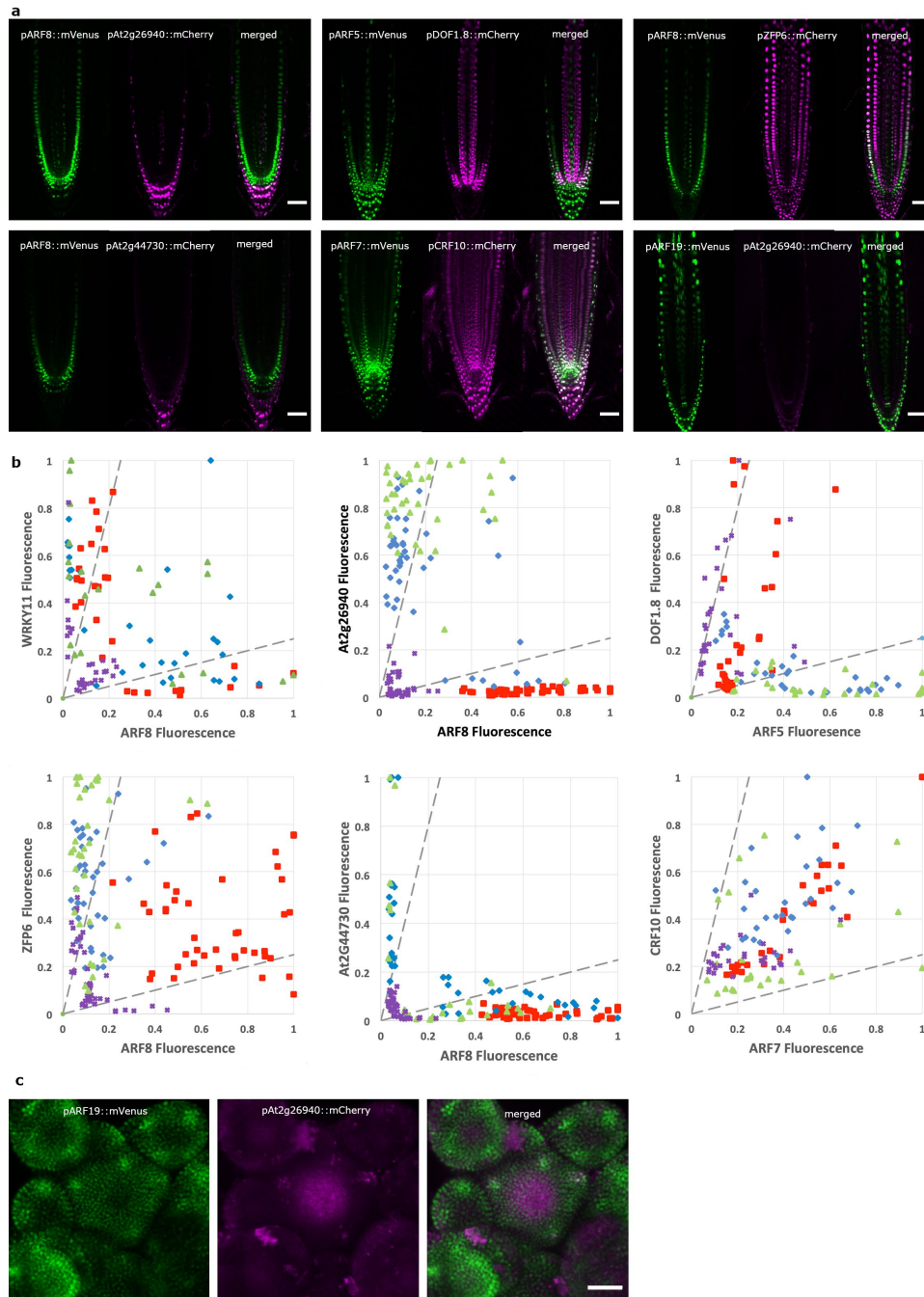
Extended Data Fig. 3 | Characterization of the TFs and TF binding sites that regulate class A *ARF* expression. **a**, Yeast one-hybrid promoter–transcription factor interaction network for class A *ARF* genes. Green boxes correspond to the class A *ARF*; pink boxes are transcription factors binding to the *ARF* promoters. TF-associated functions and expression analysis are indicated in the upper and lower small boxes and colour-coded as indicated in the key. Note that when two promoter fragments were used for the screen (see Methods), 35 out of 36 regulators bound to the more proximal fragment, supporting previous observations that the majority of transcription factor binding sites reside within a few kb of the transcriptional start site³⁵. **b**, Frequency of TF gene families in the Y1H library collection (black) and in the Y1H network (white). Only families represented by at least two members in the Y1H network were analysed. The network is overrepresented with members of the WRKY and SPL TF families. Statistical analysis: hypergeometric test significant to 5% (*; $P=4e-05$ for WRKY family and $P=0.044$ for SPL family). Sample sizes for TFs in Y1H library in black/Y1H network in white: $n=29/8$ TFs (WRKY); $n=68/6$ (ZFP); $n=91/6$ (AP2/ERF); $n=44/2$ (NAC); $n=7/2$ TFs (SPL); $n=52/2$ TFs (homeobox); $n=61/2$ TFs (bHLH). **c**, TF expression in the RAM³⁸ and the SAM^{39,40}. 50% of the identified TFs are expressed in both shoots and roots, whereas 24% and 14% are expressed specifically in roots or shoots respectively. **d**, Known functions of the TFs in the Y1H network based on a literature search

(see also Supplementary Table 2). **e**, Boxplot representation of the distribution of class A *ARF* promoter ranks. For TFs with established binding models, we ranked class A *ARF* promoters among all *Arabidopsis* promoters based on the score of the predicted TF binding sites. We repeated the same operation with a set of randomly chosen TFs from different families (see Methods). The comparison of rank distributions with those of a set of randomly chosen TFs from different families revealed significantly higher ranks for eY1H-identified TFs (see also Supplementary Table 3). Statistical analysis: one-sided t -test. Sample sizes: $n=29$ for eY1H-selected TFs and $n=100$ for randomly selected TFs. Data are represented as boxplots where the middle line is the median, the lower and upper hinges correspond to the first and third quartiles, the upper whisker extends from the hinge to the largest value no further than $1.5\times$ interquartile range (IQR) from the hinge and the lower whisker extends from the hinge to the smallest value at most $1.5\times$ IQR of the hinge. All the individual values are plotted. **f**, Summary of the DAP-seq analysis for the 17 TFs (see also Supplementary Table 3). **g**, Example of DAP-seq data, here a DAP-seq peak for WRKY33 in the promoter of *ARF8*. DAP-seq (**f, g**) thus confirms experimentally inferred bindings (**e**) for 4 of the 17 (24%) TFs for which DAP-seq data are available (see also Supplementary Table 3). Note also that chromatin immunoprecipitation sequencing (ChIP-seq) confirms the binding of WUSCHEL to the *ARF8* promoter²¹.



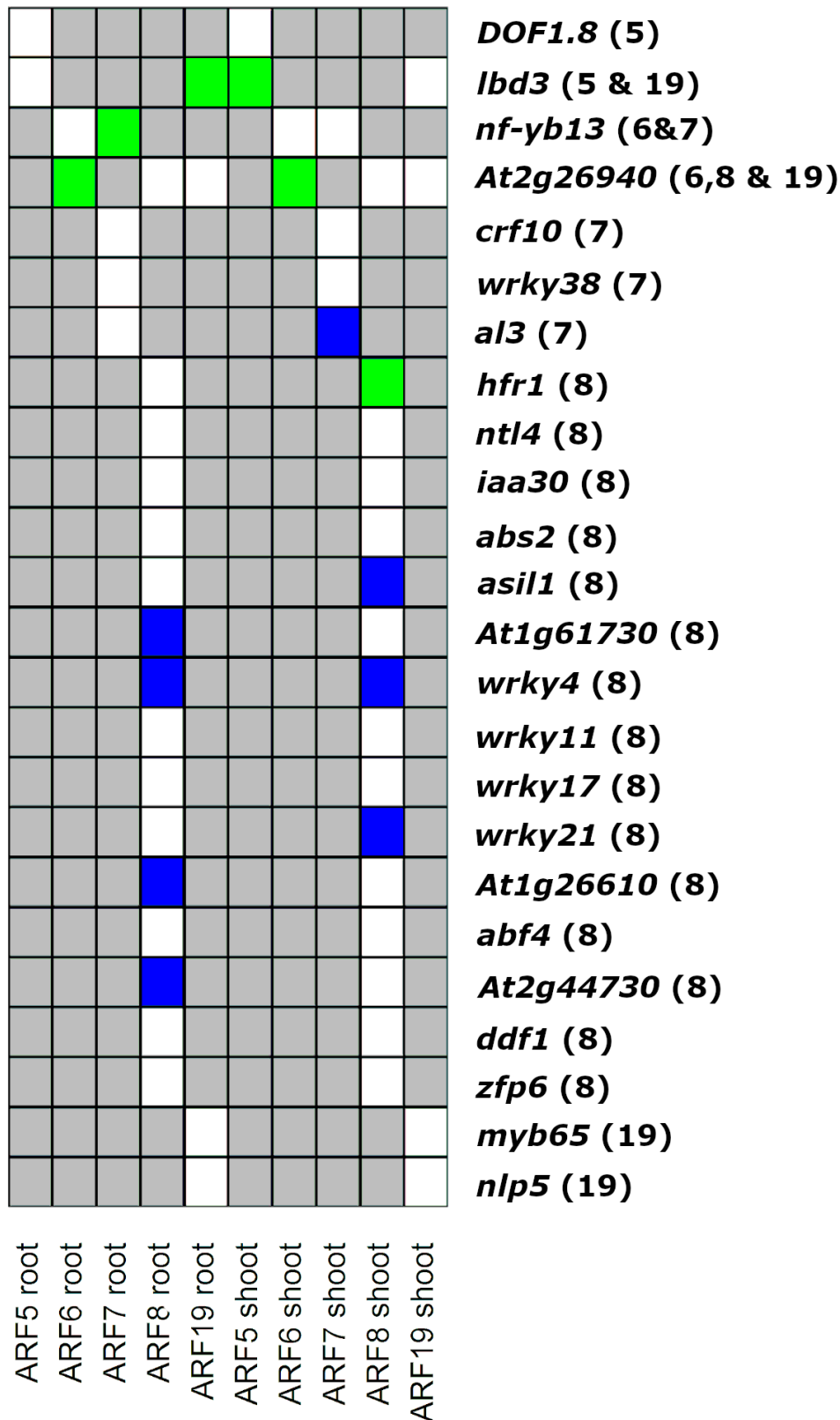
Extended Data Fig. 4 | Methodology used for the transient protoplast assay. **a**, Design of the standard reporter plasmid containing sequences upstream and downstream of the *ARF* promoter including the first intron (1), the alternative reporter plasmid containing only sequences upstream of the *ARF* promoter (2), the standard effector plasmid (3), and an alternative effector plasmid containing the VP16 domain fused to the TF coding sequence (4). **b**, Example of a nucleus of a transformed living protoplast imaged with confocal microscopy with channels for mVenus, TagBFP, mCherry and bright-field. The presence of TagBFP and mCherry specifically in the nucleus is used as a transformation control and as a test of viability of the protoplasts. Quantification: definition of the nucleus as a region of interest using ImageJ to

quantify fluorescence (see also Methods). Measurements were conducted in at least 4 independent experiments for each TF (minimum of 2 experiments for TF alone and 2 experiments for TF fused to VP16 domain). Scale bars, 10 μ m. **c, d**, Example of results using the *ARF5* reporter plasmid, with **(c)** and without **(d)** the VP16 activator domain fused to the TF coding sequence (left and right). Error bars, mean \pm s.d.; statistical analysis, one-sided Mann-Whitney *U*-test with $P \leq 0.05$ (*); *N* of protoplasts (*P* values): **(c)** control, *n* = 35; DOF1.8, *n* = 38 (0.33); KNAT1, *n* = 37 (0.11); LBD3, *n* = 38 (6e-04); SMZ, *n* = 43 (3e-10); **(d)** control, *n* = 43 (1e-07); DOF1.8-VP16, *n* = 46; KNAT1-VP16, *n* = 44 (0.37); LBD3-VP16, *n* = 32 (1e-05); SMZ-VP16, *n* = 39 (0.015).



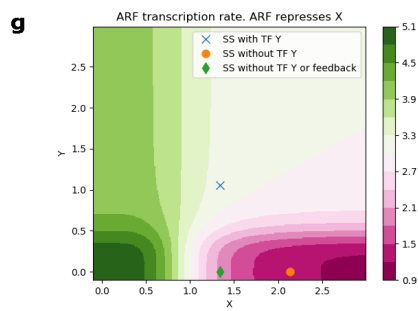
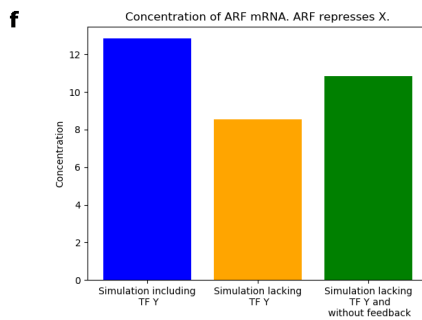
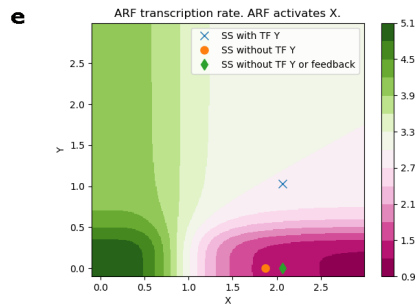
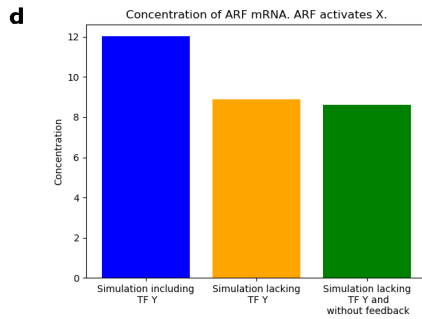
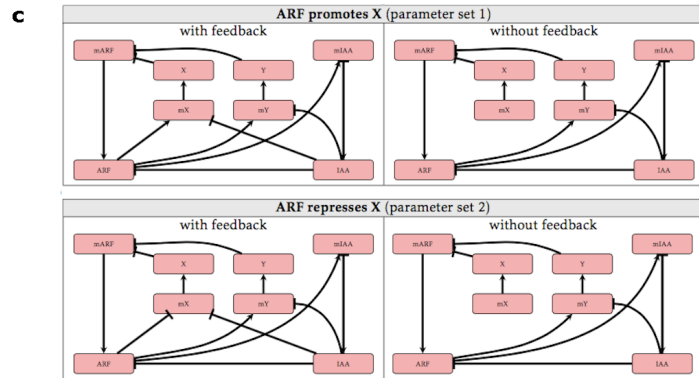
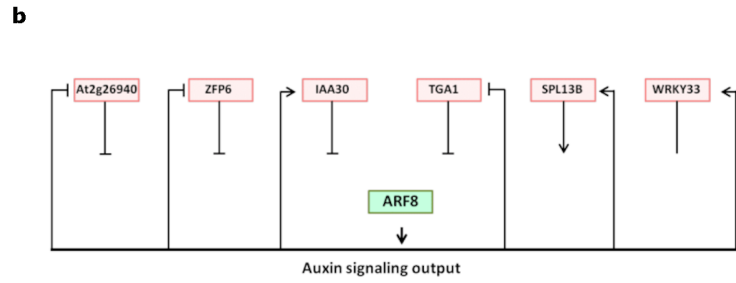
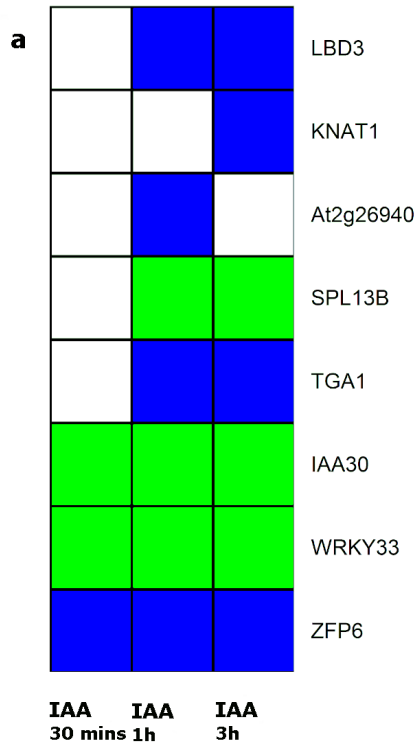
Extended Data Fig. 5 | *ARF* transcriptional regulators mostly show complementary expression patterns to their target *ARFs*. **a**, Plants carrying the *ARF* transcriptional reporters were transformed with transcriptional reporters for a subset of *ARF* regulators driving mCherry. For five out of seven constructs (see also Fig. 3), we saw complementary patterns of expression between transcriptional repressors and their *ARFs* in the root. **b**, To further quantify the complementarity of TF versus *ARF* expression, we quantified the red versus green fluorescence levels in individual nuclei from different cell types (root cap, blue diamond; columella, green triangle; epidermis, red square; vascular cells, purple cross). These values were normalized so that the brightest nucleus of each channel in each line was set to 1, and values were plotted onto scatter plots. Any value falling outside the reference lines shows a $>4\times$ bias for expression of either TF or *ARF* ($n = 3$ for *pAT2G26940::mCherry*

and *pAT2G44730::mCherry* in *pARF8::mVenus*; $n = 2$ for the remaining genotypes). In some cases there was clear complementarity in some cell types but not others. For example, *ZFP6* shows complementary expression patterns in the root cap, epidermis and columella but overlaps with *ARF8* in the vascular tissues. **c**, Analysis of *At2g26940* expression in the SAM, where it was found in organ primordia and weakly in the centre of the SAM; no clear expression was observed in roots. As previously observed with other developmental and hormonal regulators^{22,23}, co-localization of repressors and their target *ARF* occurs in some cells as in the case of *ZFP6/ARF8* in the root epidermis (**a, b**) and *At2g26940/ARF19* in shoot organ primordia (**c**), suggesting potential regulatory interactions to modulate transcription levels. Scale bars, 60 μm (**a**) and 40 μm (**c**). Experiments were done twice (**a, c**).



Extended Data Fig. 6 | Expression of class A ARF in mutants for the regulatory transcription factors. Expression of class A ARF in 24 mutants of the regulatory TFs measured with qRT-PCR, in whole root and whole shoot tissue of 7-d-old seedlings. Green boxes indicate statistically significant upregulation of the corresponding ARF in the mutant background compared to

wild-type control, and blue boxes indicate statistically significant downregulation. Statistical analysis was performed using a one-sided Mann-Whitney test and a threshold at $P \leq 0.1$. For simplicity, only the interactions predicted by the YIH are shown, with other combinations shaded with a grey box. The full data set is available in Supplementary Table 6.

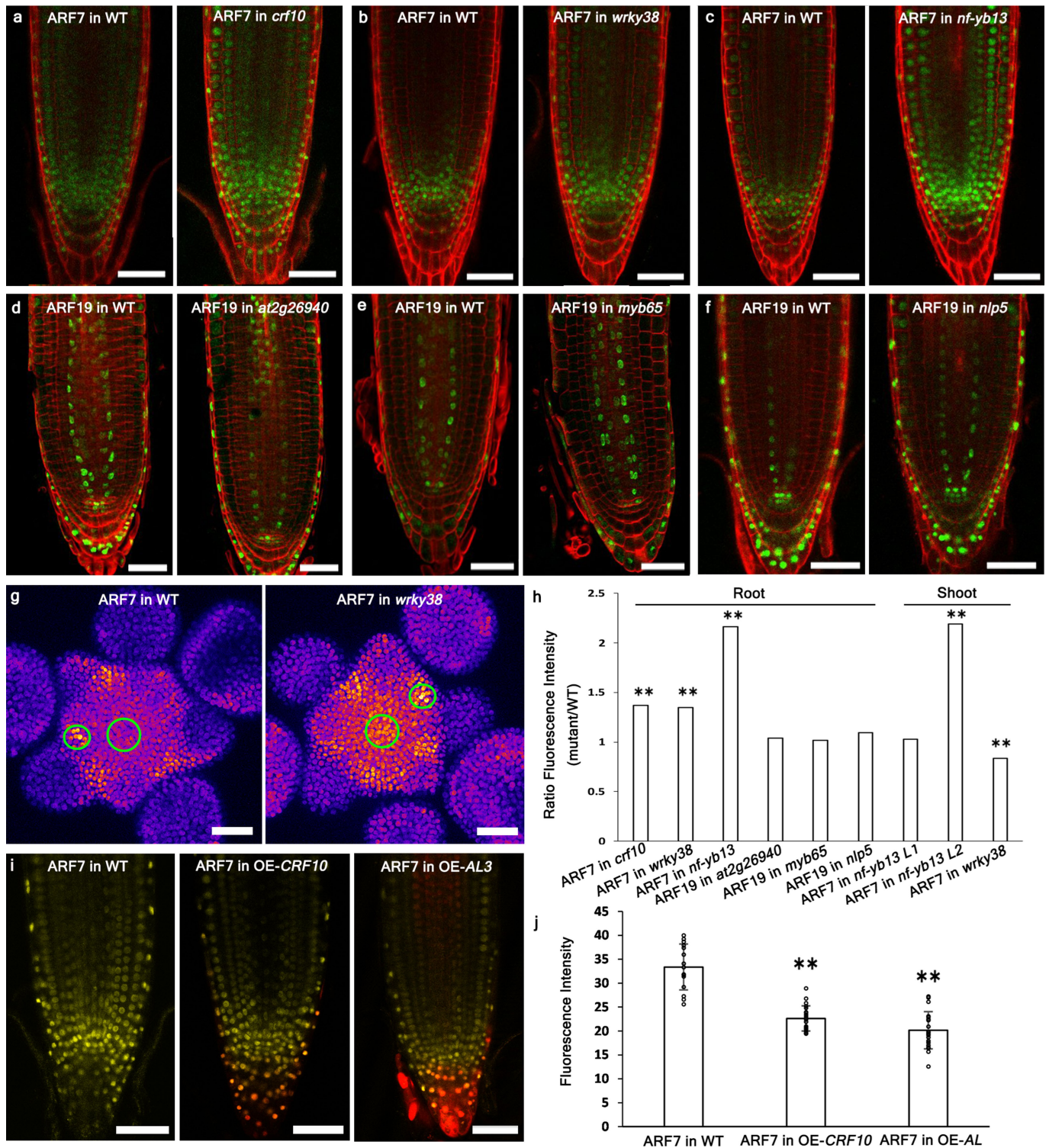


Extended Data Fig. 7 | See next page for caption.

Extended Data Fig. 7 | Feedback regulations between the transcription factors and auxin signalling. **a**, Expression of several TFs are regulated by auxin, which provides feedback regulation from auxin signalling output primarily on *ARF8* expression. Expression was measured after treatment with 1 μ M IAA for 30 min, 1h or 3h⁵⁶. Green boxes indicate upregulation, blue boxes indicate downregulation of gene expression compared with a mock treatment. **b**, Schematic representation of *ARF8* regulation with feedbacks. Feedback from auxin signalling on regulatory TFs is expected to induce complex nonlinear regulation of *ARF8* expression (see also Supplementary Note 2). **c**, Diagrammatic representation of the interactions taking place for different

instances of model analysed in Supplementary Note 2. The two diagrams on the right (without feedback) are identical. However, for comparison with the models with feedback the parameters used for these differ (see Supplementary Note 2). **d-g**, left, bar chart displaying concentrations before and after knock out of transcription factor X, where Y is activated (**d**) or repressed (**f**) by ARF. Right, contour plot displaying ARF transcription rate before and after knock out of transcription factor X relative to Y and X populations, where Y is activated (**f**) or repressed (**g**) by ARF. Steady-state (SS) values corresponding to the bar plot are also reported. These results are discussed in Supplementary Note 2.

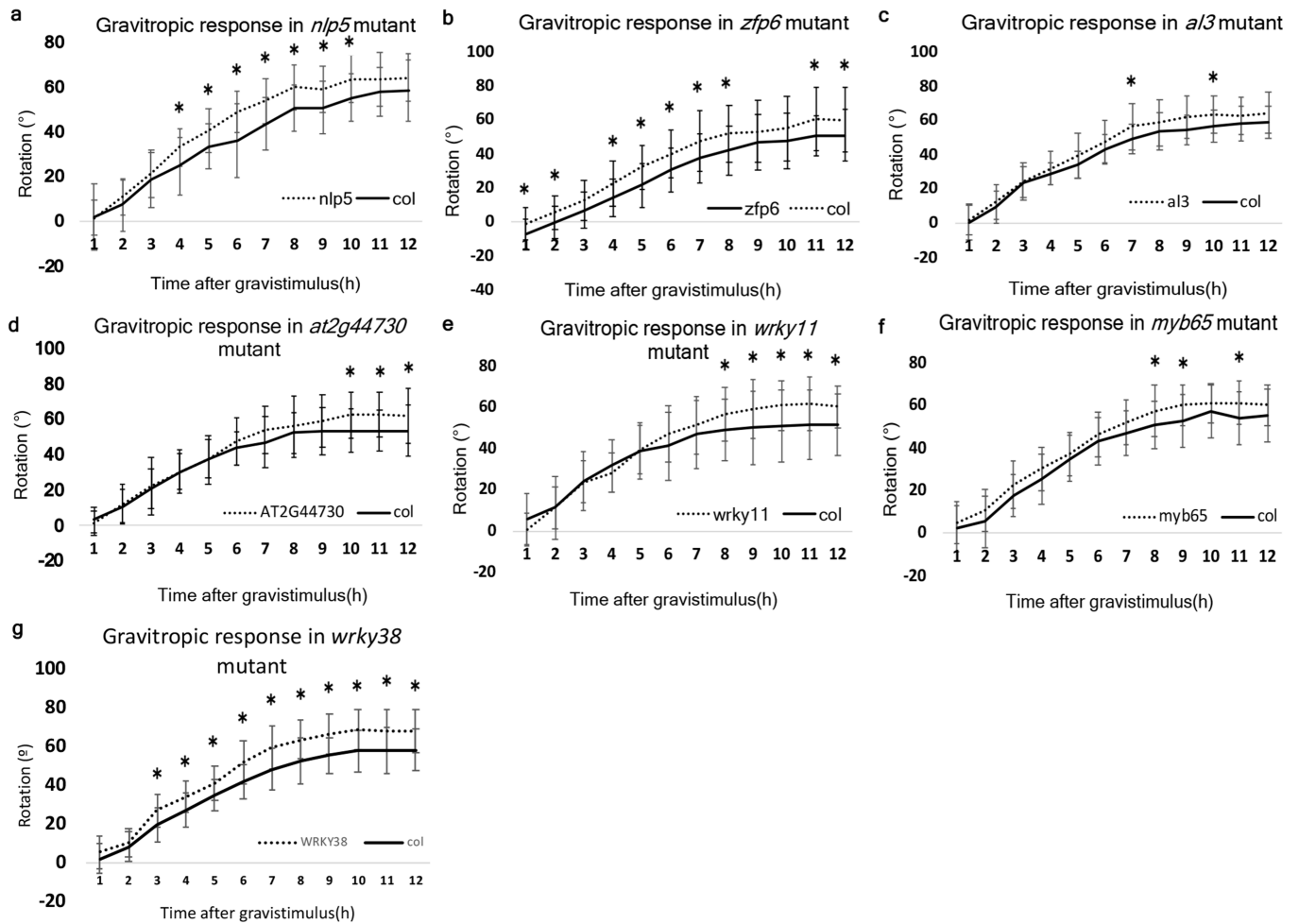
Article



Extended Data Fig. 8 | See next page for caption.

Extended Data Fig. 8 | Modulating the levels of ARF transcriptional regulators regulates the expression of associated ARFs. **a–f**, Comparison of ARF expression in wild-type versus mutants in roots. **g**, Comparison of *pARF7::VENUS* expression in wild-type versus *wrky38* shoot. For quantification (see **f**), fluorescence was measured in the central zone and primordia 2 (green circles). **h**, Quantification of fluorescence changes shown as relative changes in mean fluorescence level in mutant compared to wild type (single value). Quantifications are shown for **a–g** and for Fig. 3c,d. In roots, the total *pARF7/19*-driven fluorescent signal was quantified within a standardized zone covering the stele meristem zone and quantified relative to the wild-type controls. In the shoot, L1 and L2 correspond to quantification in the corresponding layers in the SAM of wild-type and *nf-yb13* (see also Fig. 3c, d). Quantification demonstrated a significant change in pattern in *wrky38* mutant SAMs (**g**), with an increase of *pARF7* activity in the centre and a loss of the differential expression between the SAM centre and lateral organs. Statistical analysis:

unpaired two-sided *t*-test with $P \leq 0.01$ (**). Number of samples observed and quantified: for mutant/wild type roots, 13/13 for *crf10*, 12/14 for *wrky38*, 9/9 for *nf-yb13*, 9/8 for *At2g26940*, 12/11 for *myb65*, 12/10 for *nlp5*; 7 shoots for *nf-yb13* and wild-type controls; 7 shoots for *wrky38* and 6 wild-type controls. *P* values from left to right: 0.003, 2e-05, 3e-08, 0.26, 0.57, 0.11, 0.84, 0.007, 0.009. Raw data are provided in Supplementary Table 11. **i**, Inducible constitutive overexpression of *CRF10:mCherry* and *AL3:mCherry* in the *pARF7::VENUS* line. *pARF7::VENUS* is shown in yellow and the transcription factors fused to mCherry in red following a 24h induction with β -oestradiol. **j**, Both lines shown in **i** show a significant reduction in *pARF7::VENUS* expression. Unpaired two-sided *t*-test: $P = 4e-10$ (*CRF10*) and $2e-10$ (*AL3*). Number of plants: wild-type control, $n = 15$; *CRF10*, $n = 21$; *AL3*, $n = 20$. Error bars: mean \pm s.d.. Scale bars: 45 μ m for root images; 50 μ m for shoot images. For each analysis, the confocal settings were identical in the compared genetic backgrounds. All experiments were done two times.



Extended Data Fig. 9 | Mutations in transcriptional regulators of class A ARF genes accelerate the root gravitropic response. a–g. Kinetics of perturbed gravitropic responses of TF mutants (dashed line) compared to wild-type (solid line) over 12 h after application of the gravitational stimulus. Mutants with statistically significant difference in gravitropic response compared to the wild-type are shown: (a) *nlp5*, (b) *zfp6*, (c) *al3*, (d) *at2g44730*, (e) *wrky11*, (f) *myb65* and (g) *wrky38*. Statistical analyses: unpaired two-tailed *t*-test with $P \leq 0.05$ (*). *P* values from 1 h to 12 h (left to right): (a) 0.86, 0.19, 0.37, 0.004, 0.01, 0.0008, 0.0008, 0.001, 0.007, 0.004, 0.06, 0.07; (b) 0.01, 0.02,

0.05, 0.009, 0.002, 0.007, 0.01, 0.01, 0.14, 0.1, 0.01, 0.04; (c) 0.75, 0.25, 0.85, 0.12, 0.07, 0.16, 0.02, 0.1, 0.01, 0.02, 0.1, 0.06; (d) 0.40, 0.50, 0.71, 0.95, 0.86, 0.23, 0.07, 0.36, 0.12, 0.01, 0.009, 0.04; (e) 0.058, 0.97, 0.88, 0.27, 0.81, 0.16, 0.27, 0.04, 0.03, 0.01, 0.01, 0.01; (f) 0.31, 0.07, 0.09, 0.10, 0.45, 0.26, 0.08, 0.04, 0.01, 0.24, 0.02, 0.11. (g) 0.1, 0.26, 0.003, 0.003, 0.007, 0.0003, 0.0003, 0.0004, 8e-05, 0.0002, 0.001 and 0.001. Sample sizes (WT/mutant plants): (a) $n = 29/29$, (b) $n = 32/32$, (c) $n = 28/30$, (d) $n = 28/26$, (e) $n = 30/29$, (f) $n = 30/28$, (g) 29/30. Raw data are provided in Supplementary Table 12. Error bars: mean \pm s.d.

2. Methods

2.1 Material

24 T-DNA insertion mutants were obtained from NASC. The gene expression level in mutant background were checked by qRT-PCR and mutants were confirm to be homozygous. These experiments were done by Jekaterina Triskina (UoN/ENS de Lyon, Anthony Bishopp and Teva Vernoux's groups).

pARF-mVenus transcriptional reporter line was made by Jekaterina Triskina. ARF5 promoter concluded 5418bp 5'UTR upstream and 134bp downstream sequences. ARF6 promoter concluded -3255 to +197 bp. ARF7 promoter concluded -2973 bp to + 374 bp. ARF8 promoter concluded -5091 to + 42 bp. ARF19 promoter concluded -4906 to + 452 bp. *ARF5*, *6*, *8* and *19* fragments cloned into pDONR P4-P1R and recombined with a nuclear-localized mVenusN7 OCS terminator pDONR P2R-P3 and pK7m34GW to produce pARF-3x mVenus constructs. *ARF7* fragment was cloned into a pCR8/GW/TOPO and recombined with mVenusN7, 35S terminator and pK7m34GW to produce pARF7-mVenusN7 construct. The destination vector containing selection kanamycin resistance gene for in planta selection

2.2 Root phenotype analysis of TF mutants

For root length analysis, plants were grown on 1/2 Murashige and Skoog (MS) medium supplemented with 1% agar or 1/2 MS medium supplemented with 10 μ M IAA and 1% agar in 12h light/ 12h dark conditions. The mutant and Col-0 plants were grown in same plate to limit variation. The images for root length measurement were taken at 5, 10 and 15 days in light.

For gravitropic analysis, plants were grown on 1/2 MS medium supplemented with 1% agar in 12h light/ 12h dark conditions for 5 days. At the end on the 12h light period they were turned by 90° and imaged every 1 hour for the next 12h hours in the dark with an infrared camera. Again, the mutant and Col-0 plants were grown on the same plate.

The root length and the tip angle were measured via RootNav. Two-tail T-test

was used to test for statistical significance, and $p \leq 0.05$ was considered to be significant.

2.3 Inducible overexpression of TFs

Multisite Gateway cloning technology was used to generate 15 inducible TF overexpression lines. The chimeric transcription activator, XVE, expressed under UBQ10 promoter were inserted into pDONR P4-P1R and recombined with TF coding sequence (lacking STOP codon) in pDONR211 and the 2A-mCherry-term pDONR P2R-P3 (containing the self-cleaving 2A peptide followed by mCherry coding sequence, a NLS and a nosT terminator) and pB7m34GW (the destination vector containing basta resistance gene for in planta selection) to produce pUBQ10-XVE-TF-2A-mCherry estradiol-inducible constructs. These constructs were made by Jekaterina Truskina.

I transformed these constructs in *Agrobacterium tumefaciens* GV3101 via electroporation and transformed into the pARF7-mVenus transcriptional reporter line background via floral dip method. For selection of transgenic plant, *Arabidopsis* T1 seeds were plated on 1% agar containing 1/2 MS medium and 20 $\mu\text{g}/\text{mL}$ phosphinothricin. After a 2d stratification period, seeds grew in 21°C with 6 h light, 48 h dark and 24 h light (Harrison et al., 2006).

For the overexpression analysis, plants were grown for 5 days on 1/2 MS medium, then plants transferred to 1/2 MS medium with 10 μM β -estradiol for 24h induction. Roots were imaged using the TCS-SP8 (Leica) confocal microscope, with excitation at 514 nm and emission at 526-560 nm for mVenus and excitation and emission at 587nm and 610-670nm respectively for mCherry. The fluorescent intensity of ARF was measured via Fiji. T-test was used to test for statistical significance, and $p \leq 0.05$ was considered to be significant.

Chapter 2

1. Manuscript

The novel Dual Expression Anatomy Lines (DEAL) Vector System allows simultaneous visualization of gene expression and anatomical features during live imaging of Arabidopsis roots.

Britta MC Kümpers^{1,2}, Jingyi Han¹, John Vaughan-Hirsch^{1,3}, Nicholas Redman¹, Alexander Ware¹, Jonathan A Atkinson¹, Nicola Leftley¹, George Janes¹, Giuseppe Castiglione^{1,4}, Paul T. Tarr⁵, Kevin Pyke¹, Ute Voß¹, Darren M Wells^{1*} and Anthony Bishopp^{1*}

1 School of Bioscience, University of Nottingham, Sutton Bonington Campus, Loughborough, LE12 5RD, UK

2 Currently at: Biosciences, College of Life and Environmental Sciences, University of Exeter, Geoffrey Pope Building, Stocker Road, Exeter EX4 4QD, UK.

3 Currently at: Department of Biosystems, University of Leuven, Leuven, 3001, Belgium.

4 Currently at: Dipartimento di Scienze della Vita, Università degli Studi di Trieste, Via Licio Giorgieri 5, Trieste, 34127, Italy.

correspondance: darren.wells@nottingham.ac.uk and anthony.bishopp@nottingham.ac.uk

ABSTRACT

Studying the developmental genetics of plant organs, requires following gene expression in specific tissues. To facilitate this, we have developed the Dual Expression Anatomy Lines (DEAL) which incorporate a red plasma membrane marker alongside a fluorescent reporter for a gene of interest in the same vector.

Here, we adapted the GreenGate cloning vectors to create two destination vectors showing strong marking of cell membranes in either the whole root or specifically in the lateral roots. As proof of concept, we follow both gene expression and anatomy during lateral root organogenesis for a period of over 24h, and coupled with the development of a flow cell and perfusion system, we follow changes in activity of the DII auxin sensor following application of auxin.

INTRODUCTION

The primary and lateral roots of *Arabidopsis* provide well-studied systems for cell fate acquisition. Proliferative cell divisions in the root meristem lead to a stereotypic anatomical pattern in which a diarch vascular cylinder is surrounded by radially symmetric layers of outer cells (Dolan et al., 1993). Decades of research into the mechanisms underlying cell fate specification have provided us with a broad set of cell-type specific promoters that can be used to investigate identity of individual files. Whilst we have a good understanding of the mechanistic processes through which a selection of cell identities are established, there are gaps in this knowledge relating to either specific cell types or in understanding how these developmental programmes are altered by external stimuli. In addition, anatomical patterning has been well studied in the primary root, but there is much less data over the spatial and temporal control of cell fate specification in the lateral roots. Recent advances in both confocal and light sheet microscopy (Komis et al., 2018; Ovečka et al., 2018) alongside approaches for downstream image analysis have increased our opportunity to follow changes in gene activity over long periods of time, and follow cell fate specification in emerging organs.

Following changes in gene expression patterns over time requires both resolving the temporal and spatial dynamics of genes of interest and superimposing these upon the underlying tissue geometry. Whilst genetically encoded fluorescent proteins provide an obvious choice for visualizing either transcription patterns or domains of protein accumulation, there are a greater number of options available with which to resolve the tissue structure. Transmitted light can be used to reconstruct the outline of organs, but it offers little cellular resolution and is unsuitable for creating 3D representations, as it is not possible to obtain z-stacks.

The most used alternative is to counterstain with a fluorescent dye such as propidium iodide or calcofluor white to mark cell walls, and this approach has become the 'go to' standard approach for many scientists. This method is suitable for fixed time points, but suffers a number of drawbacks. Firstly, such stains tend to be absorbed strongly within membranes of the outer layers (such as epidermis) and penetrate the innermost layers poorly. In addition, in differentiated root tissues, penetration of dyes such as propidium iodide is blocked by the endodermis leading to virtually no staining of the stele cells. In fact, exclusion of propidium iodide from the stele is used as an assay to test for endodermal differentiation (Alassimone et al., 2010). Imaging of deep tissues can be improved by fixing and clearing roots using high refractive index mounting media, such as ClearSee (Kurihara et al., 2015) or pseudo-Schiff propidium iodide (PS-PI) staining (Truernit et al., 2006). These techniques have been modified and used extensively with either fluorescent or GUS reporters (Truernit et al., 2008; Ursache et al., 2018), however due to the invasive process of fixation they are unsuitable for live tissues.

The long-term treatment of Arabidopsis roots needed for live imaging with dyes such as propidium iodide can introduce problems associated with growth and development. Exposure of cells to extended periods at high levels of propidium iodide can render cell membranes vulnerable to permeation. When this occurs, the PI enters the cells and binds to the nucleus preventing its usefulness as a plasma membrane marker. Alternatively, if roots are treated with very low levels the intensity of the PI fades over time, making long term imaging challenging. Genetically encoded fluorescent proteins to mark plasma membranes in a different colour to the gene of interest have been used to create a set of different vectors that can be used to co-visualise anatomical structure whilst following genes of interest, e.g. WAVE lines (Geldner et al., 2009) or fusions between GFP and the Low-Temperature-Inducible protein, Lti6a or 6b, (Cutler et al., 2000; Grebe et al., 2003; Martinière et al., 2012). However, combining such lines with existing reporter lines requires an extensive crossing programme and can delay research by several months.

To facilitate the rapid development of a dual marker system, we incorporated a

reporter for a defined gene of interest with a fluorescent plasma-membrane marker with which to observe root anatomy into a single plasmid. Such a system allows long term imaging of reporters, whilst reducing the labour required to combine them with genetically encoded membrane markers. The associated red membrane marker is expressed robustly and is bright enough to use as either a selectable marker or proof of transformation for new reporter lines where expression may be close to or below the level of detection. We have used this construct exclusively for Arabidopsis roots but the membrane marker is also expressed in above-ground tissues. We also developed a variant of this destination vector which outlines cells within the lateral root primordia and the stele suitable for long term imaging of lateral root organogenesis. We have named these new destination vectors Dual Expression Anatomy Lines (DEAL) and these destination vectors can be easily adapted and customised for any tissue of interest. For long-term imaging and to allow different treatments, we designed a flexible flow cell and perfusion system to maintain healthy roots orientated for imaging for the extended periods made possible by the new marker system. Using this customized flow cell, we followed the expression of our dual markers, observing changes in the dynamics of gene expression following auxin treatment.

RESULTS

An efficient method for dual visualization of gene expression and root anatomy

We sought to develop a vector system where we could introduce a single plasmid to plants to simultaneously report gene expression alongside root anatomy. To do this we first tested several different plasma membrane localized fluorophores to identify one with suitable expression in root cells. We selected the pUBQ10::tdTomato 29-1 reporter (Segonzac et al., 2012). This marker gave us consistently good results in all tissues of the primary root of Arabidopsis, although the expression levels were higher in some tissues, such as the root cap.

We have previously used the GreenGate technology for generating novel plasmid

vectors. This is a simple and efficient method that uses the BsaI type IIS restriction endonuclease to combine six insert modules into a binary destination vector (Lampropoulos et al., 2013). We cloned promoters into the pGGA module for 11 genes that are expressed in a cell type-specific manner and represent most of the common root cell lineages. We also included the constitutively expressed 35S and G1090 promoters, the synthetic cytokinin reporter TCSnew (Pfeiffer et al., 2016) as well as AUX1 which is expressed across a variety of tissues in a subset of columella, lateral root cap, and stele cells.

We tried the methods of using intermediate vectors for double constructs and the oligo duplex method for triple markers as described in the original GreenGate method, but these methods did not work reliably for us. We therefore designed a destination vector including a red membrane vector within the plasmid backbone into which our new reporters could be assembled. Our rationale was that any transcriptional/translational reporter could be cloned into this destination vector using a single GreenGate recombination reaction to produce a dual marker highlighting both the gene of interest (e.g. in GFP) and the underlying cell geometry (tdTomato). For this we used the pGGZ003 destination vector and inserted a DNA sequences encoding the UBQ10::tdTomato 29-1 reporter between the t-DNA right border and the restriction site for the A-module overhang to make our first DEAL marker backbone (Figure 1). This means that the two promoters encoding the red membrane marker and the gene of interest are back to back, and therefore read in opposite directions. We chose the pGGZ003 destination vector, rather than pGGZ001 because pGGZ003 has the resistance cassette at the left border, meaning that the resistance cassette is the last part to be inserted into the genome, making it more likely that resistant plants contain the entire constructs.

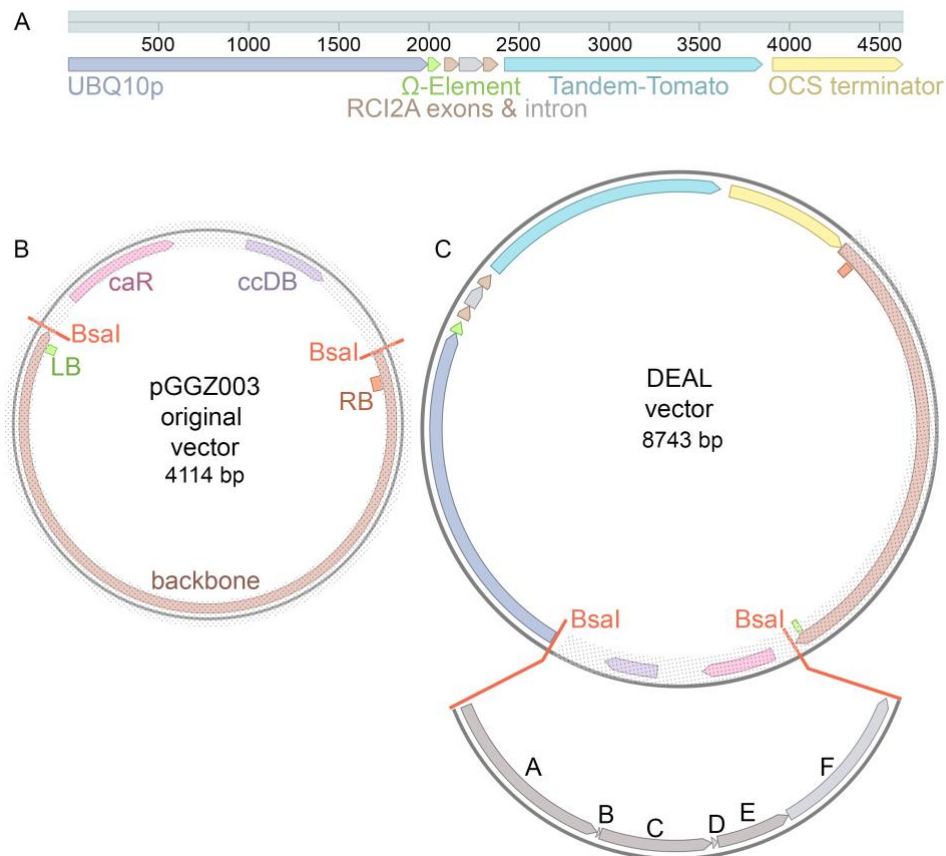


Figure 1. Construction of the DEAL marker system. **A**, Schematic representation of the UBQ10::tdTomato 29-1 red plasma membrane marker developed by Segonzac et al. (2012) that was introduced into the dual marker system. This consists of consists of a long UBIQUITIN10 (UBQ10, AT4G05320) promoter (2kb) followed by an Ω element and the RARE-COLD-INDUCIBLE 2A gene (RC12A, AT3G05880) coding sequence with intron included fused to tandem tomato (tdTomato), followed by the OCS terminator. The UBQ10 promoter drives expression in all cell types and the RC12A sequence targets the tdTomato to the plasma membrane. **B**, Schematic representation of the empty pGGZ003 destination vector developed by Lampropoulos et al. (2013). This contains a ccdB cassette and chloramphenicol acetyltransferase (CaR) gene flanked by two Bsal sites with A and G overhangs, into which GreenGate modules can be cloned. These Bsal sites in turn are flanked by left (LB, shown in green) - and right border (RB, shown in orange) sequences. The backbone requires the presence of the helper plasmid pSOUP in agrobacteria. **C**, Schematic of the pGGZ003-derived DEAL vector incorporating UBQ10::tdTomato 29-1 next to the RB in the pGGZ003 backbone. For clarity the original pGG003 vector part is shaded. Genes of interest can be inserted into the DEAL vector using the Bsal sites as indicated by the modules shown in grey. Typically, A modules would contain a promoter,

B modules an N-tag, C modules a coding sequence, D modules a C-tag, E modules a terminator region and F modules a resistance marker for expression in planta. Constructs have been visualized using Benchling software (Benchling, 2020).

We used our DEAL destination vector to assemble transcriptional reporters with 14 promoter modules using a standard GreenGate protocol. In each reaction we recombined each A module with the pGGB003 B-module containing a dummy sequence, the pGGC012 C-module containing a nuclear localized GFP or a C-module containing DII-Venus YFP, the pGGD002 D-module containing a dummy sequence, pGGE001 E-module containing the RBCS terminator sequence from pea and the pGGF007 F-module encoding Kanamycin resistance. Despite the size of the destination vector increasing from 4114bp to 8743bp, we did not notice an appreciable change in cloning efficiency using this vector, and typically observed in excess of 10 colonies per GreenGate reaction.

These constructs were transformed into *Arabidopsis* using the floral dip method. There was no appreciable difference in transformation efficiency compared to smaller single marker constructs and a good number of independent transformants was recovered for each line. We also noted whilst we selected primary transformants by antibiotics, that the membrane marker was strong enough to score segregation under a fluorescent dissecting scope and could potentially be used to screen for primary transformants from an early stage.

The membrane marker shows a good expression throughout the primary root including the vasculature, illustrating that this marker is highly suitable for observing cell anatomy in these tissues (Figure 2A-D). We observed high fluorescence within the primary root cap. By setting the gain on the confocal detector, we were able to produce good quality images of different tissues despite the differences in fluorescence levels. This caused some imaging complications where cells of different ages were located close to each other, such as in the columella root cap and in lateral root primordia (Fig 2A and 2E). Here the older cells had much higher levels of fluorescence. In the case of the root apical meristem, higher gain was required to image the young meristem cells (Fig. 2A)

whilst reducing this gain provided optimal exposure for the columella cells (Fig. 2B). These two exposures could be merged to render a high resolution composite (Fig. 2C). Using propidium iodide as a stain also creates differences in staining intensity, with the outermost cells having the strongest signal (Fig. 2F). Overall, the image quality within the meristem zone is comparable to those images taken that have been counterstained with propidium iodide. When we look at more mature zones of the root, we can see that the membrane marker outlines the cells throughout the root, including the vascular tissues (Fig. 2D), in contrast vascular cells are completely unstained following PI application (Fig. 2G). This shows that the membrane marker is suitable for analysis of all cell types within the main root (Fig. 3). One area where the membrane marker does not excel is in imaging of lateral root primordia (LRP). Unlike in PI-stained samples (Fig. 2G) the cell membranes are still marked, however this is at a much lower level than the adjacent cells (Fig. 2E). To image LRPs the gain must be set at a level in which both inner and outer layers are over-exposed. This will not be a problem for recording images at fixed timepoints but would make the recording of movies challenging. This marker is also expressed in some above-ground organs, but this was not further investigated in this project.

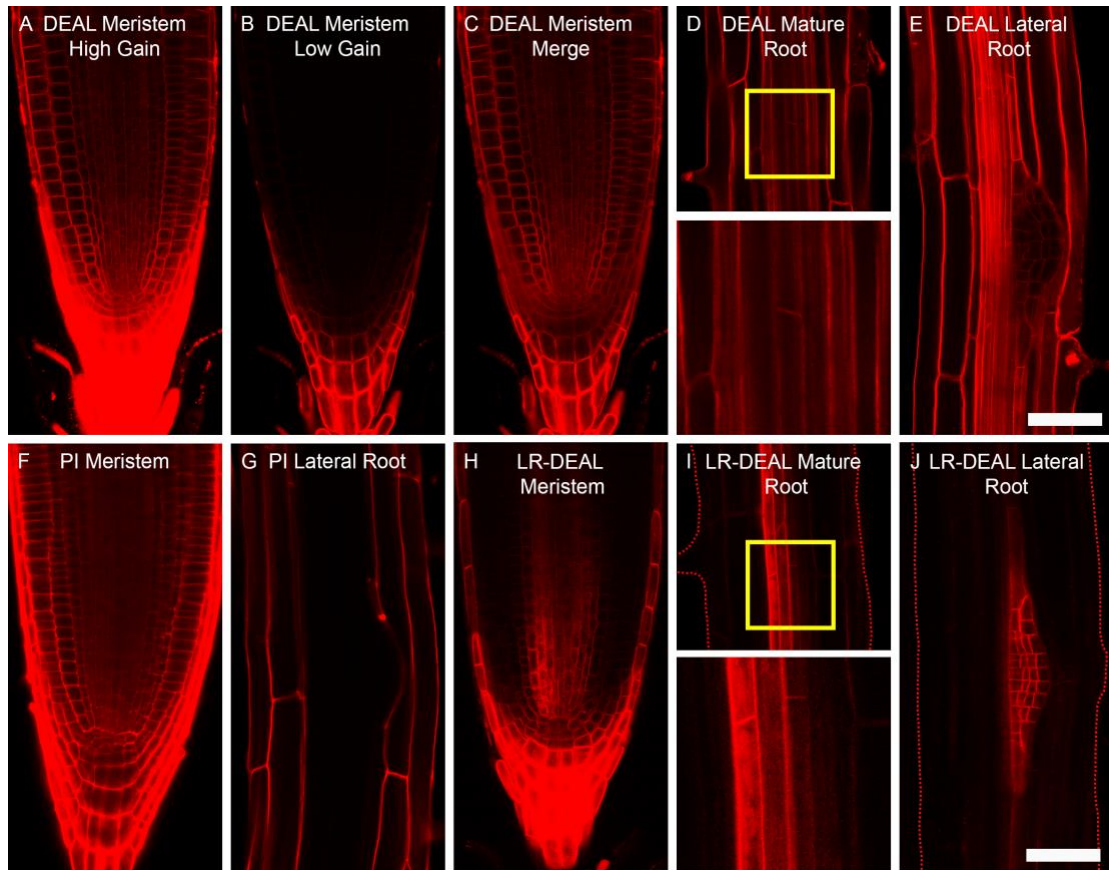


Figure 2. Comparison of the DEAL system with roots counterstained with propidium iodide. **A-C**, images taken of the root apical meristem of the dual marker system at different confocal settings. **A**, At high gain settings (500 V) all meristematic cells can be clearly distinguished, however the older cells in the columella and root cap are saturated. **B**, At reduced gain (50 V) these cells can be differentiated clearly, although the meristematic cells are barely visible. **C**, These images can be overlaid using software analysis software such as GIMP to give a high quality composite with every cell being clearly defined. **D**, Similar to the columella cells, fluorescent intensity is high in the mature tissues. Cell outlines can be clearly defined for all tissues. The yellow box defines a region zoomed in below to showing vascular cell anatomy more clearly. **E**, Staining in lateral root primordia is very weak compared with the overlaying tissues. **F&G**, Comparable images of control roots counterstained with propidium iodide. Note that in the meristem, vascular tissues are not stained as intensely as the dual marker system. In mature roots, propidium iodide is unable to enter either the vascular tissues or lateral root primordia. **H ,I & J**, The lateral root specific dual marker system marks cell membranes only in the vasculature, columella and the lateral root primordia. Cells within the lateral root primordia are defined clearly, and without fluorescence from the surrounding cells, these

primordia can be followed at high resolution. Dashed lines have been used where roots outlines are not readily visible. All images are taken from 7 days old Arabidopsis plants. The scale bar is 50 μ m.

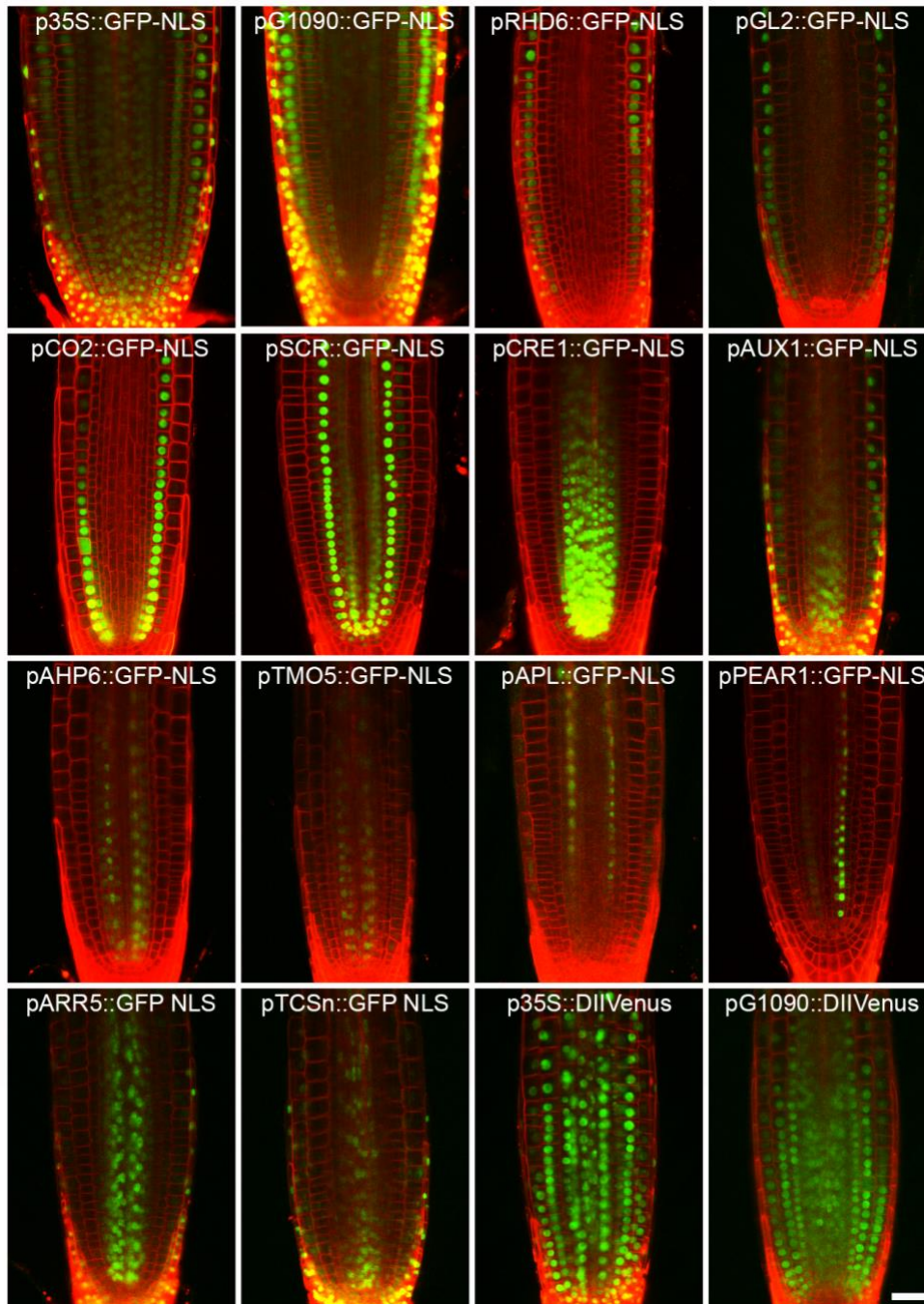


Figure 3. The DEAL constructs allow the identification of most major cell types as well as auxin and cytokinin responses. As proof of concept, 16 different constructs were transformed into Arabidopsis covering the following cell types, epidermis, cortex, endodermis, stele, procambium, xylem and phloem, alongside the constitutive promoters 35S and G1090, the cytokinin TCSn reporter and the DII-Venus auxin sensor. Most of

these lines contain a nuclear-localised GFP in the C module, expect two lines with a DII-Venus module. Primary roots imaged at 7-21 days after germination. Scale bar (bottom right): 30µm.

An optimized version for investigating lateral root organogenesis

We wanted to consider how these markers could be applied to investigate changes in gene expression during lateral root organogenesis. In Arabidopsis, the formation of a lateral root primordia (LRP) occurs via a stereotypical series of cell divisions defined by 8 stages (Malamy and Benfey, 1997). These stages cover a developmental time series starting by the first asymmetric division in the founder cell through to the establishment of a well-defined primordia. Before the lateral root emerges through the epidermis all major radial cell types are present, although the stage in which vascular cell fates are assigned is less clear. This process from the early stages of division until the establishment of a primordia in which radial cell fate has been defined takes about 24h (Guseman et al., 2015). As formation of the lateral root involves the de-novo specification of cell fate it provides an excellent template within which to investigate cell type specification.

This process has been followed in real time using either Light Sheet Fluorescence Microscopy (Von Wangenheim et al., 2016) or using confocal laser scanning microscopy (Goh et al., 2016). In both cases genetically encoded plasma membrane markers were used to define plasma-membranes. In addition to using the WAVE131Y (Geldner et al., 2009) which expresses a plasma-membrane-localized YFP under a ubiquitous promoter, the study by Goh and colleagues (2016) also made use of the pAUX1::AUX1-YFP reporter (Swarup et al., 2004) which highlights membranes within the LRP with minimal marking of the overlaying tissue. We first looked at our constructs built with the DEAL system at fixed timepoints during lateral root organogenesis to examine their suitability (Fig. 2E). Although the membrane marker marked the plasma-membrane within the lateral root primordia, this was not as clear as for the primary root. Therefore, we designed a second destination vector (LR-DEAL) where we exchanged the UBQ10 promoter with the AUX1 promoter using Gibson assembly. Plants transformed

with this vector only had cells within the vasculature, the root tip and the LRPs marked (Fig 2 H-J). As before, we cloned each of our reporters into this vector and followed the expression during lateral root formation (Fig. 4). As proof of concept, we applied the confocal imaging approach used by Goh (2016) and took z-stacks of lateral root primordia at 10 minute intervals. We imaged development from stage III through to post-emergence over a period of 24h (Fig. 5 and Supplemental Movie 1). In this time-series we observed that the AHP6 promoter drove high level expression within all cells of the primordia at stage II/III, but gradually became restricted to two poles within the vascular tissue as the primordia developed and reached the emergence stage. This demonstrates the utility of our plasmid vectors for uncovering further investigation of gene patterns during lateral root formation, and by producing a series of cell-type specific markers, we allow future researchers to investigate specification of major cell lineages within the LRP.

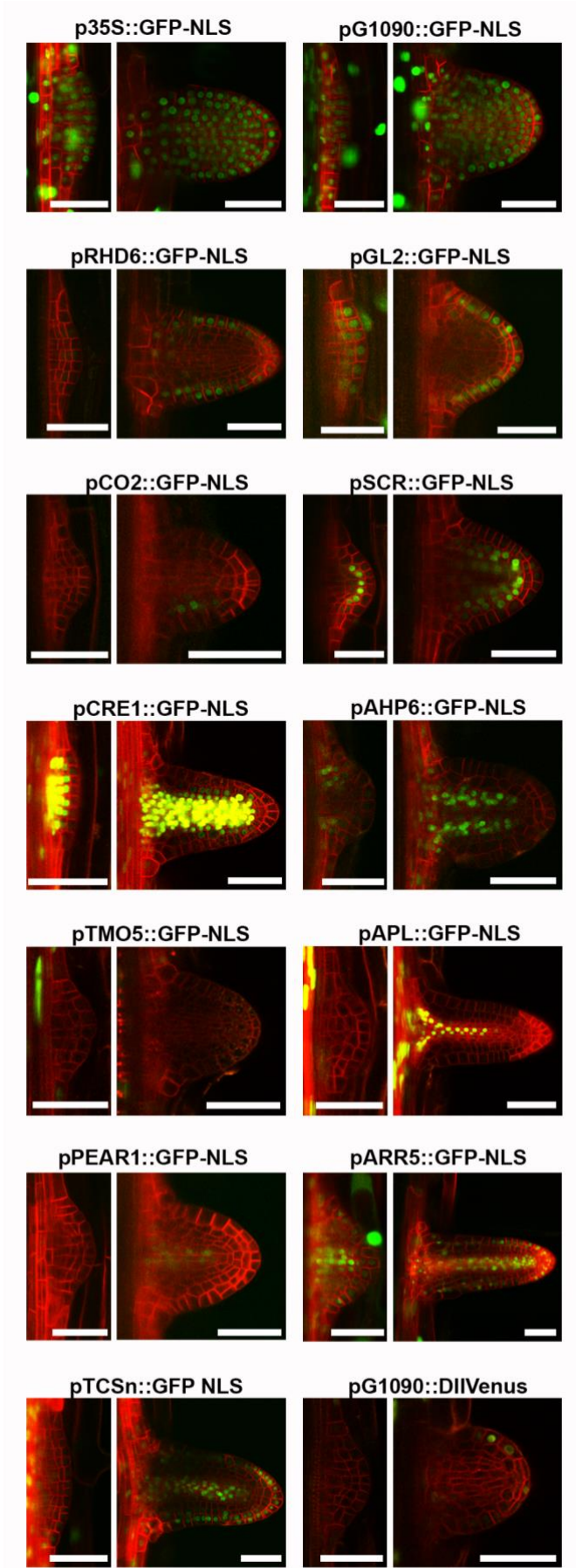


Figure 4. The lateral root specific DEAL constructs allow cell fate and auxin/cytokinin response to be observed in lateral roots of different developmental stages.

14 different lateral root specific DEAL constructs to show expression of markers at different stages of lateral root development. For each construct we show the lateral root primordium pre-emergence and the emerged lateral root. As for the other DEAL constructs, we used cell-type specific promoters, the constitutive promoters 35S and G1090 and the cytokinin TCSn reporter and the DII-Venus auxin sensor. In the constitutive promoter lines 35S and G1090, there is also GFP expression in the epidermal cells overlaying the lateral root primordium and in the stele. In the pARR5::GFP-NLS lines there is also some expression visible in the epidermis overlaying the lateral root primordium. In several lines (e.g. pRHD6, pPEAR1) there is no GFP expression in the early primordia, but GFP is expressed in later stages. Lateral roots were imaged from 2 weeks after germination. Scale bars: 50µm

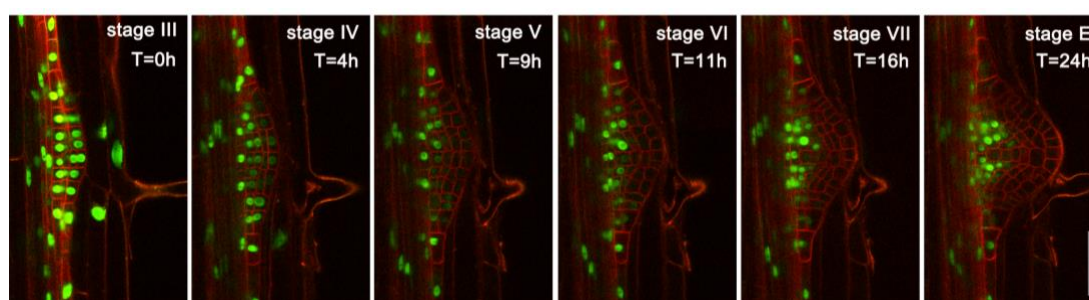


Figure 5: The dual marker system allows imaging of lateral roots for over 24h. Time lapse image series of AHP6::GFP/LR marker showing progression from stage III through to post emergence. Images were taken every 10 minutes and represent one plane selected from a z-stack. The approximate times and stages of LR development are indicated. See also Supplemental Movie 1. Scale bar: 50 µm

Visualizing dynamic changes in gene expression over time

Advances in both microscopy and the development of fluorescent biosensors make live imaging a powerful tool for the study of plant processes at the cellular level. However, keeping plant material alive and orientated to allow imaging during long-term studies is difficult and has resulted in limited adoption of these techniques (Wells et al., 2013; Calder et al., 2015). To allow imaging of roots

expressing the DEAL system, we designed a flow cell and perfusion system to maintain healthy roots orientated for long-term confocal microscopy studies. This comprises a 3D-printed flow cell (Fig. 6A) connected to a constant-pressure perfusion and extraction system (Fig. 6B) to allow rapid changes between up to five growth and test media whilst maintaining the sample root orientated for imaging for prolonged periods on the stage of a confocal laser scanning microscope. The use of 3D-printed components allows flexibility in design of chamber volume and flow characteristics as required.

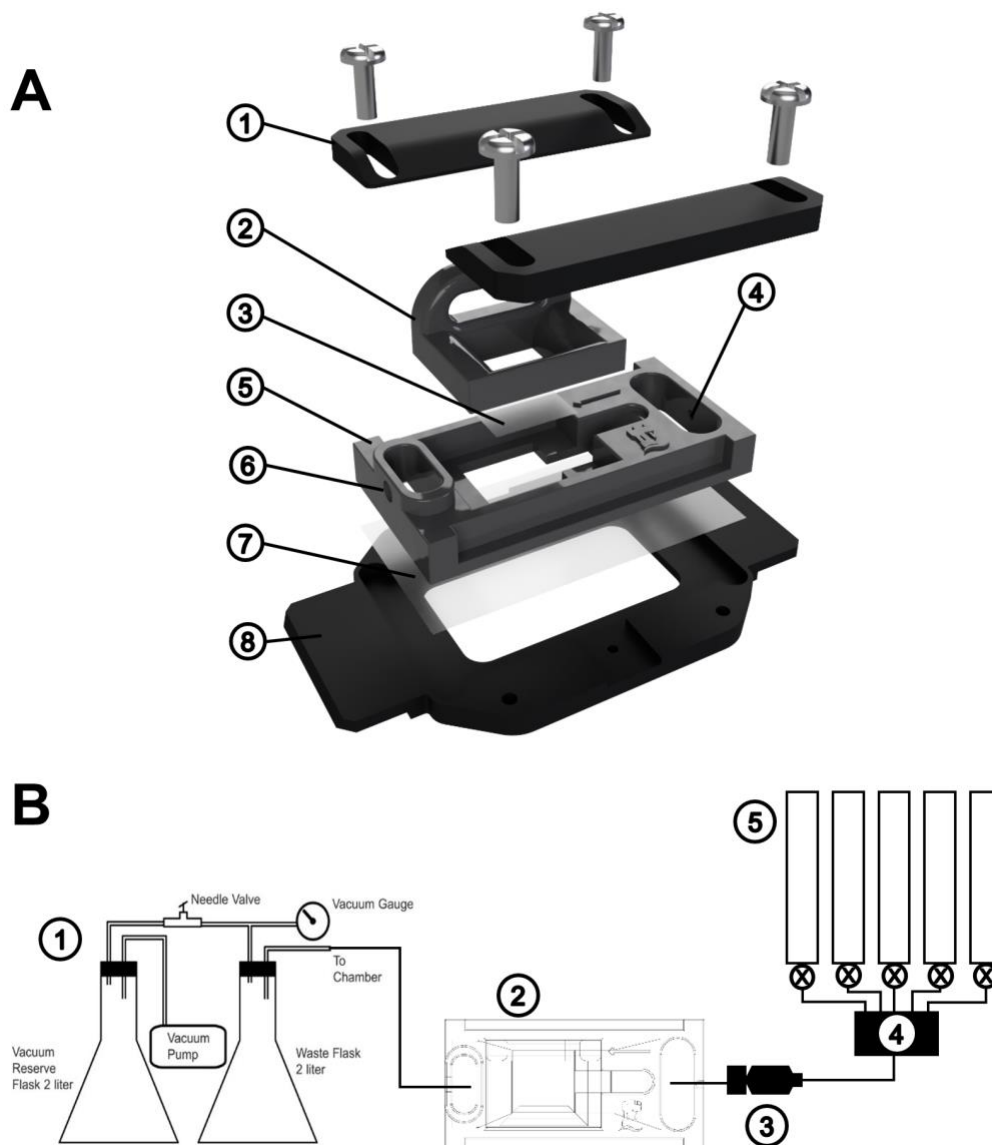


Figure 6. Flow cell and perfusion system. A. Flow cell components. (1) clamps; (2) top support; (3) top coverslip; (4) inlet port; (5) outlet port; (6) flow cell body; (7) cell coverslip; (8) stage adapter. **B.** Perfusion system. (1) vacuum pump and waste handling; (2) flow cell; (3) flow control valve; (4) manifold; (5) constant volume syringes.

The flow cell and perfusion system in combination with the DEAL marker system offers unique advantages for studying root development. Long term imaging systems such as those developed here are susceptible to the previously outlined issues of cytotoxicity, photobleaching and subcellular re-localisation of cell wall stains, if employed. This can make the assessment of fluorescence levels over time difficult to resolve spatially with regard to their exact cellular position in the root. The red membrane marker vector provides a means to circumvent the above issues, and to obtain positional information for the fluorescence output of a given cell. As a proof-of-concept, we imaged a line harbouring the DEAL destination vector with the auxin reporter line DII-venus in the flow cell system, subjected to a brief auxin perfusion treatment (5 minutes, 1nM IAA) followed by 1 hour of recovery, and imaged every two minutes throughout. This permitted clear visualisation of the degradation and accompanying loss of signal of DII-Venus in response to the auxin stimulus, with clear resolution of the location of individual nuclei allowing their anatomical position to be called with confidence. For example, it is easy to discern the more rapid loss of DII-Venus signal in the outer cortical cell layers versus the stele. Furthermore, the membrane marker remained well defined throughout the experiment (Fig. 7).

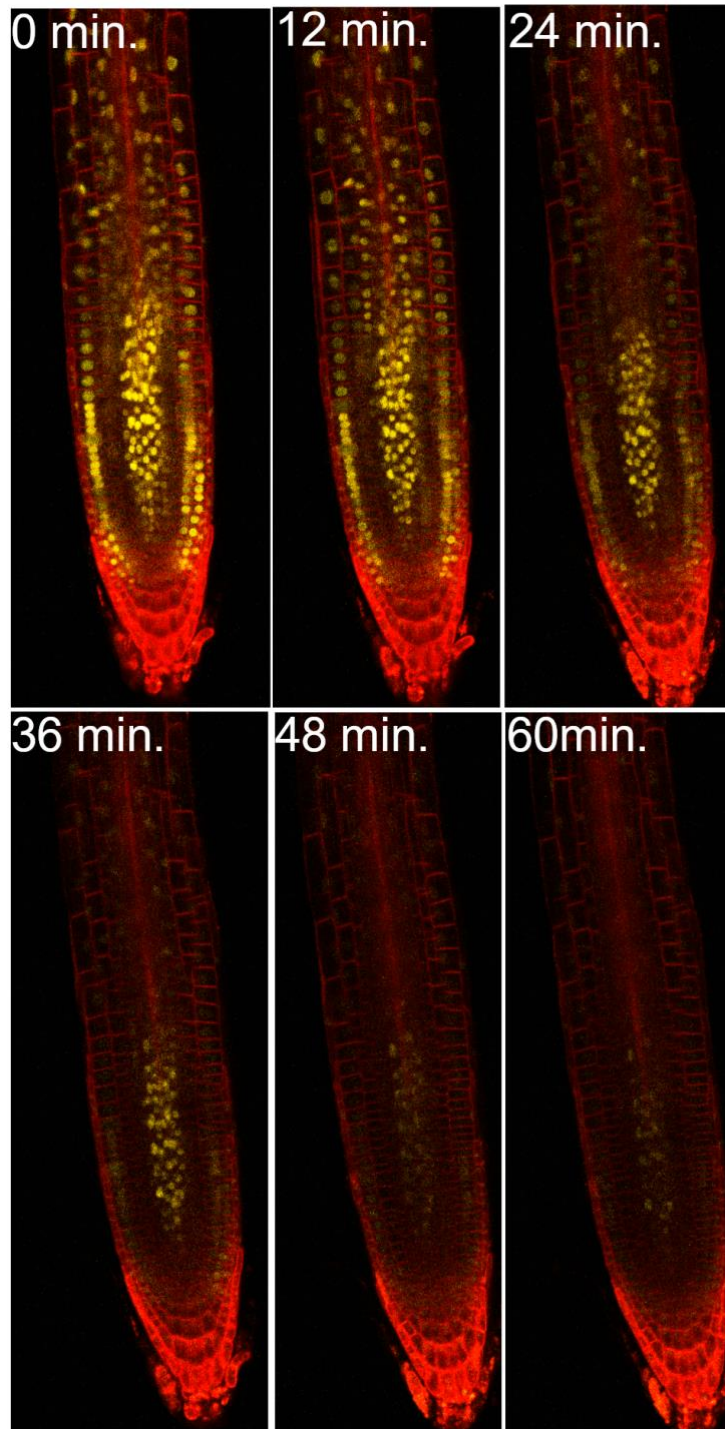


Figure 7. DEAL lines facilitate flow cell imaging without the need for counterstaining.

A line harbouring the DEAL destination vector with the auxin reporter line DII-venus was imaged using the flow cell and perfusion system over the course of 70 minutes and subjected to a brief auxin perfusion treatment (1nM NAA, 5 minutes) between minutes 5 and 10. Representative images from z-stacks taken at the 6, 12, 24, 36, 48, and 60 minute timepoints are given in the panel. See also Supplemental Movie 2.

DISCUSSION

We have developed a comprehensive set of dual expression and anatomical marker lines alongside a flow cell and perfusion system to facilitate long-term live imaging of plants. In addition to providing a suite of marker lines covering most cell lineages in the root, we have developed a GreenGate destination vector that rapidly allows the user to clone their gene of interest into the DEAL system. The two versions of the DEAL system, driven under either the UBQ10 or AUX1 promoter, provide high resolution images in a variety of root tissues. This system can be easily adapted to drive expression of the plasma membrane marker in any organ or cell-type of choice by exchanging the UBQ10/AUX1 promoter with the desired promoter. In this way it could be utilized for other non-root tissues. DEAL has several advantages over the conventional method of counterstaining roots with propidium iodide; the tdTomato signal is stable over time allowing long-term imaging, particularly in mature roots, we also see vastly improved signal from vascular tissues and by using variants that are expressed in discrete tissues – such as the LR variant – we can focus specifically on the desired structure. When combined with our newly developed flow cell, these lines provide an efficient way to observe how gene expression or cell identity changes following either environmental stimuli or changes in hormone activity. As proof of concept, we evaluated the response of a new DII-Venus line to auxin. Compared with the propidium iodide control this provided a vast improvement in methodology, allowing us to observe differences in auxin levels in individual cell types. We were able to follow the process of lateral root organogenesis for over 24h with no appreciable deterioration in signal.

Whilst the pUBQ10::tdTomato 29-1 or similar membrane marker lines can be introduced into plants individually, incorporating this into a single plasmid offers a significant reduction in experimental time. DEAL also offer a time saving advantage when combined with existing markers by genetic crossing; as both the gene of interest and the anatomical marker are on the same plasmid, they

segregate as a single loci. Our labs have now used this system for over 50 transgenic lines, we can produce high numbers of primary transformants by dipping relatively few plants. We also uncovered a number of advantages in the DEAL system that we did not anticipate. Although we select primary transformants using the conventional antibiotic selection, the red fluorescence is sufficiently high that we can easily screen transgene segregation using a simple fluorescent binocular scope, often before the antibiotic selection becomes apparent. We have also found DEAL an ideal method for generating new reporters that might show low or even no expression, such as in promoter dissection experiments. In this case the red plasma membrane marker acts as a positive control that the transgene is active.

By providing a suite of pre-made lines, we provide the research community with a toolbox enabling them to pursue projects such as investigating the de-novo assignment of cell fate in Arabidopsis lateral roots, or to investigate how hormone responses are modulated by external stimuli. These lines will also be suitable for investigating other adaptive changes such as during biotic or abiotic stresses.

MATERIALS AND METHODS

Cloning

Greengate entry module construction

Primers with GreenGate overhangs were designed following the Greengate protocol. Control primers were designed at the same time for colony screens and sequencing.

Construction of destination vectors with red membrane included

For our first DEAL destination vector, a red membrane marker construct was added to the original GreenGate pGGZ003 destination vector by amplifying the red membrane marker sequence, amplifying the empty destination vector and combining them using Gibson assembly (Gibson et al., 2009). The red membrane marker construct pUBQ10::tdTomato 29-1 (Segonzac et al., 2012) consists of a

long UBIQUITIN10 (UBQ10, AT4G05320) promoter (2kb) followed by an Ω element and the RARE-COLD-INDUCIBLE 2A gene (RCI2A, AT3G05880) coding sequence with intron included (297bp total) fused to tandem tomato (tdTomato), followed by the OCS terminator at 723 bp in length. This was amplified as a whole from the original construct including the original scar sequences between the different components.

For the lateral root-specific LR-DEAL vector, the first DEAL vector was amplified without the UBQ10 promoter and the promoter was replaced with the AUX1 promoter (AT2G38120, 2212kb upstream of ATG) using Gibson assembly.

The newly assembled DEAL destination vectors were transformed into chemically competent *E. coli* DB3.1 which are resistant to the ccdB gene product located in the empty destination vector. The DEAL and LR-DEAL destination vectors were then used in the same way as the original pGGZ003 backbone when assembling GreenGate constructs (Lampropoulos et al., 2013).

GreenGate assembly

GreenGate assemblies were done using the NEB GoldenGate mix as this was overall more efficient for us than buying the enzymes separately. All entry modules were checked by sequencing and assembled destination vectors had all seven module borders checked by sequencing to ensure that all modules were present.

Transformation using floral dipping

Entry modules and destination vectors were multiplied using chemically competent *E. coli* DH5 α and were transformed into plants using the floral dip method and electrocompetent agrobacterium GV3101 (with pSoup). All destination vectors used in this study had kanamycin resistance *in planta* and were dipped into Col-0 *Arabidopsis thaliana* plants. T1 seeds were screened on ½ MS plates with Kanamycin (50 μ g/ml) and transformants transferred to soil after 2-3 weeks.

Microscopy

For the primary root image microscopy, T3 plants were grown on 1/2 MS medium supplemented with 1% agar in 16h light/8h dark condition for 5 days. For the lateral root primordium image microscopy, T3 plants were grown on 1/2 MS medium supplemented with 1% agar in 16h light/8h dark condition for 8 or 10 days. Imaging was performed on either a Leica SP5 or SP8 confocal microscope using sequential scans and either a 40x air or 63x water objective. The tdTomato signal was excited with a 560nm laser and light between 567-701 nm was collected using a Hybrid Detector (Hybrid GaAsp/APD (HyD)). In the propidium iodide comparison figure, roots were stained in 10 µg/ml propidium iodide for three minutes and washed in distilled water. For the long term imaging lateral root movie microscopy we used a set up similar to Goh et al. (2016). T3 plants were grown on 1/2 MS medium supplemented with 1% agar and 1% sucrose in 16h light/8h dark condition for 8 days. Seedlings were removed from the agar plate and placed in a one-well Nunc™ Lab-Tek™ II Chamber Slide™ with a slice of agar covering the root. Light was supplied externally using a 10mins illumination/ 1 min dark cycle (in which images were collected) over 24 hours. Images were generated with a 63x water objective, and with Zeiss Immersol W. 1.334 used in place of water to prevent evaporation. To speed up data acquisition small z-stacks of only 3 stacks were taken. Both the tdTomato and GFP were examined with excitation at 488 nm and emission at 496-550 nm for GFP and 590-700 nm for tdTomato.

Flow cell

The sample holding system consists of a flow cell designed to fit most inverted microscope stages, with dimensions compatible with standard 50 mm x 22 mm glass coverslips (Fig. 5A). The flow cell is 3D printed to allow modification to accommodate different size roots and flow characteristics. Components were designed using Fusion 360 CAD software (Autodesk Ltd.) and printed on a stereolithographic 3D printer (Model Form2, FormLabs Inc.) using photocurable resin (Black Tough Resin, FormLabs Inc.). Printer files (*.obj) and original design files (*.f3D) are provided in the Supplementary material. Components and

suppliers for the system are given in Supplementary Table. The flow cell consists of a main body with inlet and outlet perfusion ports and an imaging chamber with a support ramp to position the shoot. A 12 x 12 mm coverslip is fitted to the base of a top support that locates on top of the chamber to control the perfusion volume and prevent excessive movement of the root. A 50 mm x 22 mm coverslip is fitted to the bottom of the main body and sealed with vacuum grease. Once the coverslip has been sealed, the main body of the flow cell is clamped to a stage adapter using two adjustable clamps – this ensures a distortion-free seal for the coverslip. Different stage adapters may be employed for different microscope configurations. To fit Leica microscopes, we employed a modified P-1 adapter (Warner Instruments LLC). Before transferring a seedling, a small volume of perfusion solution is pipetted into the imaging chamber. A seedling is then positioned in the chamber with root in the solution and the stem and cotyledons resting on the support ramp. The top support is then fitted, and the chamber filled via the inlet port. This creates a chamber of approximately 27mm³ volume in which a root can be maintained for several days.

Once assembled, the flow cell is moved to the microscope stage and connected to the perfusion and extraction systems (Fig. 5B). The perfusion system consists of five 60 ml constant flow syringes connected to a five-position manifold with 1.14 mm OD polyethylene tubing (Harvard Apparatus Inc.). The output of the manifold is connected to the inlet port of the flow cell via a flow valve (Model FR-50S, Harvard Apparatus), allowing fine control (0 – 10 ml/min) of solution flow into the cell at a constant pressure head irrespective of the volume of solution in the syringes. The outlet of the flow cell is connected to a vacuum pump with self-contained liquid waste system (Model DWV, Warner Instruments). Balancing the inlet and outlet flows produces a constant flow rate through the root growth chamber. Typically, a rate of 1 ml/min is employed, allowing rapid application and removal of test solutions.

For the DII-VENUS experiments, the perfusion media employed was liquid $\frac{1}{2}$ MS, pH 5.8. For the treatment, roots were initially imaged for 5 minutes on control media, followed by a 5-minute treatment of $\frac{1}{2}$ MS media containing 1nM NAA. Following the NAA treatment, the media was reverted to $\frac{1}{2}$ MS alone for a further hour. The media flow rate was 1 ml/min.

Imaging was undertaken at 2 minute intervals from the initial $\frac{1}{2}$ MS treatment on a Leica SP8 confocal using a 20x/0.75 dry objective and the HeNe 633 laser line. Z-stacks consisting of 61 steps were acquired at each time point. Gain values were consistent throughout the time course. Following image acquisition, the resulting stacks were transformed using the SurfaceProject plugin (Band et al., 2014) in the FIJI image processing package (Schindelin et al., 2012) in order to correct for the root's inconsistent position in the Z-axis. The red (wall marker) channel stacks only were contrast-adjusted using the Enhance Local Contrast (CLAHE) plugin (Zuiderveld, 1994) to reduce the impact of brightness differences between the root cap and stele.

REFERENCES

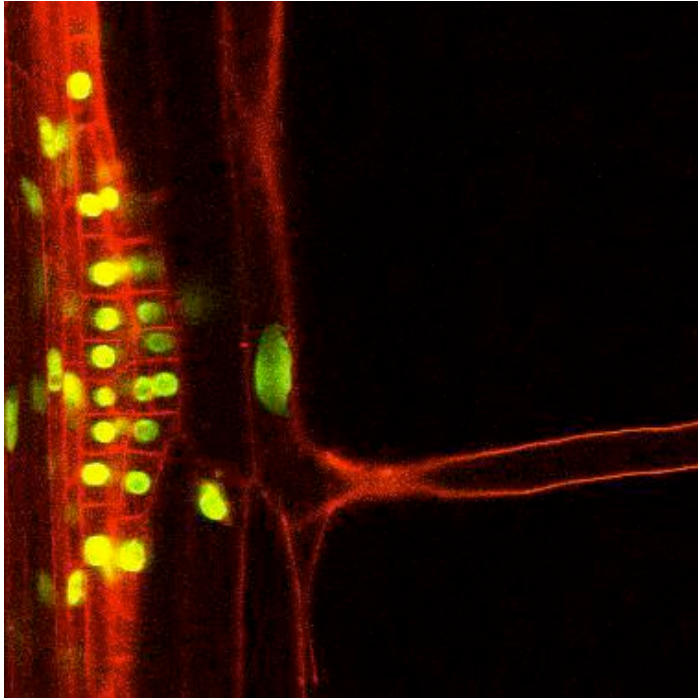
- Alassimone J, Naseer S, Geldner N (2010) A developmental framework for endodermal differentiation and polarity. *Proc Natl Acad Sci U S A* 107: 5214–5219
- Band LR, Wells DM, Fozard JA, Ghetiu T, French AP, Pound MP, Wilson MH, Yu L, Li W, Hijazi HI, et al (2014) Systems analysis of auxin transport in the Arabidopsis root apex. *Plant Cell* 26: 862–875
- Benchling (2020) Benchling [Biology Software]. <https://benchling.com>
- Bonke M, Thitamadee S, Mähönen AP, Hauser M-T, Helariutta Y (2003) APL regulates vascular tissue identity in Arabidopsis. *Nature* 426: 181–186
- Calder G, Hindle C, Chan J, Shaw P (2015) An optical imaging chamber for viewing living plant cells and tissues at high resolution for extended periods. 1–10
- Cutler SR, Ehrhardt DW, Griffitts JS, Somerville CR (2000) Random GFP::cDNA fusions enable visualization of subcellular structures in cells of Arabidopsis at a high frequency. *Proc Natl Acad Sci U S A* 97: 3718–3723

- D'Agostino IB, Deruère J, Kieber JJ (2000) Characterization of the response of the Arabidopsis response regulator gene family to cytokinin. *Plant Physiol* 124: 1706–1717
- Dolan L, Janmaat K, Willemsen V, Linstead P, Poethig S, Roberts K, Scheres B (1993) Cellular organisation of the Arabidopsis thaliana root. *Development* 119: 71–84
- Gallagher KL, Paquette AJ, Nakajima K, Benfey PN (2004) Mechanisms Regulating SHORT-ROOT Intercellular Movement. *Curr Biol* 14: 1847–1851
- Geldner N, Déneraud-Tendon V, Hyman DL, Mayer U, Stierhof YD, Chory J (2009) Rapid, combinatorial analysis of membrane compartments in intact plants with a multicolor marker set. *Plant J* 59: 169–178
- Gibson D, Young L, Chuang R (2009) Enzymatic assembly of DNA molecules up to several hundred kilobases. *Nat Methods* 6: 343–345
- Goh T, Toyokura K, Wells DM, Swarup K, Yamamoto M, Mimura T, Weijers D, Fukaki H, Laplace L, Bennett MJ, et al (2016) Quiescent center initiation in the Arabidopsis lateral root primordia is dependent on the SCARECROW transcription factor. *Dev* 143: 3363–3371
- Grebe M, Xu J, Möbius W, Ueda T, Nakano A, Geuze HJ, Rook MB, Scheres B (2003) Arabidopsis Sterol Endocytosis Involves Actin-Mediated Trafficking via ARA6-Positive Early Endosomes. *Curr Biol* 13: 1378–1387
- Guseman JM, Hellmuth A, Lanctot A, Feldman TP, Moss BL, Klavins E, Calderón Villalobos LIA, Nemhauser JL (2015) Auxin-induced degradation dynamics set the pace for lateral root development. *Dev* 142: 905–909
- Ishige F, Takaichi M, Foster R, Chua N, Oeda K (1999) A G-box motif (GCCACGTGCC) tetramer confers high-level constitutive expression in dicot and monocot plants. *Plant J* 18: 443–448
- Komis G, Novák D, Ovečka M, Šamajová O, Šamaj J (2018) Advances in imaging plant cell dynamics. *Plant Physiol* 176: 80–93
- Kurihara D, Mizuta Y, Sato Y, Higashiyama T (2015) ClearSee: A rapid optical clearing reagent for whole-plant fluorescence imaging. *Dev* 142: 4168–4179
- Lampropoulos A, Sutikovic Z, Wenzl C, Maegele I, Lohmann JU, Forner J (2013) GreenGate---a novel, versatile, and efficient cloning system for plant transgenesis. *PLoS One* 8: e83043

- Lee J-Y, Colinas J, Wang JY, Mace D, Ohler U, Benfey PN (2006) Transcriptional and posttranscriptional regulation of transcription factor expression in Arabidopsis roots. *Proc Natl Acad Sci USA* 103: 6055–60
- Mähönen AP, Bishopp A, Higuchi M, Nieminen KM, Kinoshita K, Törmäkangas K, Ikeda Y, Oka A, Kakimoto T, Helariutta Y (2006) Cytokinin signaling and its inhibitor AHP6 regulate cell fate during vascular development. *Science* (80-) 311: 94–98
- Malamy JE, Benfey PN (1997) Organization and cell differentiation in lateral roots of Arabidopsis thaliana. *Development* 124: 33–44
- Martinière A, Lavagi I, Nageswaran G, Rolfe DJ, Maneta-peyret L, Luu D, Botchway SW, Webb SED, Mongrand S, Maurel C, et al (2012) Cell wall constrains lateral diffusion of plant plasma-membrane proteins. *PNAS* 109: 12805–12810
- Menand B, Yi K, Jouannic S, Hoffmann L, Ryan E, Linstead P, Schaefer DG, Dolan (2007) An Ancient Mechanism Controls the Development of Cells with a Rooting Function in Land Plants. *Science* (80-) 316: 1477–1481
- Miyashima S, Roszak P, Sevilem I, Toyokura K, Blob B, Heo J, Mellor N, Help-rinta-rahko H, Otero S, Smet W, et al (2019) Mobile PEAR transcription factors integrate positional cues to prime cambial growth. *Nature* 565: 490–494
- Ovečka M, von Wangenheim D, Tomančák P, Šamajová O, Komis G, Šamaj J (2018) Multiscale imaging of plant development by light-sheet fluorescence microscopy. *Nat Plants* 4: 639–650
- Pfeiffer A, Janocha D, Dong Y, Medzihradzsky A, Schöne S, Daum G, Suzaki T, Forner J, Langenecker T, Rempel E, et al (2016) Integration of light and metabolic signals for stem cell activation at the shoot apical meristem. *Elife* 5: 1–21
- Schindelin J, Arganda-Carreras I, Frise E, Kaynig V, Longair M, Pietzsch T, Preibisch S, Rueden C, Saalfeld S, Schmid B, et al (2012) Fiji: An open-source platform for biological-image analysis. *Nat Methods* 9: 676–682
- Schlereth A, Möller B, Liu W, Kientz M, Flipse J, Rademacher EH, Schmid M, Jürgens G, Weijers D (2010) MONOPTEROS controls embryonic root initiation by regulating a mobile transcription factor. *Nature* 464: 913–6
- Segonzac C, Nimchuk ZL, Beck M, Tarr PT, Robatzek S, Meyerowitz EM, Zipfel C (2012) The Shoot Apical Meristem Regulatory Peptide CLV3 Does Not

- Activate Innate Immunity. *Plant Cell* 24: 3186–3192
- Swarup R, Kargul J, Marchant A, Zadik D, Rahman A, Mills R, Yemm A, May ST, Williams L, Millner P, et al (2004) Structure-Function Analysis of the Presumptive Arabidopsis Auxin Permease AUX1. *Plant Cell* 16: 3069–3083
- Truernit E, Bauby H, Dubreucq B, Grandjean O, Runions J, Barthélémy J, Palauqui J-C (2008) High-resolution whole-mount imaging of three-dimensional tissue organization and gene expression enables the study of Phloem development and structure in Arabidopsis. *Plant Cell* 20: 1494–503
- Truernit E, Siemerling KR, Hodge S, Grbic V, Haseloff J (2006) A map of KNAT gene expression in the Arabidopsis root. *Plant Mol Biol* 60: 1–20
- Ursache R, Andersen TG, Marhavý P, Geldner N (2018) A protocol for combining fluorescent proteins with histological stains for diverse cell wall components. *Plant J* 93: 399–412
- Von Wangenheim D, Fangerau J, Schmitz A, Smith RS, Leitte H, Stelzer EHK, Maizel A (2016) Rules and self-organizing properties of post-embryonic plant organ cell division patterns. *Curr Biol* 26: 439–449
- Wells DM, Laplaze L, Bennett MJ, Vernoux T (2013) Biosensors for phytohormone quantification : challenges , solutions , and opportunities. *Trends Plant Sci* 18: 244–249
- Zuiderveld K (1994) Contrast limited adaptive histogram equalization. *In* PS Heckbert, ed, *Graph. gems IV*. Academic Press Professional, Inc., pp 474–485

Movie S1. Long term imaging of AHP6::GFP using the DEAL(LR) line. See also Figure 5. Z-stacks were taken every 10 minutes over a 24h period and a single plane used to assemble the movie.

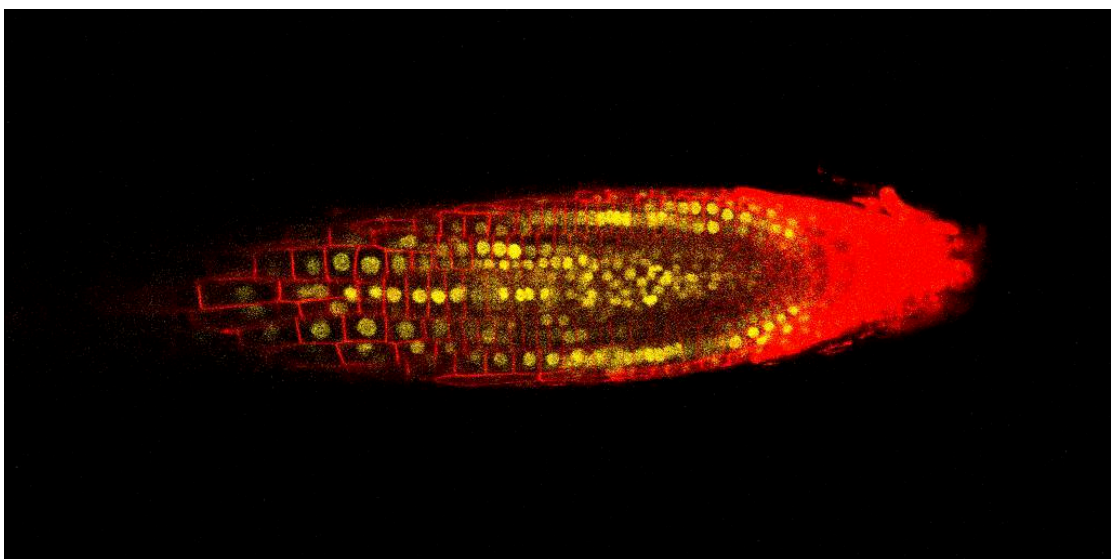


<https://uniofnottm->

[my.sharepoint.com/:v:/g/personal/jingyi_han_nottingham_ac_uk/EQDeulhqrl9JhmC2tOHsiycB5](https://uniofnottm-my.sharepoint.com/:v:/g/personal/jingyi_han_nottingham_ac_uk/EQDeulhqrl9JhmC2tOHsiycB5)

[MKAdlMpHpT6qRg5bdhcWg?e=9WsNcd](https://uniofnottm-my.sharepoint.com/:v:/g/personal/jingyi_han_nottingham_ac_uk/EQDeulhqrl9JhmC2tOHsiycB5MKAdlMpHpT6qRg5bdhcWg?e=9WsNcd)

Movie S2. Flow cell imaging of DII-venus using the DEAL line. See also Figure 7. Z-stacks were taken over 70 minutes.



https://uniofnottm-my.sharepoint.com/:v:/g/personal/jingyi_han_nottingham_ac_uk/EdOmf-

[bOzrRCqP44Wt57dGYBLBJ7bhBPgemHdO-QR18DCg?e=Uql2iP](https://uniofnottm-my.sharepoint.com/:v:/g/personal/jingyi_han_nottingham_ac_uk/EdOmf-bOzrRCqP44Wt57dGYBLBJ7bhBPgemHdO-QR18DCg?e=Uql2iP)

2. Methods

2.1 Material

DEAL lines were made by Britta Kümpers et.al, including 16 primary root lines and 14 LR lines.

2.2 Microscopy

For the root tip and lateral root microscopy, T3 plants were grown on 1/2 MS medium supplemented with 1% agar in 16h light/ 8h dark conditions for 5 days (root tips) or 8 days (lateral roots). For the lateral root movie microscopy, T3 plants were grown on 1/2 MS medium supplemented with 1% agar and 1% sucrose in 16h light/8h dark condition for 8 days. Seedlings were removed from the agar plate and placed in a one-well Nunc™ Lab-Tek™ II Chamber Slide™ with a slice of agar covering the root. Light was supplied externally using a 10mins illumination/ 1 min dark cycle (in which images were collected) over 24 hours. Images were generated with a 63x water objective, and with Zeiss Immersol W. 1.334 used in place of water to prevent evaporation. To speed data acquisition small z-stacks of only 3 stacks were taken. Both the tdTomato and GFP were examined with excitation at 488 nm and emission at 496-550 nm for GFP and 590-700 nm for tdTomato in the TCS-SP5 confocal microscope (Leica).

Chapter 3

1. Methods

1.1 Constructs of transcriptional reporter lines

All constructs were produced by DEAL (Kümpers et al., 2021), a modified version of the GreenGate cloning system (Lampropoulos et al., 2013) to include a red plasma membrane marker showing anatomy. All modules are showed in Supplemental table 3. All primers used in cloning showed in Supplemental table 3.

Promoter sequences contain 5'UTR upstream fragment and different length of downstream sequences were cloned by PCR with Q5 High-Fidelity DNA Polymerase (NEW ENGLAND BioLabs). These fragments were inserted into the empty Entry module vector. In the line pARF7^{UTR-INT}::GFP, the promoter A module was edited to inserted the intron into 5'UTR via Gibson cloning system (Gibson et al., 2009). The fragment of promoter and intron with splicing sites were cloned from ARF7 promoter A module and EX1-2 B module. These two fragments recombined to a new A module by Gibson Assembly Master Mix kit (NEW ENGLAND BioLabs). The four deletion and three single NAC mutations were edited from the EX1-2 B module, by Site-Directed Mutagenesis Kit (NEW ENGLAND BioLabs). The MYB and NAC multiple mutation plasmids were synthesized in plasmids already incorporating Bsal sites from Eurofins. The NAC and MYB mutations made by exchange 2bp within the appropriate binding motif sequences. The sequences of deletions and mutations showed in Supplemental table 2. These entry modules were recombined in order, with GFP:NLS (C module) and D-dummy and RBCS terminator and HygromycinR (for plant selection) and Destination vector DEAL (Kümpers et al., 2021) by Golden Gate Assembly Kit (NEW ENGLAND BioLabs). All primers used in cloning showed in Supplemental table 3.

These constructs were transformed in *Agrobacterium tumefaciens* GV3101 via electroporation and transformed into Col-0 via floral dip method. For selection of

transgenic plants, Arabidopsis T1 seeds were plated on 1% agar containing 1/2 MS medium and 20 µg/L Hygromycin B. After a 2d stratification period, seeds grew in 21°C with 6 h light, 48 h dark and 24 h light (Harrison et al., 2006).

1.2 Microscopy

For the root microscopy, T2 plants were grown on 1/2 MS medium supplemented with 1% agar in 16h light/ 8h dark conditions for 5 days (for primary roots) or 8 days (for lateral roots). Plant cell membranes were visualized by with Red Membrane Marker incorporating tdTomato (Kümpers et al., 2021). The roots were examined in the TCS-SP5 confocal microscope (Leica) with excitation at 488 nm and emission at 496-550 nm for GFP and 590-700 nm for tdTomato.

1.3 Expression level analysis by qRT-PCR

For reporter lines analysis, T2 plants grown on 1/2 MS medium supplemented with 1% agar in 16h light/ 8h dark conditions for 5 days (for root meristem) or 10 days (for leaf). Each construct was tested in 3 independent lines. Each RNA was extracted by dissecting 2mm root tips from around 50 plants. The leaf sample of each line contained 3 plant leaves. Qiagen RNeasy Plant Mini Kit was for RNA extraction. DNAase digestion and cDNA synthesised by RevertAid First Strand cDNA Synthesis kit (Thermo Scientific) with 200ng RNA. The cDNA was diluted 3:20 for qRT-PCR reaction. The SensiMix SYBR Hi-Rox Mastermix (BIOLINE) used for qRT-PCR reaction. The qTOWER3 84 G was used for reaction. The control gene was UBC and the test gene is GFP. Primers were showed in Supplemental table 3. The statistical analysis was done by T-test.

1.4 Transcript splicing analysis by RT-PCR

The cDNA synthesised for reporter line expression was used for RT-PCR. The forward primer located on 5'UTR and revers primer located on GFP shown in Supplemental table 3. The fragments were amplified by homemade Taq DNA polymerase. The fragments separated by 1.5% agarose gel.

1.5 Methodology for motif analysis

We first used AT5G20730.1 as a representative model to obtain the 1st intron

sequence (Chromosome 5: 7021458..7021139; minus strand; reverse complemented) of Auxin Response Factor 7 (ARF7). Next, we scanned this input sequence using PlantRegMap tool (Jin et al., 2015; Jin et al., 2017; Tian et al., 2020) for the presence of any manually curated 674 non-redundant and high-quality binding motifs derived from various experiments, literature and ChIP-seq datasets. We specifically used Binding Site Enrichment tool (with settings: species = *Arabidopsis thaliana* and Threshold p-value $\leq 1e-4$) that uses modified FIMO (Find Individual Motif Occurrences) to search TF binding sites in the input sequence.

To cross-validate the above predictions, we used recent DNA affinity purification sequencing data (DAP-seq) to scan input region (Chromosome 5: 7021458..7021139) for peaks (with FRiP $\geq 5\%$ i.e. fraction of reads in peaks) of 46 different transcription factors (O'Malley et al., 2016). The overlap between predicted and Dap-Seq derived TF binding sites (termed as selected binding sites) were considered for further analysis.

Next, to understand whether these selected binding sites could be unique and essential we aimed to study their conservation across different *Arabidopsis thaliana* genetic variants. In this context, we first identified 1st intron sequences of ARF7 from Arabidopsis 1001 genomes. Next, we MAFFT aligned all sequences, overlaid selected binding sites of AtARFs and visualised using Benchling.

2. Manuscript

NACs and MYBs specify ARF7 expression patterns in the root apical meristem through binding sites in the first intron.

Jingyi Han, Rahul Bhosale, Ute Voß, Anthony Bishopp

Abstract

Auxin regulates plant growth and development through the transcription factors of the AUXIN RESPONSE FACTOR (ARF) gene family. ARF7, is one of five activators

that bind DNA and elicit downstream transcriptional responses. In roots, ARF7 regulates root growth, gravitropism and redundantly with ARF19, lateral root organogenesis. In shoots, ARF7 controls leaf expansion and senescence. *ARF7* is expressed broadly throughout the root and shoot apical meristems. However, it is unknown whether specific *cis* regulatory elements drive expression in roots and shoots. Our previous work has shown a role for sequences 3' to the transcriptional start site in regulating *ARF7* expression in roots but not shoots. In this study we functionally dissected the *ARF7* promoter and used these dissected fragments to drive GFP. The results indicated the promoter and first intron led to a broader expression in root tip compared with only promoter. The first intron, therefore, plays an important role in transcriptional regulation in the root meristem. A swap experiment in which the first intron was moved to the 5'-UTR showed the position of intron is not essential for correct expression. Therefore, we propose that it is sequences within this intron that are required and that key transcription factors bind to this region. We identified several NACs and MYBs binding sites within the first intron and propose that these may play a role in regulating *ARF7* expression in root apical meristem.

Keywords: auxin response factor, intron, transcription factor

Introduction

Auxin plays an essential role in regulating many growth and developmental processes in plants, such as the formation of shoot apical meristem (SAM) and root apical meristem (RAM), vascular patterning, establishment of phyllotaxy, shoot phototropism, root gravitropism and female gametophyte development (Avsian-Kretchmer et al., 2002; Berleth et al., 2000; Beyer, 1972; Krogan et al., 2016; Liu et al., 2018). Together, several gene families comprise the auxin signalling network and mediate transcription of downstream response genes based on cellular auxin levels. The binding of auxin promotes the interaction between the SCF^{TIR1} ubiquitin protein ligase complex and the Aux/IAA co-repressors (X. Tan et al., 2007). The SCF-type complex comprises an F-box protein (such as TIR1) alongside the Skp1 and Cullin proteins (Smalle & Vierstra, 2004). This complex transfers an activated ubiquitin from a ubiquitin activating enzyme and conjugates

the Aux/IAAs (Dharmasiri et al., 2005; Kepinski & Leyser, 2005). The Aux/IAAs themselves act to stabilize auxin binding, leading to them being considered as co-receptors for auxin (Tiwari et al., 2001). Following the ubiquitination of the Aux/IAAs, these proteins are degraded by the 26S proteasome (Dharmasiri & Estelle, 2004; Gagne et al., 2002). A group of transcription factors (ARFs) bind to Auxin Response elements (AuxRE) within DNA (Ulmasov et al., 1999). The Aux/IAA proteins bind these ARFs and inhibit their transcriptional activity (Ulmasov et al., 1997). Under high auxin concentrations, the Aux/IAA proteins are degraded, allowing ARFs to regulate thousands of downstream responses (Worley et al., 2000; Zenser et al., 2001).

All of these auxin signalling components are present as large gene families. For example, the Arabidopsis genome encodes 23 ARF proteins that control distinct developmental processes (Okushima et al., 2005). They were divided to 3 classes based on phylogenetic analysis. Class A has 5 members, including ARF5, ARF6, ARF7, ARF8 and ARF19 (Finet et al., 2013). Of these, 5 have been shown to be transcriptional activators (Okushima et al., 2005). As activators, they bind in promoter or enhancers region of downstream genes to increase transcription. Alongside these activators, a group of ARF repressors bind similar regions to inhibit the expression of downstream genes.

These five activator ARFs have tissue specific expression patterns in both the SAM and RAM as well as in other organs (Krogan et al., 2016; Nagpal et al., 2005; Okushima et al., 2005; Truskina et al., 2021). Whilst there is a certain degree of genetic redundancy within these components, there is evidence that the spatial patterns of ARF response are important for controlling auxin specificity. Accordingly, either individual ARFs or pairs of ARFs have been associated with specific developmental responses.

ARF5 is arguably the most critically required, and is the only single mutant with a lethal phenotype (Berleth & Jurgens, 1993). It is essential for patterning of the embryonic root (Berleth & Jurgens, 1993). Besides its role during embryogenesis, ARF5 also targets *TMO5* to regulate vascular tissue development (Schlereth et al.,

2010). The BODENLOS/IAA12-ARF5 complex is also required in lateral root initiation (De Smet, 2010). In the SAM, ARF5 regulates stem cell homeostasis by regulating CLV3 via the repression of *DORNROSCHEN* and *ENHANCER OF SHOOT REGENERATION1* (Luo et al., 2018). Roles have also been identified in flower primordia where ARF5 promotes flowering through LEAFY (Yamaguchi et al., 2013).

ARF6 and ARF8 act redundantly in flower maturation (Nagpal et al., 2005). ARF6 and ARF8 also act together to modulate jasmonic acid homeostasis, as well as controlling adventitious root initiation (Gutierrez et al., 2012; Lakehal et al., 2019). ARF8 has also been shown to regulate nitrogen response in lateral root emergence (Gifford et al., 2008), and a recent network of factors acting upstream of ARFs predicts that ARF8 is regulated by many genes associated with biotic and abiotic response. NAC92 repressed *ARF8* to inhibit primary root development (Xi et al., 2019). ARF6 with BZR1 and PFI4 formed a BAP regulatory module (Boure et al., 2019) to regulated cell elongation in hypocotyl (Oh et al., 2014).

In roots, ARF7 and ARF19 are well known for their redundant role in regulating lateral root organogenesis via activation of the transcription factors LBD16 and 29 (Harper et al., 2000; Okushima et al., 2007; Okushima et al., 2005). ARF7 and 19 have also been shown to control other processes within the root, such as cell wall composition and pectin dynamics during root hair tip growth through ERULUS (Schoenaers et al., 2018), adventitious root formation via regulating LBD16 and LBD18 (Lee et al., 2019) as well as in tropic responses such as gravitropism (Okushima et al., 2005; Weijers et al., 2005).

In the aerial parts of the plant, *ARF7* is expressed in veins of maturing leaves, especially in older procambial strands, where it works together with other activating ARFs to control leaf formation (Schuetz et al., 2019). ARF7 works redundantly with ARF19 to control expansion of leaf cells. *arf19* mutants have little effect on leaf elongation by themselves, but can enhance the effect of an *arf7* mutation to reduce leaf cell expansion (Wilmoth et al., 2005). Consequently, the leaf blade area and rosettes of *arf7 arf19* are reduced. ARF7 also works alongside

ARF5 to control leaf organogenesis, with the double *arf5 arf7* mutant either not forming leaves or halting leaf initiation after the formation of one or two leaves (Schuetz et al., 2019). ARF7 and ARF19 are both induced by senescence (Ellis et al., 2005). Whilst miss-expression of these ARFs alone cannot affect the senescence of leaves, manipulation of these genes can enhance the ARF2 effect, which in turn regulates leaf senescence and floral organ abscission (Ellis et al., 2005).

The genetic analyses above show that either individual or pairs of activating ARFs can regulate distinct developmental processes, although further roles may be masked by genetic redundancy. In order to understand how ARFs can mediate such diverse functions, researchers have mapped the expression of ARFs at the cellular scale (Rademacher et al., 2011; Truskina et al., 2021). In both the root and shoot apical meristems, each ARF shows a unique but partially overlapping expression pattern. It is likely that each ARF or combination of ARFs regulate a different subset of targets. Consistently, over-expression of ARFs causes distinct phenotypes that are not present when other ARFs are overexpressed. For example, overexpression of *ARF5* can restore the *arf7* hypocotyl elongation phenotype, but overexpression of *ARF7* cannot restore the vascular defects in *arf5* (Hardtke et al., 2004).

Such specificity could be underlined by difference in expression patterns, but it could also be the result of post-transcriptional modification of auxin signalling machinery. Recently, there have been several studies identifying posttranscriptional regulation of ARFs. *ARF6* and *ARF8* can be repressed by miR167 (Yao et al., 2019; Zheng et al., 2019). ARF7 and ARF19 have also been shown to be a target for differential polyadenylation under different concentrations of auxin (Hong et al., 2018). ARF7 is a target of SUMOylation, through which root branching pattern is adapted in response to water availability (Orosa-Puente et al., 2018). Both ARF7 and ARF19 can be phosphorylated by BIN2, and this inhibits the interaction of ARFs and AUX/IAA (Cho et al., 2014).

Recently we investigated the regulatory networks acting upstream of the five Class

A activating ARFs and found that at these loci, chromatin was generally open and that transcription was predominantly controlled by a collection of transcriptional repressors (Truskina et al., 2021). The genomic structure of these ARFs, generally featured a large first intron. As intronic sequences had previously been implicated in regulating expression patterns (Bradnam & Korf, 2008; Friede et al., 2017), the expression of all five activating ARFs was investigated in transgenic reporters containing either only sequence 3' to the transcriptional start site or in reporters containing an in-frame fusion of GFP to the second exon (Truskina et al., 2021). *ARF7* showed an interesting expression pattern, that deviated to those we observed for the other ARFs. Whilst for ARFs 5,6,8 and 19, there was no discernible difference between the two promoter fragments, there was a clear difference in the *ARF7* expression pattern. A broad expression of *ARF7* was observed in root tips only in the second reporter, whilst both reporters produced similar expression patterns in shoots. This study suggested the presence of regulatory elements either in the first intron or associated sequences that guide expression in roots but not shoots. Given that these regulatory sequences appeared to increase GFP transcription, transcriptional activators likely bound these sequences. This was in sharp contrast with the majority of components identified within the ARF regulatory networks that were predicted to be transcriptional repressors. In this paper, we explore the role that sequences 3' of the transcriptional start site (including intron) play in regulating *ARF7* expression, and identify a group of transcription factors that modulate *ARF7* expression through these sites to coordinate root growth and development.

Results

The first intron is required for *ARF7* expression in the Root apical meristem.

Our previous work had shown different expression patterns for *ARF7* in the root when driven by a promoter including only sequence 5' of the translational start site (TSS) to those when the Venus was present as an in-frame fusion to the second exon (Truskina et al., 2021). To test whether these differences were due to the inclusion of the first intron, rather than as a result of either binding sites or

increased translatability resulting from the first exon, we designed a series of constructs to separate these possibilities. We exploited recent advances in greengate cloning (Lampropoulos et al., 2013) using the Dual Expression and Anatomy Lines (DEAL) system (Kümpers et al., 2021). We initially created two constructs that contained only 5' sequence upstream of the TSS or included an in-frame fusion to the second exon (Fig.1A). Similar to previous reports, the construct containing only 5' sequence (pARF7::GFP) showed virtually no GFP fluorescence in the root apical meristem, whilst the construct containing both the first exon and first intron (pARF7::ARF7^{EX1-2}:GFP) showed broad expression in the RAM, including within the stele, endodermis, cortex and epidermis (Fig.1B).

To test whether sequences in the first exon or first intron were responsible for the altered pattern, we created a new reporter line including an in-frame fusion with the first exon (pARF7::ARF7^{EX1}:GFP). Similar to reporter constructs driven by the 5' sequence alone, we saw a very little expression within the root meristem. The expression was quantified by qRT-PCR. The pARF7::GFP and pARF7::ARF7^{EX1}:GFP had a low expression, but the pARF7::ARF7^{EX1-2}:GFP had a significant higher expression level (Fig.1C). As the coding sequence included within pARF7::ARF7^{EX1}:GFP and pARF7::ARF7^{EX1-2}:GFP constructs differed by only 8bp, these results indicated it is the first intron, rather than first exon, that plays an important role in defining ARF7 expression expression specifically within the root apical meristem .

To test if first intron effected *ARF7* expression in other tissues, we observed different tissues with pARF7::ARF7^{EX1}:GFP and pARF7::ARF7^{EX1-2}:GFP. For the root, in the elongation zone and maturation zone, pARF7::ARF7^{EX1-2}:GFP showed slightly higher expression in vascular cylinder (Suppl. Fig. A). The different stages of lateral root also had similar expression (Suppl. Fig. B). We tested levels within the leaves using qRT-PCR, and these results indicated that the intron does not affect *ARF7* levels in leaves (Suppl. Fig. C). Therefore, we propose that the first intron is only required to drive expression within the RAM.

Regulation of gene expression is an essential aspect in controlling development

and differentiation of cells. Whilst for most genes, the majority of essential regulatory elements are located 5' to the transcription start site (TSS), there are several examples in which introns play an important role in transcription (Bradnam & Korf, 2008; Friede et al., 2017). Introns can increase the level of gene expression, and in these examples greater quantities of mRNA are seen in constructs incorporating introns (Callis et al., 1987). Introns can also change the spatial expression patterns of tissue-specific genes (Emami et al., 2013; Giani et al., 2009). For instance, the second intron of *AGAMOUS* (*AG*) contains enhancer elements are sufficient to confer a normal *AG* expression pattern (Deyholos & Sieburth, 2000). Also, binding sites within the second intron of *GLABRA3* (*GL3*) regulate its expression in trichomes (Friede et al., 2017).

Introns can influence transcription via many different mechanisms. For instance, they may contain enhancer sites that recruit transcription factors, affect mRNA accumulation or boost translation. Whilst enhancers can work in either orientation and can sometimes be large distances from the transcriptional start site (Zabidi & Stark, 2016), to increase mRNA levels via Intron Mediated Enhancement (IME), introns must be within transcribed sequences less than 1kb downstream of the transcriptional start site (Gallegos & Rose, 2017; Rose, 2004, 2018). To test whether the position of the first *ARF7* intron is required to drive expression in the root, we made a construct (pARF7^{UTR-INT}::GFP), in which we moved the intron to 5'UTR. This was inserted in -46 nt upstream from the ATG translational start site (Fig.1A). For most plants, introns are transcribed to pre-mRNA then spliced to form mRNA. To enable correct splicing of this intron, we also inserted exon-intron junction in both sides. To verify that this new intron was correctly spliced, we used RT-PCR with a pair of primers located within the 5'UTR and the GFP coding sequence (Fig.1A). We compared the size of amplified band between several lines. Transgenic lines harbouring the pARF7::GFP or pARF7::ARF7^{EX1}:GFP constructs did not contain an intron, and gave bands of 300bp and 323bp respectively. In plants with the pARF7::ARF7^{EX1-2}:GFP construct, the size of the fragment with splicing or without splicing should be 332bp or 652bp. For the pARF7^{UTR-INT}::GFP lines, the fragment spliced or without splicing should be 312bp or 632bp. The gel results showed correct transcript splicing of all constructs (Fig.1D). These results were

confirmed by Sanger sequencing of amplified fragments. Plants harbouring the pARF7^{UTR-INT}::GFP showed expression patterns in the root apical meristem that were indistinguishable from (pARF7::ARF7^{EX1-2}:GFP) (Fig.1B). Quantification of mRNA levels via qRT-PCR also showed comparable levels of expression between these two constructs (Fig.1C). These data indicated the position of intron is not a determinant of its ability to drive broad expression in the root apical meristem.

These results show that the position of the intron is not crucial to driving expression of *ARF7* in the root meristem, and are more consistent with a role of the first intron exerting its role on *ARF7* expression via the presence of transcription factor binding sites.

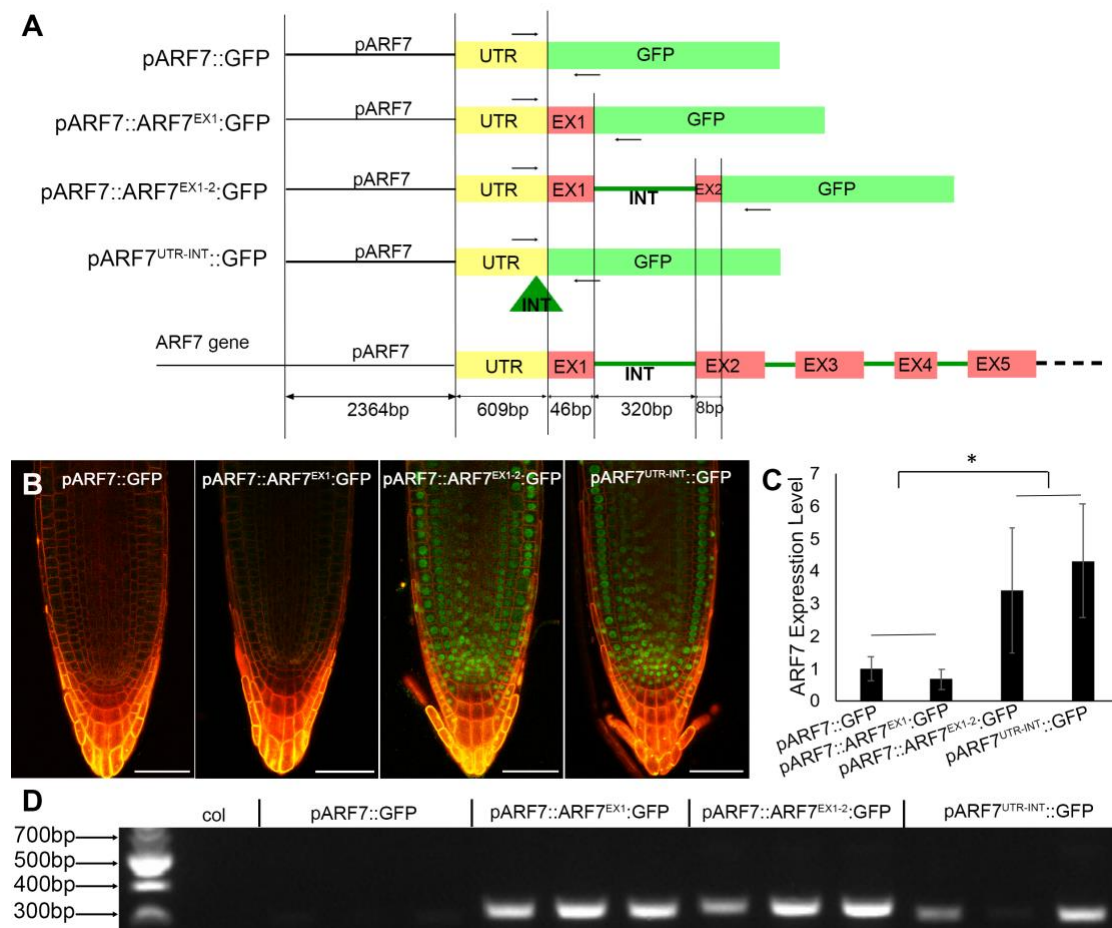


Figure 1. Analysis of *ARF7* expression in RAM with different lengths of promoter demonstrates a requirement for the first intron in driving expression in the root meristem. (A) Schematic diagram showing different *ARF7* promoter configurations used in this project. Pro, promoter; EX, exon; INT, intron. (B) Confocal images showing expression of *ARF7* in RAM with constructs in (A). Scale bars are 50µm. (C) *ARF7* expression level quantified

by qRT-PCR in 2mm root tips. The expression with first intron is significantly higher than without first intron, $p < 0.01$. Significant test was done by T-test. Error bar are standard deviation of three independent transgenic lines. (D) RT-PCR showed splicing of *ARF7* with different length promoter. Primers indicated in (A) as arrow. Each construct had three independent lines.

The first intron contains potential *cis*-elements.

Our analysis revealed the first intron is vital element for *ARF7* transcriptional regulation and expression analysis suggested the possibility that the first intron contains relevant TFs binding sites. To identify potential regulatory elements, we first examined conservation of the intronic sequence within the 1001 Genomes Sequencing project. The alignment of the sequences of first intron in these lines indicated a high degree of sequence conservation within the first intron, supporting the possibility that this region could have important binding sites.

The PlantRegMap (Plant Transcription Regulatory Map) provides a high-quality resource of TFs and target genes, including a set of high-quality, non-redundant TF binding motifs derived from experiments and regulatory elements identified from high-throughput sequencing data (Jin et al., 2017). When a threshold p -value $< 1e-4$ was applied, this intron has 33 putative binding sites of 28 TFs, including 19 NAC family genes (Suppl.Table.1). Simultaneously, we examined DNA affinity purification sequencing (DAP-seq) data, showing in-vitro-expressed TFs interacting with genomic DNA (O'Malley et al., 2016). This data identified 4 transcription factor gene families binding to the region of intron, these are bHLH, C2H2, NAC and WRKY. All these NAC binding sites aligned with those previously identified using the PlantRegMap analysis. We used this knowledge of binding sites to probe the 1001 genome sequences in more detail. We examined the previously identified binding sites and found that these TF binding sites were highly conserved.

Taken together these results identified several potential TF binding sites that may define expression within the root (Fig2).

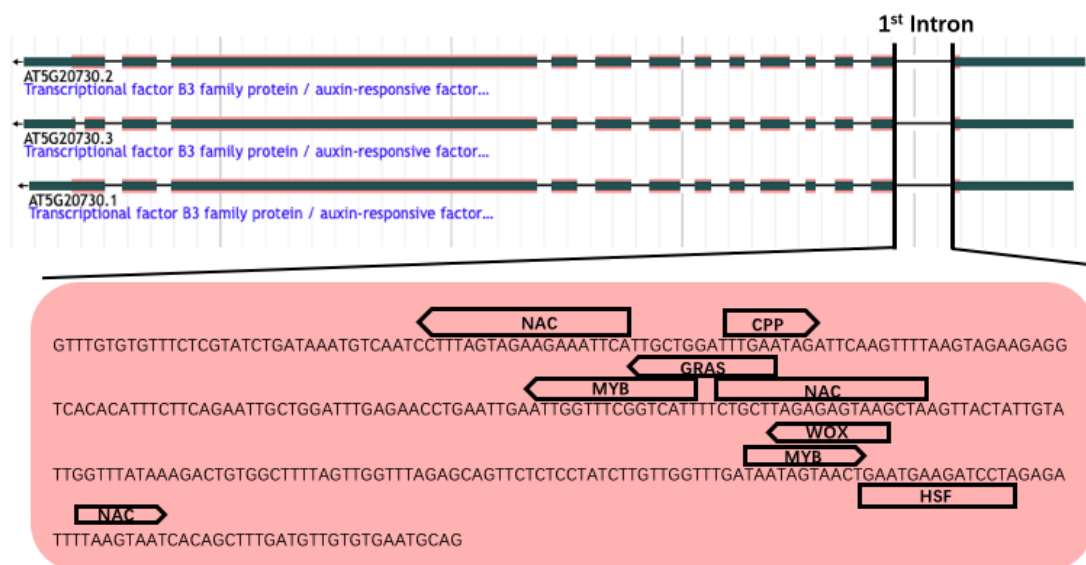


Figure 2. Bioinformatic analysis of first intron identified potential NAC and MYB Transcription factor binding sites. The sequence shadowed in pink is ARF7 first intron. The rectangles with arrow show the motif is in forward or reverse strand. The rectangles show they bind in both strands

Multiple TFs binding sites are required for regulation of *ARF7* transcription

In order to functionally dissect the *ARF7* intron and identify the location of key binding sequences, the intron was divided into four overlapping parts, with each of these being sequentially deleted. Each deletion (D1-4) was 90bp and contained different combinations of the *cis*-regulatory elements identified previously. We combined these intron dissections with the rest of the promoter and used these to drive GFP (pARF7::*ARF7*^{EX1-2(ΔD1-D4)}:GFP). From the fluorescent images, it can be seen that all these deletions showed GFP expression within the root apical meristem (Fig.3B). Whilst deletions D1, D3 and D4 showed expression level similar to pARF7::*ARF7*^{EX1-2}, only D2 had a significant decrease quantified by qRT-PCR, but not to the levels seen in lines without an intron (Fig.3C).

This suggested that multiple binding sites may be required within the introns. We then focused on transcription factors that were predicted to bind to multiple locations within the intron. Our previous bioinformatics analysis had identified

multiple binding sites for both NAC and MYB transcription factors. The three NAC binding sites were located in D1, the overlap of D2 and D3, and D4. The two MYB sites were located in D2 and D4 deletions.

We next investigated the importance of each of these NAC binding sites by making three constructs in which NAC sites were deleted (pARF7::ARF7^{EX1-2(ΔNAC)}:GFP). In these 2bp in the core NAC binding sequence were altered (Fig.3A) based on the TFs position frequency matrices and TFs flexible models provided by JASPAR (Stormo GD, 2013). Combining the position information from JASPAR and the sequences from PlantRegMap, we selected motifs to target to modulate the interaction of NAC proteins with the intronic sequence. However, no significant differences were found in the GFP levels in these constructs with mutated NAC sites (Fig.3B). The mRNA levels of GFP were quantified by qRT-PCR (Fig.3C), and again we did not see a significant reduction in GFP transcript. This indicated that no single NAC binding was solely responsible for controlling expression in the root, and that deletion of the second NAC binding site alone was not sufficient to explain the reduced expression of ARF7 mRNA in the deletion D2. We therefore assumed that the effect that this intron had on transcription was regulated either by multiple TFs or a single TF complex binding to multiple sites.

As MYB and NAC TFs had multiple binding sites, we made two constructs in which both MYB sites and all 3 NAC sites were deleted and used this to drive GFP (Fig.3A). In both constructs the level of *ARF7* expression level was slightly decreased when either the MYB or NAC binding sites were mutated (Fig.3B). These differences in GFP were consistent with reductions in the level of GFP mRNA quantified via qRT-PCR (Fig.3C). In these experiments, *ARF7* was still expressed in the RAM with mutations within NAC and MYB binding motifs. Collectively, these results support a theory that MYB or NAC could not bind DNA within intron independently. Both MYB and NAC might bind DNA within intron together as transcriptional complex.

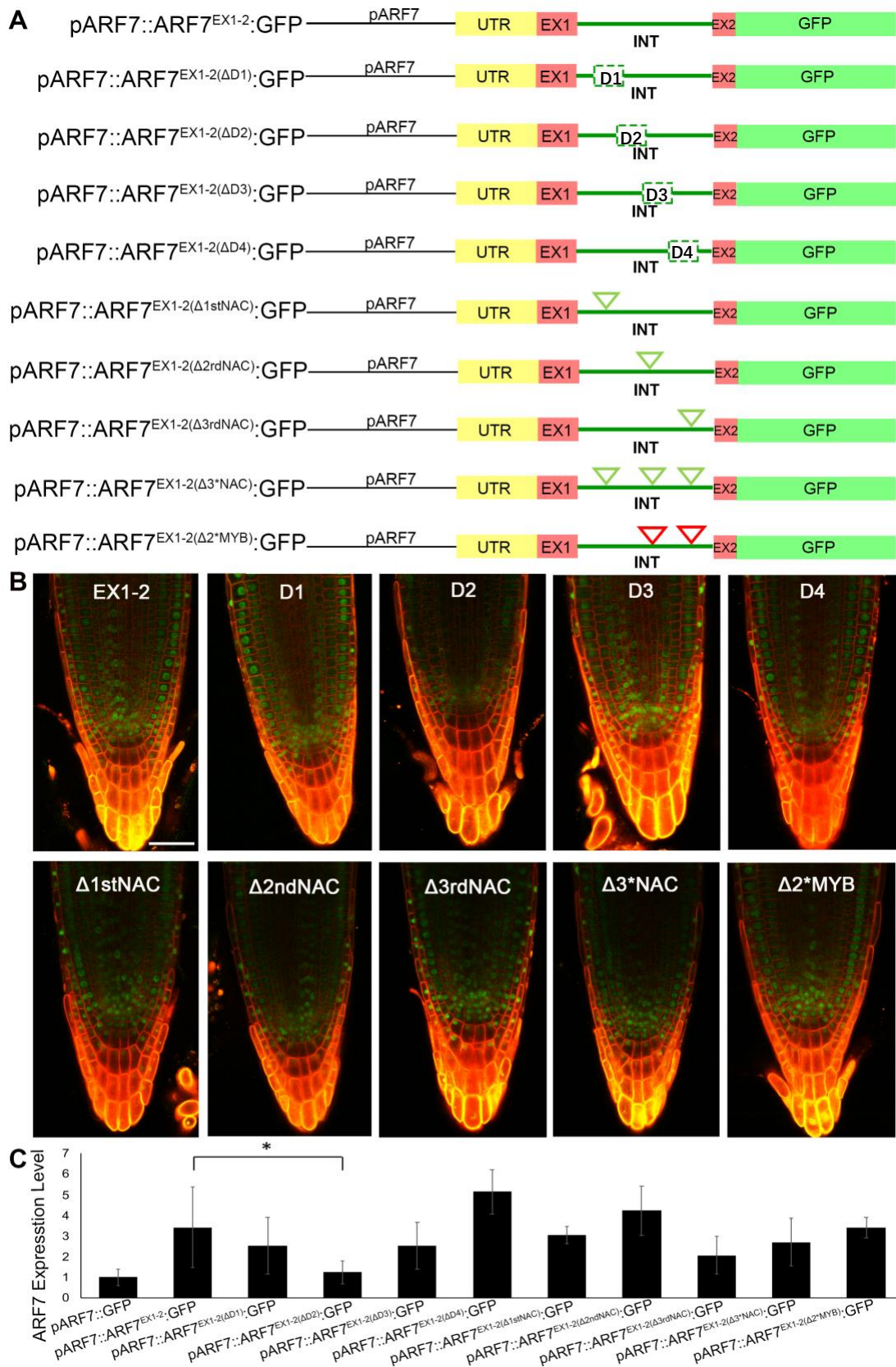


Fig3. Functional Dissection of first intron reveals that multiple regions are required to drive expression in the root apical meristem. (A) Schematic description of intron dissection constructs. The deletion sequence and each key binding sites exchanged 2bp

showed in methods and is shown with a dotted green line. NAC binding sites are shown with green triangles and MYB binding sites with red triangles (B) Confocal images showed ARF7 expression with dissected intron constructs in RAM. Scale bar is 50 μ m. (C) ARF7 expression level quantified by qRT-PCR in 2mm root tips. The expression of second deletion construct decreased compared with full length intron, $p < 0.05$. The significance test was done by T-test. Error bar are standard deviation of three independent transgenic lines.

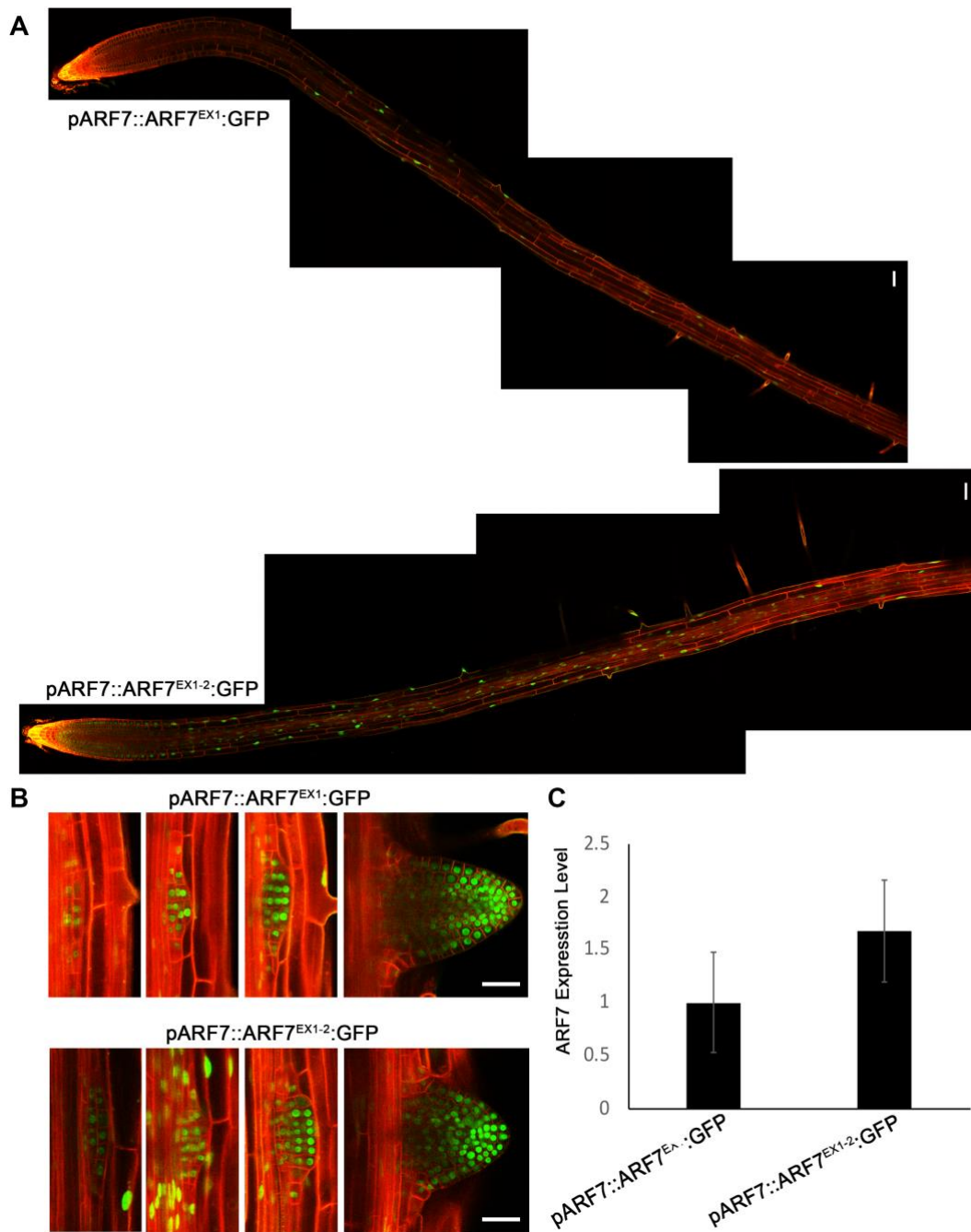
Discussion

This study developed a series constructs which collectively indicated that the first intron of *ARF7* is required for broad expression in RAM. It suggested that the intron plays an important role in transcription regulation in the root. Interestingly, our previous work (Truskina et al., 2021) shows that the presence of sequences 3' of the translational start site have no effect on expression in the SAM, suggesting a root-specific requirement for this intron. This root specific requirement is also intriguing as whilst the presence/absence of the first intron has a profound effect on ARF7 levels in the 5 days old primary root, it has almost no difference in expression in the lateral root meristem. This raises the question what is different about these two tissues? Could it be due to age? If this were true, we may predict that very young (i.e. 1-2 days old roots) may display higher levels of ARF7 or that lateral roots may lose expression of ARF7 as they mature. Either way this raises a very interesting question in which a different set of regulators must control ARF7 expression in either an age-dependent manner or a root class- (i.e. lateral versus primary) dependent manner.

As introns regulate transcription via different mechanisms, we sought to determine the effect that the first intron on *ARF7* had on its expression. Introns can direct the site of transcript initiation. For example, deleting 303 nucleotides of the TRP1 promoter including all known TSSs and all but 18 nucleotides of the 5'UTR had virtually no effect on the level of gene expression as long as the UBI10 first intron containing stimulatory sequences was included (Gallegos & Rose, 2017). Introns can also have regulatory elements, such as enhancers (Beaulieu et

al., 2011). Enhancers can work over distance and downstream of the TSS. Especially, this is common for genes in which the first introns are large (Chorev & Carmel, 2012). For example, AGAMOUS LIKE 24 (AGL24) had a large first intron (721bp). The intron contains homotypic clusters of transcription factor binding sites, which are required to direct floral expression (Hussain et al., 2019). To investigate if ARF7 first intron contain *cis*-elements, we moved the first intron to UTR. Transgenic lines with the intron within the sequences 5' of the start codon still showed comparable expression with lines in which the intron was in the UTR. As the position of the intron plays a crucial role in determining transcript levels in cases of intron mediated enhancement (Rose et al., 2019) and as there have not been reports of tissue specific IME, this suggested that TF binding motifs within the intron were likely involved in its regulation. To explore this further, the new constructs could be generated that move the sequence for the intron further upstream.

The promoter dissection results suggested that NACs and MYBs multiple binding sites may be required within the intron as no single deletion within the intron was sufficient to abolish expression. Our bioinformatic results analysis of the literature suggested some likely candidates that may bind within this intron. The NAC proteins, the triple mutant *vnd1vnd2vnd3* failed to recover lateral root development in response to the change of light conditions (T. T. Tan et al., 2018). For MYBs, MYB33 expression can be detected in the whole seedling, and mostly in root tips and leaves (Allen et al., 2007; Liang et al., 2013). MYB65 is mainly expressed in roots, leaves and pollen grains (Liang et al., 2013). MYB101 expressed mostly in mature pollen grains (Allen et al., 2007; Liang et al., 2013; Xue et al., 2017). Previous studies have shown MYB33 and MYB65 expressed in the root tip (Allen et al., 2007; Xue et al., 2017) and overlaps with where *ARF7* is expressed. Furthermore, a prior study has linked MYB33, MYB65 and MYB101 to root development as lines with elevated expression of these genes have increased primary root growth (Xue et al., 2017). miR159 inhibited primary root growth by mediated repression of *MYB33*, *MYB65* and *MYB101* (Xue et al., 2017). In the future, we could focus on these NACs and MYBs candidate to reveal the interaction of NAC and MYB and the intron.



Supplementary Figure. *ARF7* have similar expression pattern with different length promoter in root and leaf (A) Confocal images showing *ARF7* expression with or without intron constructs in primary roots. *ARF7* is slightly expressed in vascular and epidermis. Scale bar is 50 μ m. (B) Confocal images showed *ARF7* expression with or without intron constructs in lateral root primordia. *ARF7* is expressed in primordia with both constructs, but it is stronger in vascular with intron. Scale bar is 50 μ m. (C) qRT-PCR result showed *ARF7* expression level with or without intron constructs in whole leaves. $p < 0.05$. Significant test was done by T-test. Error bar are standard deviation of three independent transgenic lines.

Discussion

Auxin is a vital plant hormone and regulates almost every developmental process however it is unclear how one molecule can regulate so many aspects of plant development. In Arabidopsis, each component of the auxin signalling machinery is represented by a multigene family. These have subfunctionalised so that many proteins may have distinct biochemical properties. The resulting diverse range of binding specificities, protein turnover or enzymatic properties gives rise to multiple auxin responses that can regulate diverse and highly specialised processes. In all plants in which the auxin signalling pathway has been studied (from Arabidopsis to Marchantia), ARFs bind to the promoters of a large number of downstream genes to regulate different developmental processes in a spatial and temporal manner. ARFs are regulated by specific Aux/IAs, which in turn add a regulatory layer through which specific developmental responses may be defined (Weijers et al., 2005). In order to understand how this complexity has enabled the evolution of novel auxin responses it is important to study both the expression patterns and biochemical properties of all auxin signalling components. This is a huge task, and therefore, in this thesis, I have focused on the Class A ARFs and ask specifically what regulates their tissue specificity in terms of expression patterns.

1. Class A ARFs have unique expression pattern in RAM and SAM

ARFs are divided into 3 classes. Class A ARFs have previously been shown to have unique expression patterns in the RAM and SAM (Rademacher et al., 2011; Vernoux et al., 2011). Class B ARFs expression patterns were also reported, such as ARF1 and ARF2 are expressed in all cell types of RAM and the periphery of SAM (Rademacher et al., 2011; Vernoux et al., 2011). Most of the Class B ARF loss of function mutants do not show clear phenotypes, however functional roles have been investigated based on gain-of-function phenotypes (Okushima et al., 2005). Compared with Class B ARFs, there are several advantages why focusing this study

on Class A ARFs is a more tangible way to explore ARF regulation. Firstly, in Arabidopsis this group is smaller, and comprises only five members compared with 15 members for Class B ARFs (Finet et al., 2013; Okushima et al., 2005). Secondly, Class A ARFs have been associated with specific auxin responses; for example, ARF7 and ARF19 control LR development and ARF6 and ARF8 control flower maturation. Also, their mutants have clear phenotypes. The only single mutant with a lethal phenotype is ARF5 (Berleth & Jurgens, 1993). Although *arf6* and *arf8* showed few differences with wild type, *arf6arf8* double mutant do not produce seeds and development is completely arrested (Nagpal et al., 2005). *arf7* displays an altered phototropic response and fewer lateral roots than wildtype (Okushima et al., 2005). *arf7arf19* fail to form lateral roots and have a gravitropic defect of (Okushima et al., 2005). In Manuscript 1, we investigated the expression of these 5 ARFs and showed that they have unique expression in root and shoot apical meristems.

Our study highlighted the need to use the correct promoter in order to reproduce the desired expression patterns. A previous study generated an expression map in the RAM of all ARFs via reporter lines based on promoters including 2kb of sequence upstream of each ARF start codon (Rademacher et al., 2011). We used different reporter lines, that have longer promoters containing 3-5kb 5' of the ATG and 3' of the ATG up to the end of the first intron. These lines produced some different expression patterns to those previously observed. For example, our lines did not show that ARF7 expression is limited to the QC, but is strongly expressed throughout RAM. There is a study which produced an expression map of all ARFs in SAM via in situ hybridization (Vernoux et al., 2011). Our reporter lines showed a more consistent expression pattern in SAM, in line with the in-situ, indicating that they produce a more faithful transcriptional pattern. Especially, using a longer promoter for ARF6 was essential. Like the in-situ, our 3255kb showed enriched expression in the boundary domain. This is much more restricted than in the 2kb promoter, and supports a mechanism in which binding sites associated with transcriptional repression are missing in the 2kb promoter. These expression data demonstrated these ARFs have unique expression patterns in different tissues. For example, in the RAM ARF5, 6 and 7 are expressed in most

of the RAM, but ARF5 is not expressed in cortex and endodermis, ARF6 shows less expression in the columella. ARF8 is expressed in epidermis. ARF19 is restricted to root cap and protoxylem.

In addition, our reporter lines indicated an interesting expression pattern for ARF7. ARF7 had a different expression in RAM and similar expression in SAM when comparing both promoter lengths. This suggested the specific RAM expression of ARF7 required the first intron.

The tissue-specific expression pattern might be due to the chromatin accessibility. DNA is packaged by four histone proteins. Polycomb group proteins are multi-protein complexes that can modify histones to repress gene expression, especially trimethylation of Histone H3 Lys 27 (H3K27³) methylation (Kim & Sung, 2014). PcG proteins mainly maintain the gene stable transcriptional states by histone modification H3K27me3 which can be applied in a tissue- and time-specific manner (Kim & Sung, 2014). However, our chromatin status analysis showed H3K27me3 is largely absent in all Class A ARFs and these loci have accessible regulatory regions. It suggests the chromatin accessibility of Class A ARFs loci is not the main mechanism to define tissue-specific expression.

2. The repressor network is a crucial part for Class A ARFs regulation

After determining that the Class A ARFs had spatially specific expression in the both the root and shoot meristems, we determined what factors regulated their expression. To do this we performed a Y1H screen using libraries of transcription factors expressed in root and shoot apical meristems. Then we classified most of TFs are repressors by following expression of ARFs when co-transformed with the TFs in a transient protoplast assay. To further explore the functional role of these TFs in planta, we obtained mutant lines from the stock centre. After confirming the presence of t-DNA inserts, and performing qRT-PCR analyses to ensure that the levels of transcripts were altered, we finally identified 24 TF mutants. Levels of ARFs were assayed using qRT-PCR in mutants of individual transcription factors to determine the role that they exerted on their transcription.

As this network was identified in yeast, we cannot assume that the protein DNA interactions that we observed in yeast occur *in planta*. The protoplast work helped to address this, but even though this was done in Arabidopsis protoplasts it is based on ectopic expression of the factors. There are examples where interactions identified in heterologous systems do not necessarily occur in the native system. This could be, for example, because the two components may not be expressed in the same tissue, or that proteins may be miss-folded or require specific partners. Although we thought that the qRT-PCR in mutants would show this, the experiment turned out to be more complex than we first anticipated. Our hypothesis was that if transcription factor X regulated ARFY, then when transcription factor X was knocked out, then the level of ARFY mRNA should go up, due to the loss of an inhibitor. Whilst this happened in some cases, in many cases the opposite scenario occurred and the levels of mRNA went down. It is well known that the auxin signalling pathway is highly non-linear and multiple feedbacks exist, these include (but are not limited to) ARFs regulating the expression of TFs that then repress the ARFs, and scenarios in which multiple TFs converge on the same ARF. This was especially true for ARF8, for which we identified many regulating partners, and previous microarray studies indicated its levels are auxin responsive. This caused us to re-think these experiments and by taking a systems approach in which we modeled the potential TF-ARF interactions. We identified scenarios in which the ARF levels could go either up or down as a result of the removal of a repressive ARF.

This highlighted the need for much greater validation of the network to verify that the TFs identified affected ARF expression and that they did so as negative regulators. To do this we designed three experiments, these included over-expression of TFs in ARF reporter lines, generating new reporter lines to check the co-expression of TFs and ARFs in specific tissues and carefully measuring the phenotypes of TFs in processes which are known to be regulated by auxin. I was instrumental in establishing the transgenic lines for the first two experiments, but I concentrated my efforts on analyzing the over-expression lines. The long-term overexpression of TFs might lead to strong and pleiotropic phenotypes, so we

selected oestradiol inducible constructs. We used the constitutive UBQ10 promoter followed by the chimaeric transcription activator containing XVE, driving TF coding sequence and mCherry. These constructs were transformed in their corresponding ARFs reporter lines (pARF::mVenus). The mCherry is tagged to the TFs to confirm TFs are induced, and mVenus was used to show ARFs expression and analyse how ARF expression changes under overexpressed TFs. In total, we created 15 overexpression lines. I used many different induction conditions, including different β -oestradiol concentration (1-100 μ M), treatment time (2-48h) and treatment methods (dilute in medium plate or solution). Finally, I induced TFs in 1/2 MS plates with 10 μ M β -oestradiol for 24h. I only looked at plants where I saw induction, and only observed induction of mCherry in CRF10 and AL3. Over expression of CRF10 and AL3 both repressed ARF7 in our network. I measured ARF7 fluorescence intensity in a fixed area in WT, OE-CRF10 and OE-AL3 backgrounds. The ARF7 expression level reduced significantly in the two OE lines, confirming these two proteins are transcriptional repressors.

Collectively these data support the role that these TFs regulate ARF expression, but if they have a meaningful role in plants we would expect to see differences in processes that are known to be regulated by auxin. As both root length and gravitropism are controlled by auxin, I selected to investigate these processes. High auxin treatment inhibits primary root elongation (Rayle et al., 1970). Therefore, we tested root length with IAA treatment. Plants were grown on agar plates with or without 10 μ M IAA. The mutant and Col-0 control were grown on the same plates to avoid the difference due to plate-to-plate variation. I imaged 5, 10, 15 days old roots to analyse root length changes in auxin treatment. The 15 days data show more significant differences. 14 of 24 mutants showed altered auxin response. For gravitropism, plants were grown on agar plates for 5 days, then were turned 90° in dark. I imaged root during 12h in dark, then analysed root tip angle. The mutants and Col-0 control were also grown on the same plate. The final root tip angles of mutants were similar with wild type, but the speed of the response was different.

In addition, we analysed the role of auxin in various shoot processes. Collectively

these results indicated these TFs are involved in different auxin responses and provided further validation of our network.

This network provides some interesting leads that could be followed up in different projects to investigate individual processes regulated by specific TFs. For example, *LBD3* was identified in our network as a repressor of ARFs 5 and 7. This has previously been indicated to be cytokinin inducible (Brenner & Schmulling, 2012). Therefore, this provides a potential new node in CK and auxin cross talk, in which cytokinin output can restrict auxin response via modulating specific ARFs. To test if it induced by CK in the root, we divided seedlings to two groups. One group was treated with 1 μ M BA, and the other group was treated with the same volume DMSO, after 20 mins incubation +/- BA, I collected 2mm root tips for qRT-PCR. I found *LBD3* expression increased rapidly after CK treatment in root tips. CK and auxin are known to regulate several processes together in plants such as determining the size of the root meristem and regulating vascular pattern. To investigate if *lbd3* might be involved in this process I obtained a *lbd3* mutant and measured the length of the root meristematic zone. By counting the number of cortex cells prior to elongation, I observed that these were reduced slightly in *lbd3* mutant. This suggests that *LBD3* might play an important role in regulating auxin-cytokinin crosstalk during root growth. Although the *lbd3* mutant phenotype is weak, the LBDs comprise a large gene family and there may be considerable redundancy between these genes. *LBD4* is its closest homologue, so we investigated this further. *LBD4* can also be induced by CK, an observation which I tested using the same approach as with *LBD3*. The phenotype of *lbd4* is also weak, and so I obtained a *lbd3lbd4* double mutant. In addition, *lbd3lbd4* show a slight difference in vascular pattern as can be observed in plants treated with very low levels of cytokinin (2nM BA). This was observed using a similar assay for scoring protoxylem response to CK as used in Mähönen et al., (Mahonen et al., 2006). In order to follow this further, it would make sense for future researchers to construct higher order mutants, as there is likely to be considerable genetic redundancy within this family.

Collectively, this work identifies a repressor network that regulates ARF expression

in Arabidopsis. Our data provide insights into the spatial regulation of ARF but we did not consider the temporal expression. A previous study inferred a gene regulate network controlling LRP initiation based on a time-series transcriptomic data set (Lavenus et al., 2015). It indicated ARF7 can directly regulate ARF19, an interaction that was not identified in our studies despite ARF19 being present in the library. This shows that whilst our network may be representative there will be many important regulators yet to be identified.

3. Post transcriptional regulation also plays a role in Class A ARFs regulation

Although our recent work was focused on the transcriptional control of ARFs, we know that not only differences in specific expression define roles for individual ARFs in different developmental processes, but also post transcriptional regulation cause changes in their dynamic output. There are several examples of this. Alternative splicing of ARFs can produce different variants with specific functions. An alternative splice variant of ARF5 (MP11ir) lacks the ARF5 C-terminal PB1 domain (Cucinotta et al., 2021). The MP11ir variant has a specific role in ovule integument elongation, Therefore, changes in splicing define a tissue- and development-specific in ovules (Cucinotta et al., 2021). These changes are not only limited to ARF5. ARF8 was reported to have a flower-specific functional splice variant ARF8.4 (Ghelli et al., 2018). ARF8.4 is an intron-retaining variant of ARF8.2 that controls filament elongation and endothecium lignification (Ghelli et al., 2018).

Post-translational modification of ARFs can impact auxin responses. For instance, the SUMOylation and phosphorylation of ARF7 are involved in different LR developmental processes. SUMOylation of ARF7 controls the root branching pattern in response to water availability (Orosa-Puente et al., 2018). SUMOylated ARF7 recruits the Aux/IAAA repressor protein IAA3 on dry side (Orosa-Puente et al., 2018). Phosphorylation of ARF7 and ARF19 potentiate auxin response during lateral root development (Cho et al., 2014). The location of protein can also impact transcription factor activity. ARF7 and ARF19 form cytoplasmic assemblies to regulate nucleo-cytoplasmic partitioning (Powers et al., 2019). The nucleo-cytoplasmic partitioning varies in different zones of the root. Although the

mechanism regulating this is not yet understood, it has been shown to regulate auxin response in a cell-specific manner (Powers et al., 2019).

4. The Dual Expression and Anatomy Lines (DEAL) provide a robust way of imaging dynamic changes in gene response.

In order to understand ARFs promoter function in auxin responses, we need to show gene expression in different spatial and temporal distributions. Therefore, we developed a new system showing cellular anatomy which can efficiently combine with auxin sensors by Greengate cloning. We combined several specific cell-type genes with this system to give more information about cell fate acquisition within the vascular cylinders. We created two DEAL versions for Arabidopsis, one showing good expression within the primary root and the other within the lateral roots. To understand the spatial and temporal control of auxin response, we need information on auxin distribution and real time auxin response. For example, a previous study quantified auxin cell distribution in gravitropism by DII Venus reporter (Band et al., 2012). Auxin responses are quantitative responses, so the expression of genes regulating auxin response should be quantified in individual cells.

Compared with propidium iodide counterstaining, DEAL has several advantages. The tdTomato signal is stable over time allowing long-term imaging. Particularly in mature roots, we also see vastly improved signal from vascular tissues and by using variants that are expressed in discrete tissues – such as the LR variant – we can focus imaging specifically on the desired structure. When combined with a newly developed flow cell, these lines provide an efficient way to observe how gene expression or cell identity changes following either environmental stimuli or changes in hormone activity.

DEAL was especially relevant to my studies as in the last chapter I developed a series of promoter truncations to dissect functionally important domains within the ARF7 reporter. In this experiment I systematically deleted parts and compared the GFP expression in lines with and without those sections. In studies like this, if

a particular construct does not give GFP expression this could be for several reasons. It could be that the deleted promoter is insufficient to drive expression of GFP. However, it could be due to incomplete transfer of the plasmid DNA into the plant, or it could be due to gene silencing or incorporation into a heavily methylated region of DNA. However, as DEALs have both the *td Tomato* and the GFP construct in the same plasmid, this meant that every transformant effectively had a control to show that the transformation worked.

To optimise the system and check the effectiveness of the DEAL system, I analysed the expression of 16 marker genes in both primary and lateral roots. As the rationale for producing DEAL was to improve live imaging, it was essential to test the effectiveness with which DEAL could work in long term imaging scenarios. This technology opens the way for future studies to look at how cell fates are assigned in newly formed organs. This has previously been challenging as simultaneously following cell anatomy and gene activity is challenging. In order to prove that DEAL could be used in this way, I established time lapse images of AHP6 expression in a lateral root primordia over 24h. I transferred a seedling with an agar block into a chambered cover slide and took z-stacks confocal images over 24h. These showed AHP6 expression in primordia from an early developmental stage (stage III) through to the emerged primordia. This provided proof of concept that DEAL allows long term observation of tissues. In addition, another member of our lab followed auxin treatments of primary roots within this system using a newly developed flow cell. Collectively, our results showed that, this system can be used in future for observation of real time auxin response in many different temporarily treatments such as temperature and nutrients. It also provided a suitable vector system that I could use to functionally dissect the ARF7 promoter (see next section).

5. The first Intron can regulate ARF7 transcription via *cis*-regulatory elements.

The first manuscript indicted the chromatin of Class A ARFs are open and regulated by transcriptional repressors. However, ARF7 has an interesting

expression pattern in RAM. When driven under a longer promoter including sequences 3' to the transcriptional start it showed an expanded expression in the root tip. It suggested that whilst our network was mostly consisting of negative regulators, an activator of ARF7 is likely to bind to the sequences 3' of the ATG. The third manuscript used different length 3' sequence driving GFP and showed how these affected the ARF7 expression pattern. The high throughput cloning methods and reliability of having an internal transformation control, were only possible due to the DEAL system. The red membrane marker is a good control to prove the lack of GFP was due to missing regulatory elements rather than failed plant transformation. Previously it was unknown whether the regulatory region allowing expression in the root apical meristem was present in the first exon or intron. I produced a series constructs that indicated that the first intron of ARF7 is required for broad expression in RAM. It suggested that the intron plays an important role in transcriptional regulation. Introns can be involved in transcriptional regulation via different mechanisms. Introns can direct the site of transcript initiation. For example, deleting 303 nucleotides of the TRP1 promoter including all known TSSs and all but 18 nucleotides of the 5'UTR had virtually no effect on the level of gene expression as long as the UBQ10 first intron containing stimulatory sequences was included (Gallegos & Rose, 2017). Introns can also have regulatory elements, such as enhancers (Beaulieu et al., 2011). To investigate if ARF7 first intron contains regulatory *cis*-elements, we moved the first intron to the 5'UTR. Transgenic lines with the intron within the promoter still showed broader expression, suggesting that the intron contain TF binding sites.

In addition, to merely identifying potential binding sites this work identified a good ARF7 promoter, which can be use in future studies, e.g, to determine to what degree ARF specificity regulates the downstream transcriptional cascade. It is clear that ARF7/ARF19 have a specific role during LR organogenesis, but it is unclear whether this is due to specific functions attributed to these proteins or whether this is purely due to the unique transcriptional control. Although elements of this have been studied, there has not been a comprehensive study in which different ARFs have been miss- expressed under specific promoters. I used the ARF7 promoter (swap first intron to UTR) to drive other Class A ARFs in the

arf7arf19 mutant background. I focused on LR number, as that is the easiest to score phenotype associated with *arf7arf19*. Although the control plant transformation of ARF7 driving ARF7 CDS sequenced has failed, the LR number was partially complemented by pARF7::ARF5 and pARF7::ARF19, but not in pARF7::ARF6 and pARF7::ARF8 (Suppl. Fig. 1). This shows that there is functional divergence between these ARFs. To investigate this further I looked at an unrooted tree of Class A ARFs in different species (Mutte et al., 2018). This shows that ARF 5,7&19 form a subclade that is distinct from ARF6&8. The formation of this ARF subclade is already present in the fern *Ceratopteris richardii*, suggesting a very ancient branching between these class A ARFs. It is fascinating that only members of this subclade can complement the lateral root phenotype of the *arf7arf19* mutants. Lateral root formation is only one phenotype associated with these genes, these constructs are also being investigated in a gravitropism assay to understand the subfunctionalisation of ARFs in this process.

6. NAC and MYBs transcription factors could bind in ARF7 first intron

The promoter dissection results suggest that multiple binding sites may be required within the intron as no single deletion within the intron was sufficient to abolish expression in the RAM. Our bioinformatic analysis suggested 3 putative NAC and 2 putative MYB binding sites. However, expression is not significantly reduced when deleting all NAC or all MYB binding sites. Therefore, I created reporter lines deleting MYBs and NACs binding sites within the same construct. I predict it will show a lower *ARF7* expression level.

Our bioinformatic analysed TFs database and suggested some potential NAC candidates which might bind the first ARF7 intron. Some candidates were reported to have roles in root development. VASCULAR-RELATED NAC-DOMAINS (VNDs) encode NAC domain transcription factors (T. T. Tan et al., 2018). Compared with wildtype, the triple mutant *vnd1vnd2vnd3* have shorter primary roots and lack visible lateral root same in weak light condition (T. T. Tan et al., 2018). When transferred to normal light condition, *vnd1vnd2vnd3* cannot restore lateral root formation, but wild type recovers lateral root development (T. T. Tan

et al., 2018). Three potential MYBs that may bind the first ARF7 intron are MYB33 and MYB101 from our motif analysis. Also, MYB65 is closely related MYB33 (Millar & Gubler, 2005). MYB33 is expressed in the whole seedling, but is most abundant in root tips and leaves (Allen et al., 2007; Liang et al., 2013). MYB65 is mainly expressed in roots, leaves and pollen grains (Liang et al., 2013). MYB101 expressed mostly in mature pollen grains (Allen et al., 2007; Liang et al., 2013; Xue et al., 2017). Previous studies have shown MYB33 and MYB65 are expressed in the root tip (Allen et al., 2007; Xue et al., 2017) which overlaps with ARF7 expression. Furthermore, a prior study has linked MYB33, MYB65 and MYB101 to root development as lines with elevated expression of these genes have increased primary root growth (Xue et al., 2017). The microRNAs, miR159a and miR159b, regulate the levels of multiple mRNAs targets, including these three MYBs (Allen et al., 2007; Reyes & Chua, 2007). The *miR159ab* mutant has a reduced growth stature, curled leaves, shorter and fatter fruits and irregularly shaped seeds (Allen et al., 2007). Crucially, the *miR159ab* double mutant also has an increased primary root length with an increase in the root meristem size compared with wild-type (Xue et al., 2017). These changes in the *miR159ab* line are likely directly due to miss-expression of the MYB33, MYB65 and MYB101, as constructs for these MYBs in which the miR159 cleavage sites are removed (pMYB33:mMYB33, pMYB65:mMYB65 and pMYB101:mMYB101) can phenocopy the miR159ab root phenotype (Xue et al., 2017).

At the moment the link between MYBs and ARF7 is unclear. In the future, we could create reporters fusing NACs and MYBs candidates to GFP. These reporter lines can indicate their expression pattern in RAM and SAM. These can be compared with ARF7, to test if they have an overlap in expression pattern. For example, if an individual NAC showed a specific root expression overlapping with ARF7, it would indicate that the NAC might bind the regulatory regions within the intron to regulate ARF7 expression pattern in roots. These reporter lines could be treated by IAA to test if these TFs involve in auxin responses. ChIP PCR can identify which NACs and MYBs bind in the intron. We can create protein antibodies for these potential NACs and MYBs, then use ARF7 intron promoter to do PCR, to demonstrate if these TFs bind in intron in vivo.

To reveal the interaction of NAC and MYB and the intron, the ARF7 expression should be checked *in planta*. As mentioned before, *miR159* inhibited MYBs to reduce primary root growth. We reasoned that the increased primary root growth in the *miR159ab* lines could be due to elevated ARF7 levels, as we had predicted that the MYBs up-regulated in this line bind ARF7. Therefore, to confirm whether ARF7 is regulated by MYB33, MYB65 and MYB101, we examined the ARF7 expression level in *miR159ab*, *myb33myb65*. In these backgrounds, ARF7 expression did not show a significant difference as quantified by qRT-PCR (suppl. Fig. 2). These expression data do not support the role of MYB33, MYB65 and MYB101 as important regulators of ARF7 in the root.

Our previous bioinformatic analysis results suggested NACs and MYBs binding sites are adjacent. This is not something that has been observed before. This warrants further investigation and we could analyse whether the NAC and MYB coordination is highly conserved in the first intron of ARF7 in Brassica species. Further, NAC and MYB TFs might work together in transcriptional regulation of many other genes. To examine this possibility, we could analyse the frequency of NAC and MYB coordination in whole Arabidopsis genome.

In conclusion, Manuscript 1 identified a repressor network of ARFs controlling their transcriptional regulation. In manuscript 3, we focused on ARF7. By deeper analysis of the first intron, we indicated that this intron contains a crucial region of ARF7's regulatory sequences and that activators bind within intron to regulate ARF7 specifically in roots. The results suggest TFs are key regulators of ARF spatial expression, although more work is needed to identify the activator for ARF7. Collectively these studies provide a mechanism how auxin can control different developmental processes in a spatially specific way and my more recent work shows subfunctionalisation of class A ARFs, as only ARFs 5,7 and 19 can partially complement the *arf7,19* double mutant. In the future, we can investigate individual TFs to identify specific auxin response that they are involved in. This work could be further enriched by a better understanding of the gene network downstream of ARFs. This has been done for ARFs 7 and 19, but this data has not

been compared with ARFs from different subclades. As vital auxin signalling components, ARFs are regulated by multiple signalling components. This thesis explores the regulation network of other classes of auxin signalling components. This could apply to other class ARFs as well as Aux/IAAs and future research in this area will further fill the gap in understanding the specificity of auxin responses.

References

- Aida, M., Beis, D., Heidstra, R., Willemsen, V., Blilou, I., Galinha, C., . . . Scheres, B. (2004). The PLETHORA genes mediate patterning of the Arabidopsis root stem cell niche. *Cell*, *119*(1), 109-120. doi:10.1016/j.cell.2004.09.018
- Allen, R. S., Li, J., Stahle, M. I., Dubroue, A., Gubler, F., & Millar, A. A. (2007). Genetic analysis reveals functional redundancy and the major target genes of the Arabidopsis miR159 family. *Proc Natl Acad Sci U S A*, *104*(41), 16371-16376. doi:10.1073/pnas.0707653104
- An, Z., Liu, Y., Ou, Y., Li, J., Zhang, B., Sun, D., . . . Tang, W. (2018). Regulation of the stability of RGF1 receptor by the ubiquitin-specific proteases UBP12/UBP13 is critical for root meristem maintenance. *Proc Natl Acad Sci U S A*, *115*(5), 1123-1128. doi:10.1073/pnas.1714177115
- Avsian-Kretchmer, O., Cheng, J. C., Chen, L., Moctezuma, E., & Sung, Z. R. (2002). Indole acetic acid distribution coincides with vascular differentiation pattern during Arabidopsis leaf ontogeny. *Plant Physiology*, *130*(1), 199-209. doi:10.1104/pp.003228
- Bajguz, A., & Piotrowska, A. (2009). Conjugates of auxin and cytokinin. *Phytochemistry*, *70*(8), 957-969. doi:10.1016/j.phytochem.2009.05.006
- Band, L. R., Wells, D. M., Larrieu, A., Sun, J., Middleton, A. M., French, A. P., . . . Bennett, M. J. (2012). Root gravitropism is regulated by a transient lateral auxin gradient controlled by a tipping-point mechanism. *Proc Natl Acad Sci U S A*, *109*(12), 4668-4673. doi:10.1073/pnas.1201498109
- Bao, Y., Aggarwal, P., Robbins, N. E., 2nd, Sturrock, C. J., Thompson, M. C., Tan, H. Q., . . . Dinneny, J. R. (2014). Plant roots use a patterning mechanism to position lateral root branches toward available water. *Proc Natl Acad Sci U S A*, *111*(25), 9319-9324. doi:10.1073/pnas.1400966111
- Baral, A., Aryal, B., Jonsson, K., Morris, E., Demes, E., Takatani, S., . . . Bhalerao, R. P. (2021). External Mechanical Cues Reveal a Katanin-Independent Mechanism behind Auxin-Mediated Tissue Bending in Plants. *Dev Cell*, *56*(1), 67-80 e63. doi:10.1016/j.devcel.2020.12.008
- Beaulieu, E., Green, L., Elsby, L., Alourfi, Z., Morand, E. F., Ray, D. W., & Donn, R. (2011). Identification of a novel cell type-specific intronic enhancer of

- macrophage migration inhibitory factor (MIF) and its regulation by mithramycin. *Clinical and Experimental Immunology*, *163*(2), 178-188. doi:10.1111/j.1365-2249.2010.04289.x
- Bennett, M. J., Marchant, A., Green, H. G., May, S. T., Ward, S. P., Millner, P. A., . . . Feldmann, K. A. (1996). Arabidopsis AUX1 gene: a permease-like regulator of root gravitropism. *Science*, *273*(5277), 948-950. doi:10.1126/science.273.5277.948
- Berleth, T., & Jurgens, G. (1993). The role of the *monopteros* gene in organising the basal body region of the *Arabidopsis* embryo. *Development*, *118*(2), 575-587.
- Berleth, T., Mattsson, J., & Hardtke, C. S. (2000). Vascular continuity and auxin signals. *Trends Plant Sci*, *5*(9), 387-393. doi:10.1016/s1360-1385(00)01725-8
- Besnard, F., Refahi, Y., Morin, V., Marteaux, B., Brunoud, G., Chambrier, P., . . . Vernoux, T. (2014). Cytokinin signalling inhibitory fields provide robustness to phyllotaxis. *Nature*, *505*(7483), 417-421. doi:10.1038/nature12791
- Beyer, E. M. (1972). Auxin transport: a new synthetic inhibitor. *Plant Physiology*, *50*(3), 322-327. doi:10.1104/pp.50.3.322
- Bhalerao, R. P., Eklof, J., Ljung, K., Marchant, A., Bennett, M., & Sandberg, G. (2002). Shoot-derived auxin is essential for early lateral root emergence in *Arabidopsis* seedlings. *Plant J*, *29*(3), 325-332. doi:10.1046/j.0960-7412.2001.01217.x
- Bhatia, N., Bozorg, B., Larsson, A., Ohno, C., Jonsson, H., & Heisler, M. G. (2016). Auxin Acts through MONOPTEROS to Regulate Plant Cell Polarity and Pattern Phyllotaxis. *Curr Biol*, *26*(23), 3202-3208. doi:10.1016/j.cub.2016.09.044
- Bhosale, R., Giri, J., Pandey, B. K., Giehl, R. F. H., Hartmann, A., Traini, R., . . . Swarup, R. (2018). A mechanistic framework for auxin dependent *Arabidopsis* root hair elongation to low external phosphate. *Nat Commun*, *9*(1), 1409. doi:10.1038/s41467-018-03851-3
- Bishopp, A., & Lynch, J. P. (2015). The hidden half of crop yields. *Nat Plants*, *1*, 15117. doi:10.1038/nplants.2015.117
- Boure, N., Kumar, S. V., & Arnaud, N. (2019). The BAP Module: A Multisignal

- Integrator Orchestrating Growth. *Trends Plant Sci*, 24(7), 602-610. doi:10.1016/j.tplants.2019.04.002
- Bowman, J. L., & Eshed, Y. (2000). Formation and maintenance of the shoot apical meristem. *Trends Plant Sci*, 5(3), 110-115. doi:10.1016/s1360-1385(00)01569-7
- Bradnam, K. R., & Korf, I. (2008). Longer first introns are a general property of eukaryotic gene structure. *PLoS One*, 3(8), e3093. doi:10.1371/journal.pone.0003093
- Brand, U., Fletcher, J. C., Hobe, M., Meyerowitz, E. M., & Simon, R. (2000). Dependence of stem cell fate in Arabidopsis on a feedback loop regulated by CLV3 activity. *Science*, 289(5479), 617-619. doi:10.1126/science.289.5479.617
- Brenner, W. G., & Schmulling, T. (2012). Transcript profiling of cytokinin action in Arabidopsis roots and shoots discovers largely similar but also organ-specific responses. *Bmc Plant Biology*, 12, 112. doi:10.1186/1471-2229-12-112
- Callis, J., Fromm, M., & Walbot, V. (1987). Introns increase gene expression in cultured maize cells. *Genes Dev*, 1(10), 1183-1200. doi:10.1101/gad.1.10.1183
- Casimiro, I., Marchant, A., Bhalerao, R. P., Beeckman, T., Dhooge, S., Swarup, R., . . . Bennett, M. (2001). Auxin transport promotes Arabidopsis lateral root initiation. *Plant Cell*, 13(4), 843-852. doi:10.1105/tpc.13.4.843
- Chalfie, M. (1995). Green fluorescent protein. *Photochem Photobiol*, 62(4), 651-656. doi:10.1111/j.1751-1097.1995.tb08712.x
- Cho, H., Ryu, H., Rho, S., Hill, K., Smith, S., Audenaert, D., . . . Hwang, I. (2014). A secreted peptide acts on BIN2-mediated phosphorylation of ARFs to potentiate auxin response during lateral root development. *Nat Cell Biol*, 16(1), 66-76. doi:10.1038/ncb2893
- Chorev, M., & Carmel, L. (2012). The function of introns. *Front Genet*, 3, 55. doi:10.3389/fgene.2012.00055
- Cucinotta, M., Cavalleri, A., Guazzotti, A., Astori, C., Manrique, S., Bombarely, A., . . . Colombo, L. (2021). Alternative Splicing Generates a MONOPTEROS Isoform Required for Ovule Development. *Curr Biol*, 31(4), 892-899 e893.

doi:10.1016/j.cub.2020.11.026

- Davuluri, R. V., Sun, H., Palaniswamy, S. K., Matthews, N., Molina, C., Kurtz, M., & Grotewold, E. (2003). AGRIS: Arabidopsis gene regulatory information server, an information resource of Arabidopsis cis-regulatory elements and transcription factors. *BMC Bioinformatics*, *4*, 25. doi:10.1186/1471-2105-4-25
- De Rybel, B., Adibi, M., Breda, A. S., Wendrich, J. R., Smit, M. E., Novak, O., . . . Weijers, D. (2014). Plant development. Integration of growth and patterning during vascular tissue formation in Arabidopsis. *Science*, *345*(6197), 1255215. doi:10.1126/science.1255215
- De Rybel, B., Moller, B., Yoshida, S., Grabowicz, I., Barbier de Reuille, P., Boeren, S., . . . Weijers, D. (2013). A bHLH complex controls embryonic vascular tissue establishment and indeterminate growth in Arabidopsis. *Dev Cell*, *24*(4), 426-437. doi:10.1016/j.devcel.2012.12.013
- De Rybel, B., Vassileva, V., Parizot, B., Demeulenaere, M., Grunewald, W., Audenaert, D., . . . Beeckman, T. (2010). A novel aux/IAA28 signaling cascade activates GATA23-dependent specification of lateral root founder cell identity. *Curr Biol*, *20*(19), 1697-1706. doi:10.1016/j.cub.2010.09.007
- De Smet, I. (2010). Multimodular auxin response controls lateral root development in Arabidopsis. *Plant Signal Behav*, *5*(5), 580-582. doi:10.4161/psb.11495
- De Smet, I., Tetsumura, T., De Rybel, B., Frei dit Frey, N., Laplace, L., Casimiro, I., . . . Beeckman, T. (2007). Auxin-dependent regulation of lateral root positioning in the basal meristem of Arabidopsis. *Development*, *134*(4), 681-690. doi:10.1242/dev.02753
- Dello Iorio, R., Linhares, F. S., Scacchi, E., Casamitjana-Martinez, E., Heidstra, R., Costantino, P., & Sabatini, S. (2007). Cytokinins determine Arabidopsis root-meristem size by controlling cell differentiation. *Curr Biol*, *17*(8), 678-682. doi:10.1016/j.cub.2007.02.047
- Dello Iorio, R., Nakamura, K., Moubayidin, L., Perilli, S., Taniguchi, M., Morita, M. T., . . . Sabatini, S. (2008). A genetic framework for the control of cell division and differentiation in the root meristem. *Science*, *322*(5906), 1380-1384. doi:10.1126/science.1164147
- Deyholos, M. K., & Sieburth, L. E. (2000). Separable whorl-specific expression and

- negative regulation by enhancer elements within the AGAMOUS second intron. *Plant Cell*, *12*(10), 1799-1810. doi:10.1105/tpc.12.10.1799
- Dharmasiri, N., Dharmasiri, S., & Estelle, M. (2005). The F-box protein TIR1 is an auxin receptor. *Nature*, *435*(7041), 441-445. doi:10.1038/nature03543
- Dharmasiri, N., & Estelle, M. (2004). Auxin signaling and regulated protein degradation. *Trends Plant Sci*, *9*(6), 302-308. doi:10.1016/j.tplants.2004.04.003
- Ellis, C. M., Nagpal, P., Young, J. C., Hagen, G., Guilfoyle, T. J., & Reed, J. W. (2005). AUXIN RESPONSE FACTOR1 and AUXIN RESPONSE FACTOR2 regulate senescence and floral organ abscission in *Arabidopsis thaliana*. *Development*, *132*(20), 4563-4574. doi:10.1242/dev.02012
- Emami, S., Arumainayagam, D., Korf, I., & Rose, A. B. (2013). The effects of a stimulating intron on the expression of heterologous genes in *Arabidopsis thaliana*. *Plant Biotechnol J*, *11*(5), 555-563. doi:10.1111/pbi.12043
- Ercoli, M. F., Ferela, A., Debernardi, J. M., Perrone, A. P., Rodriguez, R. E., & Palatnik, J. F. (2018). GIF Transcriptional Coregulators Control Root Meristem Homeostasis. *Plant Cell*, *30*(2), 347-359. doi:10.1105/tpc.17.00856
- Finet, C., Berne-Dedieu, A., Scutt, C. P., & Marletaz, F. (2013). Evolution of the ARF gene family in land plants: old domains, new tricks. *Mol Biol Evol*, *30*(1), 45-56. doi:10.1093/molbev/mss220
- Fletcher, J. C., Brand, U., Running, M. P., Simon, R., & Meyerowitz, E. M. (1999). Signaling of cell fate decisions by CLAVATA3 in *Arabidopsis* shoot meristems. *Science*, *283*(5409), 1911-1914. doi:10.1126/science.283.5409.1911
- Friede, A., Zhang, B., Herberth, S., Pesch, M., Schrader, A., & Hulskamp, M. (2017). The Second Intron Is Essential for the Transcriptional Control of the *Arabidopsis thaliana* GLABRA3 Gene in Leaves. *Frontiers in Plant Science*, *8*, 1382. doi:10.3389/fpls.2017.01382
- Gagne, J. M., Downes, B. P., Shiu, S. H., Durski, A. M., & Vierstra, R. D. (2002). The F-box subunit of the SCF E3 complex is encoded by a diverse superfamily of genes in *Arabidopsis*. *Proc Natl Acad Sci U S A*, *99*(17), 11519-11524. doi:10.1073/pnas.162339999
- Galinha, C., Hofhuis, H., Luijten, M., Willemsen, V., Blilou, I., Heidstra, R., & Scheres,

- B. (2007). PLETHORA proteins as dose-dependent master regulators of Arabidopsis root development. *Nature*, *449*(7165), 1053-1057. doi:10.1038/nature06206
- Gallegos, J. E., & Rose, A. B. (2017). Intron DNA Sequences Can Be More Important Than the Proximal Promoter in Determining the Site of Transcript Initiation. *Plant Cell*, *29*(4), 843-853. doi:10.1105/tpc.17.00020
- Galweiler, L., Guan, C., Muller, A., Wisman, E., Mendgen, K., Yephremov, A., & Palme, K. (1998). Regulation of polar auxin transport by AtPIN1 in Arabidopsis vascular tissue. *Science*, *282*(5397), 2226-2230. doi:10.1126/science.282.5397.2226
- Geisler, M., & Murphy, A. S. (2006). The ABC of auxin transport: the role of p-glycoproteins in plant development. *FEBS Lett*, *580*(4), 1094-1102. doi:10.1016/j.febslet.2005.11.054
- Geldner, N., Denervaud-Tendon, V., Hyman, D. L., Mayer, U., Stierhof, Y. D., & Chory, J. (2009). Rapid, combinatorial analysis of membrane compartments in intact plants with a multicolor marker set. *Plant J*, *59*(1), 169-178. doi:10.1111/j.1365-313X.2009.03851.x
- Geldner, N., Richter, S., Vieten, A., Marquardt, S., Torres-Ruiz, R. A., Mayer, U., & Jurgens, G. (2004). Partial loss-of-function alleles reveal a role for GNOM in auxin transport-related, post-embryonic development of Arabidopsis. *Development*, *131*(2), 389-400. doi:10.1242/dev.00926
- Ghelli, R., Brunetti, P., Napoli, N., De Paolis, A., Cecchetti, V., Tsuge, T., . . . Cardarelli, M. (2018). A Newly Identified Flower-Specific Splice Variant of AUXIN RESPONSE FACTOR8 Regulates Stamen Elongation and Endothecium Lignification in Arabidopsis. *Plant Cell*, *30*(3), 620-637. doi:10.1105/tpc.17.00840
- Giani, S., Altana, A., Campanoni, P., Morello, L., & Breviario, D. (2009). In transgenic rice, alpha- and beta-tubulin regulatory sequences control GUS amount and distribution through intron mediated enhancement and intron dependent spatial expression. *Transgenic Research*, *18*(2), 151-162. doi:10.1007/s11248-008-9202-7
- Gibson, D. G., Young, L., Chuang, R. Y., Venter, J. C., Hutchison, C. A., 3rd, & Smith, H. O. (2009). Enzymatic assembly of DNA molecules up to several hundred

- kilobases. *Nature Methods*, *6*(5), 343-345. doi:10.1038/nmeth.1318
- Gifford, M. L., Dean, A., Gutierrez, R. A., Coruzzi, G. M., & Birnbaum, K. D. (2008). Cell-specific nitrogen responses mediate developmental plasticity. *Proc Natl Acad Sci U S A*, *105*(2), 803-808. doi:10.1073/pnas.0709559105
- Goh, T., Toyokura, K., Wells, D. M., Swarup, K., Yamamoto, M., Mimura, T., . . . Guyomarc'h, S. (2016). Quiescent center initiation in the Arabidopsis lateral root primordia is dependent on the SCARECROW transcription factor. *Development*, *143*(18), 3363-3371. doi:10.1242/dev.135319
- Gutierrez, L., Mongelard, G., Flokova, K., Pacurar, D. I., Novak, O., Staswick, P., . . . Bellini, C. (2012). Auxin controls Arabidopsis adventitious root initiation by regulating jasmonic acid homeostasis. *Plant Cell*, *24*(6), 2515-2527. doi:10.1105/tpc.112.099119
- Hamann, T., Benkova, E., Baurle, I., Kientz, M., & Jurgens, G. (2002). The Arabidopsis BODENLOS gene encodes an auxin response protein inhibiting MONOPTEROS-mediated embryo patterning. *Genes Dev*, *16*(13), 1610-1615. doi:10.1101/gad.229402
- Hardtke, C. S., Ckurshumova, W., Vidaurre, D. P., Singh, S. A., Stamatiou, G., Tiwari, S. B., . . . Berleth, T. (2004). Overlapping and non-redundant functions of the Arabidopsis auxin response factors MONOPTEROS and NONPHOTOTROPIC HYPOCOTYL 4. *Development*, *131*(5), 1089-1100. doi:10.1242/dev.00925
- Harper, R. M., Stowe-Evans, E. L., Luesse, D. R., Muto, H., Tatematsu, K., Watahiki, M. K., . . . Liscum, E. (2000). The NPH4 locus encodes the auxin response factor ARF7, a conditional regulator of differential growth in aerial Arabidopsis tissue. *Plant Cell*, *12*(5), 757-770. doi:10.1105/tpc.12.5.757
- Harrison, S. J., Mott, E. K., Parsley, K., Aspinall, S., Gray, J. C., & Cottage, A. (2006). A rapid and robust method of identifying transformed Arabidopsis thaliana seedlings following floral dip transformation. *Plant Methods*, *2*, 19. doi:10.1186/1746-4811-2-19
- Helariutta, Y., Fukaki, H., Wysocka-Diller, J., Nakajima, K., Jung, J., Sena, G., . . . Benfey, P. N. (2000). The SHORT-ROOT gene controls radial patterning of the Arabidopsis root through radial signaling. *Cell*, *101*(5), 555-567. doi:10.1016/s0092-8674(00)80865-x

- Higuchi, M., Pischke, M. S., Mahonen, A. P., Miyawaki, K., Hashimoto, Y., Seki, M., . . . Kakimoto, T. (2004). In planta functions of the Arabidopsis cytokinin receptor family. *Proc Natl Acad Sci U S A*, *101*(23), 8821-8826. doi:10.1073/pnas.0402887101
- Hochholdinger, F., & Zimmermann, R. (2008). Conserved and diverse mechanisms in root development. *Current Opinion in Plant Biology*, *11*(1), 70-74. doi:10.1016/j.pbi.2007.10.002
- Hong, L., Ye, C., Lin, J., Fu, H., Wu, X., & Li, Q. Q. (2018). Alternative polyadenylation is involved in auxin-based plant growth and development. *Plant J*, *93*(2), 246-258. doi:10.1111/tpj.13771
- Hughes, J., & McCully, M. E. (1975). The use of an optical brightener in the study of plant structure. *Stain Technol*, *50*(5), 319-329. doi:10.3109/10520297509117082
- Hussain, T., Rehman, N., Inam, S., Ajmal, W., Afroz, A., Muhammad, A., . . . Khan, M. R. (2019). Homotypic Clusters of Transcription Factor Binding Sites in the First Large Intron of AGL24 MADS-Box Transcription Factor Are Recruited in the Enhancement of Floral Expression. *Plant Molecular Biology Reporter*, *37*(1-2), 24-40. doi:10.1007/s11105-019-01136-7
- Jin, J., He, K., Tang, X., Li, Z., Lv, L., Zhao, Y., . . . Gao, G. (2015). An Arabidopsis Transcriptional Regulatory Map Reveals Distinct Functional and Evolutionary Features of Novel Transcription Factors. *Mol Biol Evol*, *32*(7), 1767-1773. doi:10.1093/molbev/msv058
- Jin, J., Tian, F., Yang, D. C., Meng, Y. Q., Kong, L., Luo, J., & Gao, G. (2017). PlantTFDB 4.0: toward a central hub for transcription factors and regulatory interactions in plants. *Nucleic Acids Res*, *45*(D1), D1040-D1045. doi:10.1093/nar/gkw982
- Kato, H., Mutte, S. K., Suzuki, H., Crespo, I., Das, S., Radoeva, T., . . . Weijers, D. (2020). Design principles of a minimal auxin response system. *Nat Plants*, *6*(5), 473-482. doi:10.1038/s41477-020-0662-y
- Kepinski, S., & Leyser, O. (2005). The Arabidopsis F-box protein TIR1 is an auxin receptor. *Nature*, *435*(7041), 446-451. doi:10.1038/nature03542
- Kerstetter, R. A., Bollman, K., Taylor, R. A., Bomblied, K., & Poethig, R. S. (2001). KANADI regulates organ polarity in Arabidopsis. *Nature*, *411*(6838), 706-

709. doi:10.1038/35079629

- Khan, M. A., Gemenet, D. C., & Villordon, A. (2016). Root System Architecture and Abiotic Stress Tolerance: Current Knowledge in Root and Tuber Crops. *Frontiers in Plant Science*, 7, 1584. doi:10.3389/fpls.2016.01584
- Khunkitti, W., Lloyd, D., Furr, J. R., & Russell, A. D. (1997). Aspects of the mechanisms of action of biguanides on trophozoites and cysts of *Acanthamoeba castellanii*. *J Appl Microbiol*, 82(1), 107-114. doi:10.1111/j.1365-2672.1997.tb03304.x
- Kim, D. H., & Sung, S. (2014). Polycomb-mediated gene silencing in *Arabidopsis thaliana*. *Mol Cells*, 37(12), 841-850. doi:10.14348/molcells.2014.0249
- Kleine-Vehn, J., Ding, Z., Jones, A. R., Tasaka, M., Morita, M. T., & Friml, J. (2010). Gravity-induced PIN transcytosis for polarization of auxin fluxes in gravity-sensing root cells. *Proc Natl Acad Sci U S A*, 107(51), 22344-22349. doi:10.1073/pnas.1013145107
- Korasick, D. A., Enders, T. A., & Strader, L. C. (2013). Auxin biosynthesis and storage forms. *J Exp Bot*, 64(9), 2541-2555. doi:10.1093/jxb/ert080
- Krogan, N. T., Marcos, D., Weiner, A. I., & Berleth, T. (2016). The auxin response factor MONOPTEROS controls meristem function and organogenesis in both the shoot and root through the direct regulation of PIN genes. *New Phytol*, 212(1), 42-50. doi:10.1111/nph.14107
- Kuroha, T., Tokunaga, H., Kojima, M., Ueda, N., Ishida, T., Nagawa, S., . . . Sakakibara, H. (2009). Functional analyses of LONELY GUY cytokinin-activating enzymes reveal the importance of the direct activation pathway in *Arabidopsis*. *Plant Cell*, 21(10), 3152-3169. doi:10.1105/tpc.109.068676
- Lakehal, A., Chaabouni, S., Cavel, E., Le Hir, R., Ranjan, A., Raneshan, Z., . . . Bellini, C. (2019). A Molecular Framework for the Control of Adventitious Rooting by TIR1/AFB2-Aux/IAA-Dependent Auxin Signaling in *Arabidopsis*. *Mol Plant*, 12(11), 1499-1514. doi:10.1016/j.molp.2019.09.001
- Lampropoulos, A., Sutikovic, Z., Wenzl, C., Maegele, I., Lohmann, J. U., & Forner, J. (2013). GreenGate---a novel, versatile, and efficient cloning system for plant transgenesis. *PLoS One*, 8(12), e83043. doi:10.1371/journal.pone.0083043
- Lavenus, J., Goh, T., Guyomarc'h, S., Hill, K., Lucas, M., Voss, U., . . . Bennett, M. J.

- (2015). Inference of the Arabidopsis lateral root gene regulatory network suggests a bifurcation mechanism that defines primordia flanking and central zones. *Plant Cell*, *27*(5), 1368-1388. doi:10.1105/tpc.114.132993
- Le, J., Vandenbussche, F., Van Der Straeten, D., & Verbelen, J. P. (2001). In the early response of Arabidopsis roots to ethylene, cell elongation is up- and down-regulated and uncoupled from differentiation. *Plant Physiology*, *125*(2), 519-522. doi:10.1104/pp.125.2.519
- Lee, H. W., Cho, C., Pandey, S. K., Park, Y., Kim, M. J., & Kim, J. (2019). LBD16 and LBD18 acting downstream of ARF7 and ARF19 are involved in adventitious root formation in Arabidopsis. *Bmc Plant Biology*, *19*(1), 46. doi:10.1186/s12870-019-1659-4
- Lee, H. W., Kim, N. Y., Lee, D. J., & Kim, J. (2009). LBD18/ASL20 regulates lateral root formation in combination with LBD16/ASL18 downstream of ARF7 and ARF19 in Arabidopsis. *Plant Physiology*, *151*(3), 1377-1389. doi:10.1104/pp.109.143685
- Leitz, G., Kang, B. H., Schoenwaelder, M. E., & Staehelin, L. A. (2009). Statolith sedimentation kinetics and force transduction to the cortical endoplasmic reticulum in gravity-sensing Arabidopsis columella cells. *Plant Cell*, *21*(3), 843-860. doi:10.1105/tpc.108.065052
- Leyser, O. (2018). Auxin Signaling. *Plant Physiology*, *176*(1), 465-479. doi:10.1104/pp.17.00765
- Liang, Y., Tan, Z. M., Zhu, L., Niu, Q. K., Zhou, J. J., Li, M., . . . Ye, D. (2013). MYB97, MYB101 and MYB120 function as male factors that control pollen tube-synergid interaction in Arabidopsis thaliana fertilization. *PLoS Genet*, *9*(11), e1003933. doi:10.1371/journal.pgen.1003933
- Liu, Z., Miao, L., Huo, R., Song, X., Johnson, C., Kong, L., . . . Yu, X. (2018). ARF2-ARF4 and ARF5 are Essential for Female and Male Gametophyte Development in Arabidopsis. *Plant Cell Physiol*, *59*(1), 179-189. doi:10.1093/pcp/pcx174
- Ludwig-Muller, J. (2011). Auxin conjugates: their role for plant development and in the evolution of land plants. *J Exp Bot*, *62*(6), 1757-1773. doi:10.1093/jxb/erq412
- Luo, L., Zeng, J., Wu, H., Tian, Z., & Zhao, Z. (2018). A Molecular Framework for

- Auxin-Controlled Homeostasis of Shoot Stem Cells in Arabidopsis. *Mol Plant*, *11*(7), 899-913. doi:10.1016/j.molp.2018.04.006
- Mahonen, A. P., Bishopp, A., Higuchi, M., Nieminen, K. M., Kinoshita, K., Tormakangas, K., . . . Helariutta, Y. (2006). Cytokinin signaling and its inhibitor AHP6 regulate cell fate during vascular development. *Science*, *311*(5757), 94-98. doi:10.1126/science.1118875
- Malamy, J. E., & Benfey, P. N. (1997). Organization and cell differentiation in lateral roots of Arabidopsis thaliana. *Development*, *124*(1), 33-44.
- Matsuzaki, Y., Ogawa-Ohnishi, M., Mori, A., & Matsubayashi, Y. (2010). Secreted peptide signals required for maintenance of root stem cell niche in Arabidopsis. *Science*, *329*(5995), 1065-1067. doi:10.1126/science.1191132
- Mayer, K. F., Schoof, H., Haecker, A., Lenhard, M., Jurgens, G., & Laux, T. (1998). Role of WUSCHEL in regulating stem cell fate in the Arabidopsis shoot meristem. *Cell*, *95*(6), 805-815. doi:10.1016/s0092-8674(00)81703-1
- Millar, A. A., & Gubler, F. (2005). The Arabidopsis GAMYB-like genes, MYB33 and MYB65, are microRNA-regulated genes that redundantly facilitate anther development. *Plant Cell*, *17*(3), 705-721. doi:10.1105/tpc.104.027920
- Moller, B., & Weijers, D. (2009). Auxin control of embryo patterning. *Cold Spring Harb Perspect Biol*, *1*(5), a001545. doi:10.1101/cshperspect.a001545
- Moubayidin, L., Perilli, S., Dello Iorio, R., Di Mambro, R., Costantino, P., & Sabatini, S. (2010). The rate of cell differentiation controls the Arabidopsis root meristem growth phase. *Curr Biol*, *20*(12), 1138-1143. doi:10.1016/j.cub.2010.05.035
- Muller, A., Guan, C., Galweiler, L., Tanzler, P., Huijser, P., Marchant, A., . . . Palme, K. (1998). AtPIN2 defines a locus of Arabidopsis for root gravitropism control. *Embo Journal*, *17*(23), 6903-6911. doi:10.1093/emboj/17.23.6903
- Muller, B., & Sheen, J. (2008). Cytokinin and auxin interaction in root stem-cell specification during early embryogenesis. *Nature*, *453*(7198), 1094-1097. doi:10.1038/nature06943
- Murray, J. A., Jones, A., Godin, C., & Traas, J. (2012). Systems analysis of shoot apical meristem growth and development: integrating hormonal and mechanical signaling. *Plant Cell*, *24*(10), 3907-3919. doi:10.1105/tpc.112.102194

- Mutte, S. K., Kato, H., Rothfels, C., Melkonian, M., Wong, G. K., & Weijers, D. (2018). Origin and evolution of the nuclear auxin response system. *Elife*, *7*. doi:10.7554/eLife.33399
- Nagpal, P., Ellis, C. M., Weber, H., Ploense, S. E., Barkawi, L. S., Guilfoyle, T. J., . . . Reed, J. W. (2005). Auxin response factors ARF6 and ARF8 promote jasmonic acid production and flower maturation. *Development*, *132*(18), 4107-4118. doi:10.1242/dev.01955
- Nakajima, K., Sena, G., Nawy, T., & Benfey, P. N. (2001). Intercellular movement of the putative transcription factor SHR in root patterning. *Nature*, *413*(6853), 307-311. doi:10.1038/35095061
- O'Malley, R. C., Huang, S. C., Song, L., Lewsey, M. G., Bartlett, A., Nery, J. R., . . . Ecker, J. R. (2016). Cistrome and Epicistrome Features Shape the Regulatory DNA Landscape. *Cell*, *166*(6), 1598. doi:10.1016/j.cell.2016.08.063
- Oh, E., Zhu, J. Y., Bai, M. Y., Arenhart, R. A., Sun, Y., & Wang, Z. Y. (2014). Cell elongation is regulated through a central circuit of interacting transcription factors in the Arabidopsis hypocotyl. *Elife*, *3*. doi:10.7554/eLife.03031
- Ohashi-Ito, K., Saegusa, M., Iwamoto, K., Oda, Y., Katayama, H., Kojima, M., . . . Fukuda, H. (2014). A bHLH complex activates vascular cell division via cytokinin action in root apical meristem. *Curr Biol*, *24*(17), 2053-2058. doi:10.1016/j.cub.2014.07.050
- Okushima, Y., Fukaki, H., Onoda, M., Theologis, A., & Tasaka, M. (2007). ARF7 and ARF19 regulate lateral root formation via direct activation of LBD/ASL genes in Arabidopsis. *Plant Cell*, *19*(1), 118-130. doi:10.1105/tpc.106.047761
- Okushima, Y., Overvoorde, P. J., Arima, K., Alonso, J. M., Chan, A., Chang, C., . . . Theologis, A. (2005). Functional genomic analysis of the AUXIN RESPONSE FACTOR gene family members in Arabidopsis thaliana: unique and overlapping functions of ARF7 and ARF19. *Plant Cell*, *17*(2), 444-463. doi:10.1105/tpc.104.028316
- Orosa-Puente, B., Leftley, N., von Wangenheim, D., Banda, J., Srivastava, A. K., Hill, K., . . . Bennett, M. J. (2018). Root branching toward water involves posttranslational modification of transcription factor ARF7. *Science*, *362*(6421), 1407-1410. doi:10.1126/science.aau3956

- Ou, Y., Lu, X., Zi, Q., Xun, Q., Zhang, J., Wu, Y., . . . Li, J. (2016). RGF1 INSENSITIVE 1 to 5, a group of LRR receptor-like kinases, are essential for the perception of root meristem growth factor 1 in *Arabidopsis thaliana*. *Cell Res*, *26*(6), 686-698. doi:10.1038/cr.2016.63
- Overvoorde, P., Fukaki, H., & Beeckman, T. (2010). Auxin control of root development. *Cold Spring Harb Perspect Biol*, *2*(6), a001537. doi:10.1101/cshperspect.a001537
- Pandey, B. K., Huang, G., Bhosale, R., Hartman, S., Sturrock, C. J., Jose, L., . . . Bennett, M. J. (2021). Plant roots sense soil compaction through restricted ethylene diffusion. *Science*, *371*(6526), 276-280. doi:10.1126/science.abf3013
- Parry, G., Calderon-Villalobos, L. I., Prigge, M., Peret, B., Dharmasiri, S., Itoh, H., . . . Estelle, M. (2009). Complex regulation of the TIR1/AFB family of auxin receptors. *Proc Natl Acad Sci U S A*, *106*(52), 22540-22545. doi:10.1073/pnas.0911967106
- Peret, B., De Rybel, B., Casimiro, I., Benkova, E., Swarup, R., Laplaze, L., . . . Bennett, M. J. (2009). Arabidopsis lateral root development: an emerging story. *Trends Plant Sci*, *14*(7), 399-408. doi:10.1016/j.tplants.2009.05.002
- Peret, B., Swarup, K., Ferguson, A., Seth, M., Yang, Y., Dhondt, S., . . . Swarup, R. (2012). AUX/LAX genes encode a family of auxin influx transporters that perform distinct functions during Arabidopsis development. *Plant Cell*, *24*(7), 2874-2885. doi:10.1105/tpc.112.097766
- Perilli, S., Di Mambro, R., & Sabatini, S. (2012). Growth and development of the root apical meristem. *Current Opinion in Plant Biology*, *15*(1), 17-23. doi:10.1016/j.pbi.2011.10.006
- Petricka, J. J., Winter, C. M., & Benfey, P. N. (2012). Control of Arabidopsis root development. *Annu Rev Plant Biol*, *63*, 563-590. doi:10.1146/annurev-arplant-042811-105501
- Porco, S., Larrieu, A., Du, Y., Gaudinier, A., Goh, T., Swarup, K., . . . Bennett, M. J. (2016). Lateral root emergence in Arabidopsis is dependent on transcription factor LBD29 regulation of auxin influx carrier LAX3. *Development*, *143*(18), 3340-3349. doi:10.1242/dev.136283
- Powers, S. K., Holehouse, A. S., Korasick, D. A., Schreiber, K. H., Clark, N. M., Jing,

- H., . . . Strader, L. C. (2019). Nucleo-cytoplasmic Partitioning of ARF Proteins Controls Auxin Responses in *Arabidopsis thaliana*. *Mol Cell*, *76*(1), 177-190 e175. doi:10.1016/j.molcel.2019.06.044
- Prigge, M. J., Platre, M., Kadakia, N., Zhang, Y., Greenham, K., Szutu, W., . . . Estelle, M. (2020). Genetic analysis of the *Arabidopsis* TIR1/AFB auxin receptors reveals both overlapping and specialized functions. *Elife*, *9*. doi:10.7554/eLife.54740
- Punwani, J. A., Hutchison, C. E., Schaller, G. E., & Kieber, J. J. (2010). The subcellular distribution of the *Arabidopsis* histidine phosphotransfer proteins is independent of cytokinin signaling. *Plant J*, *62*(3), 473-482. doi:10.1111/j.1365-313X.2010.04165.x
- Rademacher, E. H., Lokerse, A. S., Schlereth, A., Llavata-Peris, C. I., Bayer, M., Kientz, M., . . . Weijers, D. (2012). Different auxin response machineries control distinct cell fates in the early plant embryo. *Dev Cell*, *22*(1), 211-222. doi:10.1016/j.devcel.2011.10.026
- Rademacher, E. H., Moller, B., Lokerse, A. S., Llavata-Peris, C. I., van den Berg, W., & Weijers, D. (2011). A cellular expression map of the *Arabidopsis* AUXIN RESPONSE FACTOR gene family. *Plant J*, *68*(4), 597-606. doi:10.1111/j.1365-313X.2011.04710.x
- Rayle, D. L., Evans, M. L., & Hertel, R. (1970). Action of auxin on cell elongation. *Proc Natl Acad Sci U S A*, *65*(1), 184-191. doi:10.1073/pnas.65.1.184
- Redei, G. P. (1975). *Arabidopsis* as a genetic tool. *Annu Rev Genet*, *9*, 111-127. doi:10.1146/annurev.ge.09.120175.000551
- Reinhardt, D., Pesce, E. R., Stieger, P., Mandel, T., Baltensperger, K., Bennett, M., . . . Kuhlemeier, C. (2003). Regulation of phyllotaxis by polar auxin transport. *Nature*, *426*(6964), 255-260. doi:10.1038/nature02081
- Remington, D. L., Vision, T. J., Guilfoyle, T. J., & Reed, J. W. (2004). Contrasting modes of diversification in the Aux/IAA and ARF gene families. *Plant Physiology*, *135*(3), 1738-1752. doi:10.1104/pp.104.039669
- Reyes, J. L., & Chua, N. H. (2007). ABA induction of miR159 controls transcript levels of two MYB factors during *Arabidopsis* seed germination. *Plant J*, *49*(4), 592-606. doi:10.1111/j.1365-313X.2006.02980.x
- Rodriguez, R. E., Ercoli, M. F., Debernardi, J. M., Breakfield, N. W., Mecchia, M. A.,

- Sabatini, M., . . . Palatnik, J. F. (2015). MicroRNA miR396 Regulates the Switch between Stem Cells and Transit-Amplifying Cells in Arabidopsis Roots. *Plant Cell*, *27*(12), 3354-3366. doi:10.1105/tpc.15.00452
- Rogers, E. D., & Benfey, P. N. (2015). Regulation of plant root system architecture: implications for crop advancement. *Curr Opin Biotechnol*, *32*, 93-98. doi:10.1016/j.copbio.2014.11.015
- Rose, A. B. (2004). The effect of intron location on intron-mediated enhancement of gene expression in Arabidopsis. *Plant J*, *40*(5), 744-751. doi:10.1111/j.1365-3113.2004.02247.x
- Rose, A. B. (2018). Introns as Gene Regulators: A Brick on the Accelerator. *Front Genet*, *9*, 672. doi:10.3389/fgene.2018.00672
- Rosquete, M. R., von Wangenheim, D., Marhavy, P., Barbez, E., Stelzer, E. H., Benkova, E., . . . Kleine-Vehn, J. (2013). An auxin transport mechanism restricts positive orthogravitropism in lateral roots. *Curr Biol*, *23*(9), 817-822. doi:10.1016/j.cub.2013.03.064
- Roudier, F., Fernandez, A. G., Fujita, M., Himmelspach, R., Borner, G. H., Schindelman, G., . . . Benfey, P. N. (2005). COBRA, an Arabidopsis extracellular glycosyl-phosphatidyl inositol-anchored protein, specifically controls highly anisotropic expansion through its involvement in cellulose microfibril orientation. *Plant Cell*, *17*(6), 1749-1763. doi:10.1105/tpc.105.031732
- Ruzicka, K., Strader, L. C., Bailly, A., Yang, H., Blakeslee, J., Langowski, L., . . . Friml, J. (2010). Arabidopsis PIS1 encodes the ABCG37 transporter of auxinic compounds including the auxin precursor indole-3-butyric acid. *Proc Natl Acad Sci U S A*, *107*(23), 10749-10753. doi:10.1073/pnas.1005878107
- Sabatini, S., Heidstra, R., Wildwater, M., & Scheres, B. (2003). SCARECROW is involved in positioning the stem cell niche in the Arabidopsis root meristem. *Genes Dev*, *17*(3), 354-358. doi:10.1101/gad.252503
- Sarkar, A. K., Luijten, M., Miyashima, S., Lenhard, M., Hashimoto, T., Nakajima, K., . . . Laux, T. (2007). Conserved factors regulate signalling in Arabidopsis thaliana shoot and root stem cell organizers. *Nature*, *446*(7137), 811-814. doi:10.1038/nature05703
- Scacchi, E., Salinas, P., Gujas, B., Santuari, L., Krogan, N., Ragni, L., . . . Hardtke, C.

- S. (2010). Spatio-temporal sequence of cross-regulatory events in root meristem growth. *Proc Natl Acad Sci U S A*, *107*(52), 22734-22739. doi:10.1073/pnas.1014716108
- Scharwies, J. D., & Dinneny, J. R. (2019). Water transport, perception, and response in plants. *J Plant Res*, *132*(3), 311-324. doi:10.1007/s10265-019-01089-8
- Scheres, B., Wolkenfelt, H., Willemsen, V., Terlouw, M., Lawson, E., Dean, C., & Weisbeek, P. (1994). Embryonic origin of the Arabidopsis primary root and root meristem initials. *Development*, *120*(9), 2475-2487.
- Schindelman, G., Morikami, A., Jung, J., Baskin, T. I., Carpita, N. C., Derbyshire, P., . . . Benfey, P. N. (2001). COBRA encodes a putative GPI-anchored protein, which is polarly localized and necessary for oriented cell expansion in Arabidopsis. *Genes Dev*, *15*(9), 1115-1127. doi:10.1101/gad.879101
- Schlereth, A., Moller, B., Liu, W., Kientz, M., Flipse, J., Rademacher, E. H., . . . Weijers, D. (2010). MONOPTEROS controls embryonic root initiation by regulating a mobile transcription factor. *Nature*, *464*(7290), 913-916. doi:10.1038/nature08836
- Schoenaers, S., Balcerowicz, D., Breen, G., Hill, K., Zdanio, M., Mouille, G., . . . Vissenberg, K. (2018). The Auxin-Regulated CrRLK1L Kinase ERULUS Controls Cell Wall Composition during Root Hair Tip Growth. *Curr Biol*, *28*(5), 722-732 e726. doi:10.1016/j.cub.2018.01.050
- Schoof, H., Lenhard, M., Haecker, A., Mayer, K. F., Jurgens, G., & Laux, T. (2000). The stem cell population of Arabidopsis shoot meristems is maintained by a regulatory loop between the CLAVATA and WUSCHEL genes. *Cell*, *100*(6), 635-644. doi:10.1016/s0092-8674(00)80700-x
- Schuetz, M., Fidanza, M., & Mattsson, J. (2019). Identification of Auxin Response Factor-Encoding Genes Expressed in Distinct Phases of Leaf Vein Development and with Overlapping Functions in Leaf Formation. *Plants (Basel)*, *8*(7). doi:10.3390/plants8070242
- Smalle, J., & Vierstra, R. D. (2004). The ubiquitin 26S proteasome proteolytic pathway. *Annu Rev Plant Biol*, *55*, 555-590. doi:10.1146/annurev.arplant.55.031903.141801
- Sozzani, R., & Iyer-Pascuzzi, A. (2014). Postembryonic control of root meristem growth and development. *Current Opinion in Plant Biology*, *17*, 7-12.

doi:10.1016/j.pbi.2013.10.005

- Stahl, Y., Wink, R. H., Ingram, G. C., & Simon, R. (2009). A signaling module controlling the stem cell niche in Arabidopsis root meristems. *Curr Biol*, *19*(11), 909-914. doi:10.1016/j.cub.2009.03.060
- Steinmann, T., Geldner, N., Grebe, M., Mangold, S., Jackson, C. L., Paris, S., . . . Jurgens, G. (1999). Coordinated polar localization of auxin efflux carrier PIN1 by GNOM ARF GEF. *Science*, *286*(5438), 316-318. doi:10.1126/science.286.5438.316
- Strader, L. C., & Bartel, B. (2009). The Arabidopsis PLEIOTROPIC DRUG RESISTANCE8/ABCG36 ATP binding cassette transporter modulates sensitivity to the auxin precursor indole-3-butyric acid. *Plant Cell*, *21*(7), 1992-2007. doi:10.1105/tpc.109.065821
- Street, I. H., Aman, S., Zubo, Y., Ramzan, A., Wang, X., Shakeel, S. N., . . . Schaller, G. E. (2015). Ethylene Inhibits Cell Proliferation of the Arabidopsis Root Meristem. *Plant Physiology*, *169*(1), 338-350. doi:10.1104/pp.15.00415
- Su, S. H., Gibbs, N. M., Jancewicz, A. L., & Masson, P. H. (2017). Molecular Mechanisms of Root Gravitropism. *Curr Biol*, *27*(17), R964-R972. doi:10.1016/j.cub.2017.07.015
- Suzuki, T., Imamura, A., Ueguchi, C., & Mizuno, T. (1998). Histidine-containing phosphotransfer (HPT) signal transducers implicated in His-to-Asp phosphorelay in Arabidopsis. *Plant Cell Physiol*, *39*(12), 1258-1268. doi:10.1093/oxfordjournals.pcp.a029329
- Swarup, K., Benkova, E., Swarup, R., Casimiro, I., Peret, B., Yang, Y., . . . Bennett, M. J. (2008). The auxin influx carrier LAX3 promotes lateral root emergence. *Nat Cell Biol*, *10*(8), 946-954. doi:10.1038/ncb1754
- Swarup, R., Kramer, E. M., Perry, P., Knox, K., Leyser, H. M., Haseloff, J., . . . Bennett, M. J. (2005). Root gravitropism requires lateral root cap and epidermal cells for transport and response to a mobile auxin signal. *Nat Cell Biol*, *7*(11), 1057-1065. doi:10.1038/ncb1316
- Swarup, R., & Peret, B. (2012). AUX/LAX family of auxin influx carriers-an overview. *Frontiers in Plant Science*, *3*, 225. doi:10.3389/fpls.2012.00225
- Szemenyei, H., Hannon, M., & Long, J. A. (2008). TOPLESS mediates auxin-dependent transcriptional repression during Arabidopsis embryogenesis.

- Science*, 319(5868), 1384-1386. doi:10.1126/science.1151461
- Tan, T. T., Endo, H., Sano, R., Kurata, T., Yamaguchi, M., Ohtani, M., & Demura, T. (2018). Transcription Factors VND1-VND3 Contribute to Cotyledon Xylem Vessel Formation. *Plant Physiology*, 176(1), 773-789. doi:10.1104/pp.17.00461
- Tan, X., Calderon-Villalobos, L. I., Sharon, M., Zheng, C., Robinson, C. V., Estelle, M., & Zheng, N. (2007). Mechanism of auxin perception by the TIR1 ubiquitin ligase. *Nature*, 446(7136), 640-645. doi:10.1038/nature05731
- ten Hove, C. A., Lu, K. J., & Weijers, D. (2015). Building a plant: cell fate specification in the early Arabidopsis embryo. *Development*, 142(3), 420-430. doi:10.1242/dev.111500
- Tian, F., Yang, D. C., Meng, Y. Q., Jin, J., & Gao, G. (2020). PlantRegMap: charting functional regulatory maps in plants. *Nucleic Acids Res*, 48(D1), D1104-D1113. doi:10.1093/nar/gkz1020
- Tiwari, S. B., Wang, X. J., Hagen, G., & Guilfoyle, T. J. (2001). AUX/IAA proteins are active repressors, and their stability and activity are modulated by auxin. *Plant Cell*, 13(12), 2809-2822. doi:10.1105/tpc.010289
- Truskina, J., Han, J., Chrysanthou, E., Galvan-Ampudia, C. S., Laine, S., Brunoud, G., . . . Vernoux, T. (2021). Publisher Correction: A network of transcriptional repressors modulates auxin responses. *Nature*, 589(7842), E7. doi:10.1038/s41586-020-03066-x
- Truskina, J., & Vernoux, T. (2018). The growth of a stable stationary structure: coordinating cell behavior and patterning at the shoot apical meristem. *Current Opinion in Plant Biology*, 41, 83-88. doi:10.1016/j.pbi.2017.09.011
- Tsukagoshi, H., Busch, W., & Benfey, P. N. (2010). Transcriptional regulation of ROS controls transition from proliferation to differentiation in the root. *Cell*, 143(4), 606-616. doi:10.1016/j.cell.2010.10.020
- Ulmasov, T., Hagen, G., & Guilfoyle, T. J. (1999). Dimerization and DNA binding of auxin response factors. *Plant J*, 19(3), 309-319. doi:10.1046/j.1365-313x.1999.00538.x
- Ulmasov, T., Murfett, J., Hagen, G., & Guilfoyle, T. J. (1997). Aux/IAA proteins repress expression of reporter genes containing natural and highly active synthetic auxin response elements. *Plant Cell*, 9(11), 1963-1971.

doi:10.1105/tpc.9.11.1963

- van den Berg, C., Willemsen, V., Hendriks, G., Weisbeek, P., & Scheres, B. (1997). Short-range control of cell differentiation in the Arabidopsis root meristem. *Nature*, *390*(6657), 287-289. doi:10.1038/36856
- Verbelen, J. P., De Cnodder, T., Le, J., Vissenberg, K., & Baluska, F. (2006). The Root Apex of Arabidopsis thaliana Consists of Four Distinct Zones of Growth Activities: Meristematic Zone, Transition Zone, Fast Elongation Zone and Growth Terminating Zone. *Plant Signal Behav*, *1*(6), 296-304. doi:10.4161/psb.1.6.3511
- Vernoux, T., Brunoud, G., Farcot, E., Morin, V., Van den Daele, H., Legrand, J., . . . Traas, J. (2011). The auxin signalling network translates dynamic input into robust patterning at the shoot apex. *Molecular Systems Biology*, *7*, 508. doi:10.1038/msb.2011.39
- Vissenberg, K., Martinez-Vilchez, I. M., Verbelen, J. P., Miller, J. G., & Fry, S. C. (2000). In vivo colocalization of xyloglucan endotransglycosylase activity and its donor substrate in the elongation zone of Arabidopsis roots. *Plant Cell*, *12*(7), 1229-1237. doi:10.1105/tpc.12.7.1229
- Wang, X., Yu, R., Wang, J., Lin, Z., Han, X., Deng, Z., . . . Chen, H. (2020). The Asymmetric Expression of SAUR Genes Mediated by ARF7/19 Promotes the Gravitropism and Phototropism of Plant Hypocotyls. *Cell Rep*, *31*(3), 107529. doi:10.1016/j.celrep.2020.107529
- Weijers, D., Benkova, E., Jager, K. E., Schlereth, A., Hamann, T., Kientz, M., . . . Jurgens, G. (2005). Developmental specificity of auxin response by pairs of ARF and Aux/IAA transcriptional regulators. *Embo Journal*, *24*(10), 1874-1885. doi:10.1038/sj.emboj.7600659
- Wilmoth, J. C., Wang, S., Tiwari, S. B., Joshi, A. D., Hagen, G., Guilfoyle, T. J., . . . Reed, J. W. (2005). NPH4/ARF7 and ARF19 promote leaf expansion and auxin-induced lateral root formation. *Plant J*, *43*(1), 118-130. doi:10.1111/j.1365-313X.2005.02432.x
- Wisniewska, J., Xu, J., Seifertova, D., Brewer, P. B., Ruzicka, K., Blilou, I., . . . Friml, J. (2006). Polar PIN localization directs auxin flow in plants. *Science*, *312*(5775), 883. doi:10.1126/science.1121356
- Woodward, A. W., & Bartel, B. (2005). Auxin: regulation, action, and interaction.

Ann Bot, 95(5), 707–735. doi:10.1093/aob/mci083

- Worley, C. K., Zenser, N., Ramos, J., Rouse, D., Leyser, O., Theologis, A., & Callis, J. (2000). Degradation of Aux/IAA proteins is essential for normal auxin signalling. *Plant J*, 21(6), 553–562. doi:10.1046/j.1365-313x.2000.00703.x
- Wysocka-Diller, J. W., Helariutta, Y., Fukaki, H., Malamy, J. E., & Benfey, P. N. (2000). Molecular analysis of SCARECROW function reveals a radial patterning mechanism common to root and shoot. *Development*, 127(3), 595–603.
- Xi, D., Chen, X., Wang, Y., Zhong, R., He, J., Shen, J., & Ming, F. (2019). Arabidopsis ANAC092 regulates auxin-mediated root development by binding to the ARF8 and PIN4 promoters. *J Integr Plant Biol*, 61(9), 1015–1031. doi:10.1111/jipb.12735
- Xue, T., Liu, Z., Dai, X., & Xiang, F. (2017). Primary root growth in Arabidopsis thaliana is inhibited by the miR159 mediated repression of MYB33, MYB65 and MYB101. *Plant Sci*, 262, 182–189. doi:10.1016/j.plantsci.2017.06.008
- Yadav, R. K., Perales, M., Gruel, J., Ohno, C., Heisler, M., Girke, T., . . . Reddy, G. V. (2013). Plant stem cell maintenance involves direct transcriptional repression of differentiation program. *Molecular Systems Biology*, 9, 654. doi:10.1038/msb.2013.8
- Yamaguchi, N., Wu, M. F., Winter, C. M., Berns, M. C., Nole-Wilson, S., Yamaguchi, A., . . . Wagner, D. (2013). A molecular framework for auxin-mediated initiation of flower primordia. *Dev Cell*, 24(3), 271–282. doi:10.1016/j.devcel.2012.12.017
- Yao, X., Chen, J., Zhou, J., Yu, H., Ge, C., Zhang, M., . . . Zhao, Y. (2019). An Essential Role for miRNA167 in Maternal Control of Embryonic and Seed Development. *Plant Physiology*, 180(1), 453–464. doi:10.1104/pp.19.00127
- Yoshida, S., Barbier de Reuille, P., Lane, B., Bassel, G. W., Prusinkiewicz, P., Smith, R. S., & Weijers, D. (2014). Genetic control of plant development by overriding a geometric division rule. *Dev Cell*, 29(1), 75–87. doi:10.1016/j.devcel.2014.02.002
- Zabidi, M. A., & Stark, A. (2016). Regulatory Enhancer-Core-Promoter Communication via Transcription Factors and Cofactors. *Trends Genet*, 32(12), 801–814. doi:10.1016/j.tig.2016.10.003
- Zenser, N., Ellsmore, A., Leasure, C., & Callis, J. (2001). Auxin modulates the

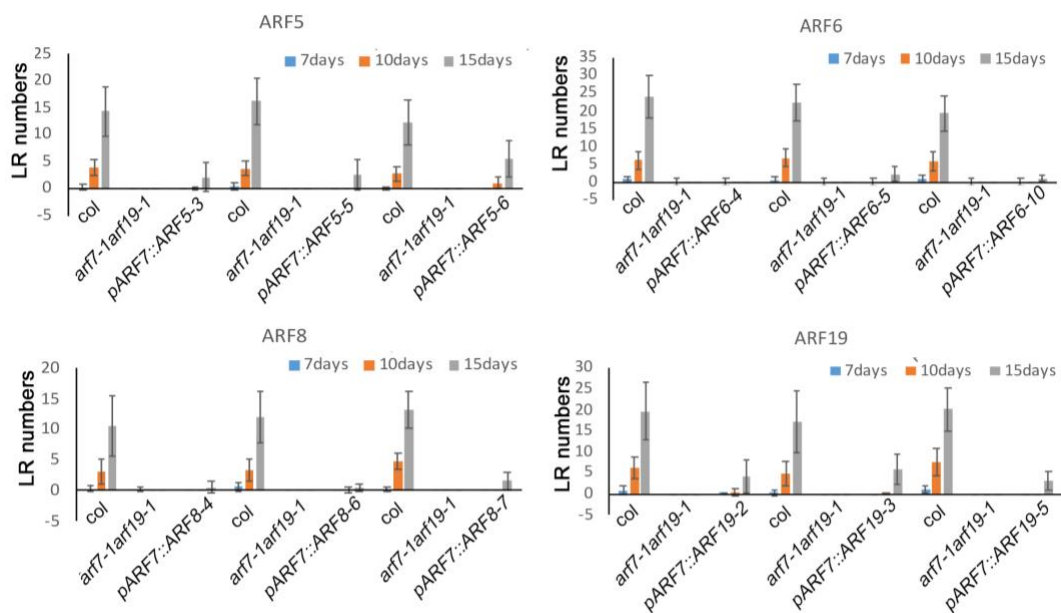
degradation rate of Aux/IAA proteins. *Proc Natl Acad Sci U S A*, *98*(20), 11795-11800. doi:10.1073/pnas.211312798

Zheng, L., Nagpal, P., Villarino, G., Trinidad, B., Bird, L., Huang, Y., & Reed, J. W. (2019). miR167 limits anther growth to potentiate anther dehiscence. *Development*, *146*(14). doi:10.1242/dev.174375

Zolman, B. K., Silva, I. D., & Bartel, B. (2001). The Arabidopsis pxa1 mutant is defective in an ATP-binding cassette transporter-like protein required for peroxisomal fatty acid beta-oxidation. *Plant Physiology*, *127*(3), 1266-1278.

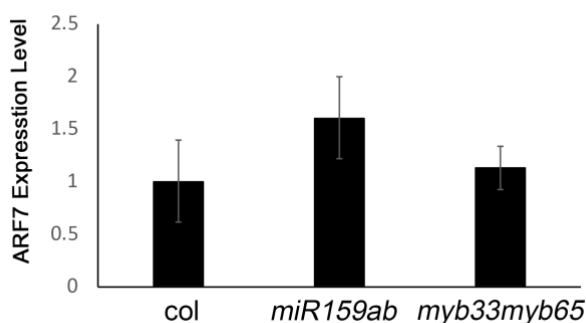
Appendix

Supplemental figure. 1 Lateral root numbers in *pARF7::ARFs*



The graph showed LR numbers in *col*, *arf7-1arf19-1* and *pARF7::ARFs*. Each ARF measured 3 independent lines with no less than 15 plants. *Col*, *arf7-1arf19-1* and *pARF7::ARFs* grew in same plates.

Supplemental figure. 2 ARF7 expression in *myb* and *miR159ab* mutants



qRT-PCR result showed ARF7 expression level in *col* and MYB related mutants in 2mm root tips. $p < 0.05$. Significant test was done by T-test. Error bar are standard deviation of three independent replicates.

Supplemental table 1. Potential transcription factor binding to first intron of ARF7

Gene	Family	Name	score	p-value	matched sequence
AT2G01760	ARR-B	RR14	10.8605	6.74E-05	AGATACGA
AT5G58080	ARR-B	RR18	10.5474	9.28E-05	TATCAGATACGAG
AT5G18090	B3	AT5G18090	11.8904	7.00E-05	TTTGATGAAGGAGCT
AT4G29000	CPP	AT4G29000	11.6224	7.35E-05	GATTTGAATA
AT5G05090	G2-like	AT5G05090	11.4894	5.84E-05	TCAGATACGAG
AT2G01570	GRAS	RGA1	11.9571	3.34E-05	CAGAAAATGACCGAAACCAA
AT1G46264	HSF	HSFB4	7.43836	5.58E-05	TGAAGATCCTAGAGA
AT2G41690	HSF	HSFB3	10.3797	7.86E-05	TCTCTAGGATCTTCA
AT3G22830	HSF	HSFA6B	9.54688	8.10E-05	TGAAGATCCTAGAGA
AT5G16820	HSF	HSF3	11.0156	4.79E-05	GAAGATCCTAGA
AT2G32460	MYB	MYB101	11.9062	3.83E-05	GACCGAAACCAATTC
AT5G06100	MYB	MYB33	11.4844	6.70E-05	GTAAGTGAATG
AT4G01550	NAC	NAC069	12.1094	4.10E-05	AGCTTACTCTCTAAG
AT2G27300	NAC	NTL8	12.4844	2.35E-05	ATTTCTTCTACTAAAGGAT
AT1G02250	NAC	NAC005	9.29688	9.19E-05	CTGCTTAGAGAGTAAGCTA
AT1G02230	NAC	NAC004	13.9062	1.24E-05	CTTACTCTCTAAGC
AT1G12260	NAC	NAC007	11.2344	6.05E-05	CTTACTCTCTAAGCA
AT3G49530	NAC	NAC062	14.1562	1.29E-05	CTTACTCTCTAAGCA
AT4G36160	NAC	NAC076	11.0469	6.80E-05	CTTACTCTCTAAGCA
AT1G12260	NAC	NAC007	11.4375	5.43E-05	CTTAGAGAGTAAGCT
AT3G49530	NAC	NAC062	13.6406	1.79E-05	CTTAGAGAGTAAGCT
AT4G36160	NAC	NAC076	11.1875	6.34E-05	CTTAGAGAGTAAGCT
AT1G32870	NAC	NAC13	8.35938	6.80E-05	CTTAGAGAGTAAGCTA
AT3G10480	NAC	NAC050	5.54688	9.12E-05	CTTAGAGAGTAAGCTA
AT5G46590	NAC	NAC096	10.0312	6.86E-05	CTTAGAGAGTAAGCTA
AT5G66300	NAC	NAC105	12.5469	2.31E-05	CTTAGAGAGTAAGCTA
AT4G01540	NAC	NTM1	13.6562	1.70E-05	GCTTACTCTCTAAGC
AT4G01540	NAC	NTM1	9.625	6.54E-05	GCTTAGAGAGTAAGC
AT2G46770	NAC	NST1	12.3438	2.98E-05	TAGCTTACTCTCTAAGC

AT1G02250	NAC	NAC005	11.2344	4.58E-05	TAGCTTACTCTCTAAGCAG
AT4G35580	NAC	NTL9	15.0577	2.49E-05	TTAAGTAAT
AT2G38880	NF-YB	NF-YB1	3.72603	8.33E-05	TCCTTCATC
AT2G17950	WOX	WUS	10.9747	7.05E-05	TCATTCAGTTA

Supplemental table 2. Dissected intron sequences

The part deleted is shown in grey and the exchanged sequence is shown in red.

Name	Sequence
Original Intron	GTTTGTGTGTTTCTCGTATCTGATAAATGTCAATCCTTTAGTAGAAGAAATTCATTGC TGGATTTGAATAGATTCAAGTTTTAAGTAGAAGAGGTCACACATTTCTTCAGAATTG CTGGATTTGAGAACCTGAATTGAATTGGTTTCGGTCATTTTCTGCTTAGAGAGTAA GCTAAGTTACTATTGTATTGGTTTATAAAGACTGTGGCTTTTAGTTGGTTTAGAGCA GTTCTCTCCTATCTTGTTGGTTTGATAATAGTAACTGAATGAAGATCCTAGAGATTTT AAGTAATCACAGCTTTGATGTTGTGTGAATGCAG
D1	GTTTGTGTGTT(<u>TCTCGTATCTGATAAATGTCAATCCTTTAGTAGAAGAAATTCATTGC</u> <u>TGGATTTGAATAGATTCAAGTTTTAAGTAGAAGAGGTCACACA</u>)TTTCTTCAGAATT GCTGGATTTGAGAACCTGAATTGAATTGGTTTCGGTCATTTTCTGCTTAGAGAGTA AGCTAAGTTACTATTGTATTGGTTTATAAAGACTGTGGCTTTTAGTTGGTTTAGAGC AGTTCTCTCCTATCTTGTTGGTTTGATAATAGTAACTGAATGAAGATCCTAGAGATTT TAAGTAATCACAGCTTTGATGTTGTGTGAATGCAG
D2	GTTTGTGTGTTTCTCGTATCTGATAAATGTCAATCCTTTAGTAGAAGAAATTCATTGC TGGATTTGAATAGATTCAAGTTTTAAG(<u>TAGAAGAGGTCACACATTTCTTCAGAATT</u> <u>GCTGGATTTGAGAACCTGAATTGAATTGGTTTCGGTCATTTTCTGCTTAGAGAGTA</u> <u>AGCTA</u>)AGTTACTATTGTATTGGTTTATAAAGACTGTGGCTTTTAGTTGGTTTAGAGC AGTTCTCTCCTATCTTGTTGGTTTGATAATAGTAACTGAATGAAGATCCTAGAGATTT TAAGTAATCACAGCTTTGATGTTGTGTGAATGCAG
D3	GTTTGTGTGTTTCTCGTATCTGATAAATGTCAATCCTTTAGTAGAAGAAATTCATTGC TGGATTTGAATAGATTCAAGTTTTAAGTAGAAGAGGTCACACATTTCTTCAGAATTG CTGGATTTGAGAACCTGAAT(<u>TGAATTGGTTTCGGTCATTTTCTGCTTAGAGAGTAA</u> <u>GCTAAGTTACTATTGTATTGGTTTATAAAGACTGTGGCTTTTAGTTGGTTTAGA</u>)GCA GTTCTCTCCTATCTTGTTGGTTTGATAATAGTAACTGAATGAAGATCCTAGAGATTTT AAGTAATCACAGCTTTGATGTTGTGTGAATGCAG

D4
GTTTGTGTGTTTCTCGTATCTGATAAATGTCAATCCTTTAGTAGAAGAAATTCATTGC
TGGATTTGAATAGATTCAAGTTTTAAGTAGAAGAGGTCACACATTTCTTCAGAATTG
CTGGATTTGAGAACCTGAATTGAATTGGTTTCGGTCATTTTCTGCTTAGAGAGTAA
GCTAAGTTACTATTGTATTGGTTTATAAAGACTGTG(GCTTTTAGTTGGTTTAGAGCA
GTTCTCTCCTATCTTGGTTGGTTTGATAATAGTAACTGAATGAAGATCCTAGAGATTTT
AAGTAATCACAJ)GCTTTGATGTTGTGTGAATGCAG

$\Delta 1^{\text{st}}$ NAC
GTTTGTGTGTTTCTCGTATCTGATAAATGTCAATCCTTcgGTAGAAGAAATTCATTGC
TGGATTTGAATAGATTCAAGTTTTAAGTAGAAGAGGTCACACATTTCTTCAGAATTG
CTGGATTTGAGAACCTGAATTGAATTGGTTTCGGTCATTTTCTGCTTAGAGAGTAA
GCTAAGTTACTATTGTATTGGTTTATAAAGACTGTGGCTTTTAGTTGGTTTAGAGCA
GTTCTCTCCTATCTTGGTTGGTTTGATAATAGTAACTGAATGAAGATCCTAGAGATTTT
AAGTAATCACAGCTTTGATGTTGTGTGAATGCAG

$\Delta 2^{\text{nd}}$ NAC
GTTTGTGTGTTTCTCGTATCTGATAAATGTCAATCCTTTAGTAGAAGAAATTCATTGC
TGGATTTGAATAGATTCAAGTTTTAAGTAGAAGAGGTCACACATTTCTTCAGAATTG
CTGGATTTGAGAACCTGAATTGAATTGGTTTCGGTCATTTTCTGtcTAGAGAGTAA
CTAAGTTACTATTGTATTGGTTTATAAAGACTGTGGCTTTTAGTTGGTTTAGAGCAG
TTCTCTCCTATCTTGGTTGGTTTGATAATAGTAACTGAATGAAGATCCTAGAGATTTTA
AGTAATCACAGCTTTGATGTTGTGTGAATGCAG

$\Delta 3^{\text{rd}}$ NAC
GTTTGTGTGTTTCTCGTATCTGATAAATGTCAATCCTTTAGTAGAAGAAATTCATTGC
TGGATTTGAATAGATTCAAGTTTTAAGTAGAAGAGGTCACACATTTCTTCAGAATTG
CTGGATTTGAGAACCTGAATTGAATTGGTTTCGGTCATTTTCTGCTTAGAGAGTAA
GCTAAGTTACTATTGTATTGGTTTATAAAGACTGTGGCTTTTAGTTGGTTTAGAGCA
GTTCTCTCCTATCTTGGTTGGTTTGATAATAGTAACTGAATGAAGATCCTAGAGATTTT
ActTAATCACAGCTTTGATGTTGTGTGAATGCAG

$\Delta 2^{\text{*}}$ MYB
GTTTGTGTGTTTCTCGTATCTGATAAATGTCAATCCTTTAGTAGAAGAAATTCATTGC
TGGATTTGAATAGATTCAAGTTTTAAGTAGAAGAGGTCACACATTTCTTCAGAATTG
CTGGATTTGAGAACCTGAATTGAATcaGTTTCGGTCATTTTCTGCTTAGAGAGTAA
CTAAGTTACTATTGTATTGGTTTATAAAGACTGTGGCTTTTAGTTGGTTTAGAGCAG
TTCTCTCCTATCTTGGTTGGTTTGATAATAGTActGAATGAAGATCCTAGAGATTTTAA
GTAATCACAGCTTTGATGTTGTGTGAATGCAG

Supplemental table 3. Primers

Entry Module Name	Forward Primers	Reverse Primers	Information
pGGA-ARF7proS	AACAGGTCTCTACCTaagagATGTCGCAAACCAGC	AACAGGTCTCGTGTGatcactcaactttactttctctgaa	Amplify
pGGA-ARF7proINTs	ttgtgtgaatgcagGAGAAAttatttattgggtttattcttcagaga	agaaacacacaaaacCTTCAAtctgaatctgagcttatacaaag	Gibson for promoter
	tgtataagctcagattcagaTTGAAGgtttgtgtttctc	agaataaacccaataaataaTTTCTCctgcattcacaca	Gibson for 1 st intron
pGGB003-B dummy			
pGGB-EX1	gcttggctcaaacaccATGAAAGCTCCTTCATCAAATGGAG	attcggctcaagcCTTCAACAGGATTAGGAGAAACTCC	Amplify
pGGB-EX1-2	gcttggctcaaacaccATGAAAGCTCCTTCATCAAATGGAG	attcggctcaagccCTTTCTCctgcattcacaca	Amplify
pGGB-EX1-2 (d1)	TTTCTTCAGAATTGCTGG	AACACACAAACCTTCAAC	For deletions
pGGB-EX1-2 (d2)	AGTTACTATTGTATTGGTTTATAAAG	CTTAAACTTGAATCTATTCAAATC	For deletions
pGGB-EX1-2 (d3)	GCAGTTCTCTCTATCTTG	ATTCAGTTCTCAAATCC	For deletions
pGGB-EX1-2 (d4)	GCTTTGATGTTGTGTGAATG	CACAGTCTTTATAAACCAATAC	For deletions
pGGB-EX1-2 (NAC)	TCATTTTCTGtcTAGAGAGTAAGCTAAG	CCGAAACCAATTCAATTC	For deletions
pGGB-EX1-2 (NAC1)	GTCAATCCTTcgGTAGAAGAAATTCATTG	ATTTATCAGATACGAGAAACAC	For deletions
pGGB-EX1-2 (NAC2)	AGAGATTTTActTAATCACAGCTTTGATGTTGTGTG	AGGATCTTCATTGATTAC	For deletions
pGGC012-GFP			
pGGC-ARF7CDS			By Nicky Leftley
pGGC-ARF7Genomic	accaggtctcgggctATGAAAGCTCCTTCATCAAATGGAGT	aacaggtctctctgAtgatttcatgttttctctctttt	Amplify
	tttggctcaGGaCTCAACGGGCAGAATCAG	tttggctcaGtCCAGGAGGCTGCTGCTGT	For Bsa I cutting site

pGGC-ARF7EX1-2CDS	accaggtctcgggctATGATGGCTTCATTGTCTTGTG	aacaggtctctctgaTTATGAAACAGAAGTCTTAAGATCG	Amplify
pGGC-ARF5CDS	tttggtctcaGAtCCGCATATCGCCTTAC	tttggtctcaGaTCTCAGCTCTCAGTTGGT	For Bsa I cutting site
	tttggtctcaGtCCGTTCAACTGAGTGTC	tttggtctcaGGaCTCAAGTTTGACCAGTT	For Bsa I cutting site
pGGC-ARF6CDS	accaggtctcgggctATGAGATTATCTTCAGCTGGGT	aacaggtctctctgaCTAGTAGTTGAATGAACCCCAA	Amplify
	tttggtctcaGGaCTCCCATCTTCCATGG	tttggtctcaGtCCAGGAGGCCACGG	For Bsa I cutting site
pGGC-ARF8CDS	accaggtctcgggctATGAAGCTGTCAACATCTGGATTG	aacaggtctctctgaCTAGAGATGGGTCGGGTTTT	Amplify
	tttggtctcaGgGACCAGCCCTCTGTTGTAA	tttggtctcaTcCCAAAAGCATCCAACAC	For Bsa I cutting site
pGGC-ARF19CDS	accaggtctcgggctATGAAAGCTCCATCAAATGG	aacaggtctctctgaCTATCTGTTGAAAGAAGCTGC	
pGGD003-D dummy			
pGGE001-RBCS			
pGGF005-Hygromycin			

Primer name	Forward Primers	Reverse Primers	Information
ARF7-TRANS	AGTTCCTCCATTTCTGATTAACG	TGAAGTGTGGCCGTTTAC	For RT-PCR
GFP-qRT	TTCAAGGACGACGGCAACTA	TCAGCTCGATGCGGTTCA	For qRT-PCR
ARF7-qRT	CGCCATTTGAAACGATCT	AGCCTCGTTTTTGCACCTT	For qRT-PCR
